

INVESTIGATION OF SO₂ REMOVAL CHARACTERISTICS WITH
LIMESTONE UNDER OXYCOMBUSTION CONDITIONS

A THESIS SUBMITTED TO
THE GRADUATE SCHOOL OF NATURAL AND APPLIED SCIENCES
OF
MIDDLE EAST TECHNICAL UNIVERSITY

BY

SEVIL AVŞAROĞLU

IN PARTIAL FULFILLMENT OF THE REQUIREMENTS
FOR
THE DEGREE OF MASTER OF SCIENCE
IN
ENVIRONMENTAL ENGINEERING

SEPTEMBER 2019

Approval of the thesis:

**INVESTIGATION OF SO₂ REMOVAL CHARACTERISTICS WITH
LIMESTONE UNDER OXYCOMBUSTION CONDITIONS**

submitted by **SEVIL AVŞAROĞLU** in partial fulfillment of the requirements for the degree of **Master of Science in Environmental Engineering Department, Middle East Technical University** by,

Prof. Dr. Halil Kalıpçılar
Dean, Graduate School of **Natural and Applied Sciences**

Prof. Dr. Bülent İçgen
Head of Department, **Environmental Eng.**

Prof. Dr. Faika Dilek Sanin
Supervisor, **Environmental Eng., METU**

Prof. Dr. Aysel Atımtay
Co-Supervisor, **Environmental Engineering, METU**

Examining Committee Members:

Prof. Dr. Ayşegül Aksoy
Environmental Engineering, METU

Prof. Dr. Faika Dilek Sanin
Environmental Eng., METU

Prof. Dr. Ahmet Yozgatlıgil
Mechanical Engineering, METU

Prof. Dr. Murat Köksal
Mechanical Engineering, Hacettepe University

Prof. Dr. Zöhre Kurt
Environmental Engineering, METU

Date: 10.09.2019

I hereby declare that all information in this document has been obtained and presented in accordance with academic rules and ethical conduct. I also declare that, as required by these rules and conduct, I have fully cited and referenced all material and results that are not original to this work.

Name, Surname: Sevil Avşarođlu

Signature:

ABSTRACT

INVESTIGATION OF SO₂ REMOVAL CHARACTERISTICS WITH LIMESTONE UNDER OXYCOMBUSTION CONDITIONS

Avşarođlu, Sevil

Master of Science, Environmental Engineering

Supervisor: Prof. Dr. Faika Dilek Sanin

Co-Supervisor: Prof. Dr. Aysel Atimtay

September 2019, 112 pages

One of the technologies to increase combustion efficiency and decrease CO₂ and other emissions is Oxy-Fuel Combustion. Combustion efficiency is higher and emissions are lower when the oxygen concentration of air is higher. In this thesis different characteristics of two indigenous Turkish lignites are investigated by Thermal Gravimetric Analysis (TGA). Pyrolysis is carried out under both N₂ and CO₂ atmospheres and combustion characteristics is also examined. CO₂ acts as an inert gas at lower temperatures. Three temperature regions in pyrolysis are due to moisture release, volatile matter release and calcite decomposition in N₂ and char gasification in CO₂ atmosphere. In combustion study, the third temperature region shows the oxidation of char. Due to Turkish lignites having high sulphur content, capturing of SO₂ emissions with limestone addition during oxy-combustion is studied. The studies showed the main effect of CO₂ concentration is to determine whether the limestone will undergo calcination (indirect sulfation) or not (direct sulfation) at the same temperature. Generating oxycombustion conditions that allow indirect sulfation, results in a more effective use of limestone to capture SO₂. At the end of eight-hour period, the sulfur conversion of **direct sulfation** at 800 °C was 30%. However, for the **indirect sulfation** sulfur conversion was 58%. For 15% CO₂, sulfur conversion

doubles at higher temperatures due to calcination and **indirect sulfation** of limestone. In sulfation studies, the other parameters that are examined were temperature, SO₂ concentration in the gas mixture, particle size and limestone type. When Çan and Çumra limestone are compared, calcination of these limestones occurred at the same condition. However, Çan limestone resulted in higher sulfur conversion values (about 60%) due to higher surface area. Dolomite results showed lower sulfur conversions (about 12% at 800 °C, and 28-37% at 900 °C) as compared to limestone samples.

Keywords: Coal, Combustion, Oxy-combustion, Emissions, SO₂ capture

ÖZ

OKSİYANMA KOŞULLARINDA KİREÇTAŞI İLE SO₂ GİDERME KARAKTERİSTİKLERİNİN İNCELENMESİ

Avşaroğlu, Sevil
Yüksek Lisans, Çevre Mühendisliği
Tez Danışmanı: Prof. Dr. Faika Dilek Sanin
Ortak Tez Danışmanı: Prof. Dr. Aysel Atımtay

Eylül 2019, 112 sayfa

Kömür yakan enerji üretim sistemlerinde yanma verimini yükseltmeyi ve açığa çıkan CO₂ ve diğer emisyonları azaltmayı sağlayabilecek teknolojilerden biri yanmanın oksijence zengin ortamda gerçekleştirilmesidir. Yanma daha yüksek oksijene sahip havayla yapıldığında yanma verimi yüksek olmakta, emisyonlar azalmaktadır. Bu çalışmada iki yerli linyit örneği termogravimetrik analiz (TGA) ile incelenmiştir. Numuneler, N₂ ve CO₂ atmosferlerinde piroliz ve yanma koşullarında incelenmiştir. CO₂'nin düşük sıcaklıklarda soy gaz gibi davrandığı görülmüştür. Piroliz deneylerinde, birinci ve ikinci sıcaklık aralığında nem ve uçucu maddenin açığa çıkması; üçüncü sıcaklık aralığında ise N₂ atmosferinde kalsit bozulması ve CO₂ atmosferinde oluşan karbonun (char) gazlaşması reaksiyonları görülmüştür. Yanma deneylerinde, üçüncü sıcaklık aralığı karbonun (char) oksidasyonunu göstermektedir. Ülkemiz linyit kömürlerinin kükürt içeriği fazla olduğundan oksi-yanma sırasında oluşan SO₂'nin sisteme eklenecek kireçtaşı ile tutulması incelenmiştir. Çalışmalar, ortamdaki CO₂ konsantrasyonuna göre aynı sıcaklıkta kireçtaşının kalsinasyona uğrayarak dolaylı sülfasyon yapmasını veya kalsine olmayarak direkt sülfasyona girmesine neden olduğunu göstermiştir. Dolaylı sülfasyona neden olacak oksi-yanma koşullarında, kireçtaşı ile SO₂ tutulmasının daha verimli olması sağlanabilir.

Sülfasyon çalıřmaları kapsamında incelenen diđer parametreler ise sıcaklık, karıřım gazındaki SO₂ konsantrasyonu, parçacık boyutu ve kireçtařı cinsidir. Çan ve Çumra kireçtařları karşılařtırılıđında, kalsinasyon reaksiyonunun aynı kořullarda gerçekteřtiđi görülmüřtür. Fakat, Çan kireçtařının yüzey alanı yüksek olduđundan daha yüksek sülfür dönüşüm deđerleri (yaklařık % 60), ancak dolomit ile kireçtařına oranla daha düşük sülfür dönüşüm deđerleri (%12 at 800 °C, and %28-37 at 900 °C) elde edilmiřtir.

Anahtar Kelimeler: Kömür, Yanma, Oksijenleme, Emisyon, SO₂ giderimi

To my dearest family...

ACKNOWLEDGEMENTS

This thesis was supervised by Assistant Professor Dr. Barış Kaymak starting from November 2014 after Prof. Dr. Aysel Atımtay's retirement. Dr. Atımtay could only be my Co-advisor according to the Rules and Regulations of the Graduate School of Middle East Technical University. Dr. Kaymak left Middle East Technical University in October 2016. After that Professor Dr. F. Dilek Sanin accepted to undertake my advisorship at an administrative level.

First and foremost, I would like to express my deepest gratitude to my Co-Adviser Prof. Dr. Aysel Atımtay for her advice, encouragement and support during the completion of this thesis. Her guidance greatly enabled this thesis study.

I would like to express my gratefulness to my supervisor Prof. Dr. F. Dilek Sanin, to accept to be my administrative advisor. It was possible for me to complete this thesis since Dr. Sanin accepted to be my advisor.

I also would like to thank Prof. Dr. Ahmet Yozgatlıgil for his guidance, advice and direction in this study. My thanks extend to Ramin Barzegar, with whom I worked in the same Air Pollution Laboratory. He supported me throughout the study with his help and friendship.

I would like to thank my jury members Prof. Dr. Murat Köksal, Prof. Dr. Ayşegül Aksoy and Assist. Prof. Dr. Zöhre Kurt for their valuable suggestions and comments on this study.

I would also like to thank my whole family, especially to my parents and my brother for all the moral support and belief in me.

Finally, I gratefully acknowledge the financial support provided by the Scientific and Technological Research Council of Turkey (TÜBİTAK) through the project entitled 'Oxygen Enriched Combustion of Lignite and Biomass in Circulating Fluidized Bed

Combustion System (Oxy-Combustion)' with project number 113M003. This thesis was a part of the project study.

TABLE OF CONTENTS

ABSTRACT	v
ÖZ	vii
ACKNOWLEDGEMENTS.....	x
TABLE OF CONTENTS	xii
LIST OF TABLES.....	xiv
LIST OF FIGURES	xv
LIST OF ABBREVIATIONS.....	xviii
CHAPTERS	
1. INTRODUCTION.....	1
2. THEORETICAL BACKGROUND	11
2.1. Carbon Capture	11
2.2. Oxy-fuel Combustion.....	13
2.3. Pyrolysis and Oxy-Fuel Combustion	16
2.4. Emissions from Oxy-fuel Combustion	17
2.5. Sulfur Retention with Limestone	20
3. MATERIALS AND METHODS	25
3.1. Experimental Setup	25
3.2. Physical and Chemical Characteristics of Coal Samples.....	30
3.3. Physical and Chemical Characteristics of Sorbents - Limestone and Dolomite Samples	33
3.4. Experimental Procedures	35
3.4.1. Experimental Procedure for Pyrolysis and Combustion Tests.....	35

3.4.2. Methods Used for the Calculations of Kinetic Data	37
3.4.3. Experimental Procedure for Limestone Sulfation Tests	42
4. Results and discussion	47
4.1. Thermogravimetric Analysis of Lignites	47
4.1.1. Thermogravimetric Analysis Results of Coal Pyrolysis.....	48
4.1.2. Kinetic Results of Coal Pyrolysis	51
4.1.3. Thermogravimetric Analysis Results of Coal Combustion	57
4.2. Thermogravimetric Analysis of Limestones and Dolomite	59
4.2.1. Thermogravimetric Analysis Results of Çan Limestone	60
4.2.1.1. Calcination of Çan Limestone in Indirect Sulfation	60
4.2.1.2. Sulfation of Çan Limestone	68
4.2.2. Thermogravimetric Analysis Results of Çumra Limestone	77
4.2.2.1. Calcination of Çumra Limestone in Indirect Sulfation	78
4.2.2.2. Sulfation of Çumra Limestone	80
4.2.3. Thermogravimetric Analysis Results of Eskişehir Dolomite	85
4.2.3.1. Calcination of Eskişehir Dolomite in Indirect Sulfation.....	85
4.2.3.2. Sulfation of Eskişehir Dolomite.....	88
5. CONCLUSION.....	95
REFERENCES.....	99
APPENDIX A Isoconversional Plots for Coal Pyrolysis.....	105

LIST OF TABLES

TABLES

Table 3-1 Technical properties of PerkinElmer Pyris 1 model TGA	28
Table 3-2 Technical properties of gas mixing unit	29
Table 3-3 Methods and instruments used in the characterization of lignites and limestones	30
Table 3-4 Proximate and ultimate analysis of the coal samples	31
Table 3-5 XRF analysis of lignite ashes	33
Table 3-6 XRF analysis of limestone samples	34
Table 3-7 XRF analysis of dolomite sample	34
Table 3-8 BET surface area analysis results of limestones and dolomite	35
Table 3-9 List of experiments for Orhaneli and Soma lignites	36
Table 3-10 List of limestone sulfation experiments	44
Table 4-1 Activation energies for Orhaneli lignite in N ₂ and CO ₂ atmospheres.....	55
Table 4-2 Activation energies for Soma lignite in N ₂ and CO ₂ atmospheres.....	55
Table 4-3 Pre-exponential factors for Orhaneli lignite in N ₂ and CO ₂ atmospheres.	56
Table 4-4 Pre-exponential factors for Soma lignite in N ₂ and CO ₂ atmospheres.....	56

LIST OF FIGURES

FIGURES

Figure 1-1 Simplified energy balances of 1973 and 2016 (International Energy Agency, 2018).....	2
Figure 1-2 1973 and 2016 source shares of electricity generation (International Energy Agency, 2018).....	3
Figure 2-1 A schematic diagram showing the three carbon capture technologies (Nemitallah et al., 2017).....	13
Figure 2-2 Flowchart of oxy-fuel combustion technology for power generation (Huang et al., 2018).....	14
Figure 2-3 Thermodynamic equilibrium curve of CaCO ₃ calcination (De Diego et al., 2011)	21
Figure 3-1 Schematic diagram of TGA and gas mixing unit.....	26
Figure 3-2 Thermogravimetric Analyzer (TGA)	27
Figure 3-3 Gas mixing unit and the MFCs.....	27
Figure 4-1 TGA and DTG curves showing the characteristic temperatures and weight loss regions for a coal sample	48
Figure 4-2 TGA and DTG graphs of pyrolysis of Orhaneli lignite in N ₂ and CO ₂ atmospheres.....	50
Figure 4-3 TGA and DTG graphs of Soma lignite in N ₂ and CO ₂ atmospheres	51
Figure 4-4 Activation energy values as a function of conversion factor in different isoconversional methods for Orhaneli lignite under N ₂ and CO ₂ atmospheres	53
Figure 4-5 Activation energy values as a function of conversion factor in different isoconversional methods for Soma lignite under N ₂ and CO ₂ atmospheres	54
Figure 4-6 TGA and DTG graphs of combustion of Orhaneli lignite in dry air.....	58
Figure 4-7 TGA and DTG graphs of combustion of Soma lignite in dry air.....	58
Figure 4-8 Comparison of Orhaneli and Soma lignites at 20 °C/min in dry air.....	59

Figure 4-9 TGA results of Çan limestone at 800 °C	62
Figure 4-10 TGA results of Çan limestone at 850 °C	62
Figure 4-11 TGA results of Çan limestone at 900 °C	63
Figure 4-12 CaCO ₃ -CaO calcination thermodynamic curve (solid line) and the curve obtained from the experimental results (dashed line) (De Diego et al., 2011).....	64
Figure 4-13 Calcination of Çan limestone at 15% CO ₂ concentration.....	65
Figure 4-14 Calcination of Çan limestone at 900 °C.....	66
Figure 4-15 Calcination of Çan limestone at different particle sizes	67
Figure 4-16 Sulfur conversion of Çan limestone at 15% CO ₂ concentration.....	69
Figure 4-17 Sulfur conversion of Çan limestone at 40% CO ₂ concentration.....	70
Figure 4-18 Sulfur conversion of Çan limestone at 60% CO ₂ concentration.....	70
Figure 4-19 Sulfur conversion of Çan limestone at 80% CO ₂ concentration.....	71
Figure 4-20 Sulfur conversion of Çan limestone at 800 °C.....	72
Figure 4-21 Sulfur conversion of Çan limestone at 900 °C.....	73
Figure 4-22 Comparison of sulfur conversion for Çan limestone at 800 °C and 900°C at different CO ₂ concentrations	74
Figure 4-23 Sulfur conversion of Çan limestone for different particle sizes at 800 °C and 60% CO ₂ concentration.....	75
Figure 4-24 Sulfur conversion of Çan limestone for different particle sizes at 900 °C and 60% CO ₂ concentration.....	76
Figure 4-25 Comparison of sulfur conversion for Çan limestone at 800 °C and 900°C at different SO ₂ concentrations	77
Figure 4-26 TGA results of Çumra limestone at 800 °C	79
Figure 4-27 TGA results of Çumra limestone at 850 °C	79
Figure 4-28 TGA results of Çumra limestone at 900 °C	80
Figure 4-29 Sulfur conversion of Çumra limestone at 15% CO ₂ concentration	81
Figure 4-30 Sulfur conversion of Çumra limestone at 40% CO ₂ concentration	82
Figure 4-31 Sulfur conversion of Çumra limestone at 60% CO ₂ concentration	82
Figure 4-32 Sulfur conversion of Çumra limestone at 800 °C	83
Figure 4-33 Sulfur conversion of Çumra limestone at 900 °C	84

Figure 4-34 Comparison of sulfur conversion for Çumra limestone at 800 °C and 900°C at different CO ₂ concentrations.....	84
Figure 4-35 TGA results of Eskişehir dolomite at 800 °C.....	87
Figure 4-36 TGA results of Eskişehir dolomite at 850 °C.....	87
Figure 4-37 TGA results of Eskişehir dolomite at 900 °C.....	87
Figure 4-38 Sulfur conversion of Eskişehir dolomite at 15% CO ₂ concentration	89
Figure 4-39 Sulfur conversion of Eskişehir dolomite at 40% CO ₂ concentration	89
Figure 4-40 Sulfur conversion of Eskişehir dolomite at 60% CO ₂ concentration	90
Figure 4-41 Sulfur conversion of Eskişehir dolomite at 80% CO ₂ concentration	91
Figure 4-42 Sulfur conversion of Eskişehir dolomite at 800 °C.....	92
Figure 4-43 Sulfur conversion of Eskişehir dolomite at 900 °C.....	93
Figure 4-44 Comparison of sulfur conversion comparison for Eskişehir dolomite at 800 °C and 900°C at different CO ₂ concentrations.....	93
Figure 4-45 Sulfur conversion of Eskişehir dolomite at 900°C at different SO ₂ concentrations	94

LIST OF ABBREVIATIONS

ABBREVIATIONS

ASU: Air Separation Unit

CFBC: Circulating Fluidized Bed

FGD: Flue gas desulfurization

FWO: Flynn-Wall-Ozawa method

IEA: International Energy Agency

IGCC: Integrated Gasification Combined Cycles

KAS: Kissinger-Akahira-Sunose method

MENR: Ministry of Energy and Natural Resources

MFC: Mass flow controllers

Mtoe: Million tons of equivalent oil

NGCC: Natural Gas Combined Cycles

PC: Pulverized coal

TGA: Thermogravimetric Analyzer

TPES: Total Primary Energy Supply

XRF: X-ray fluorescence

CHAPTER 1

INTRODUCTION

Coal has always been one of the prominent energy supplies historically, before and after the revolution as well as current times. Coal is used for the generation of electricity and heat. As of 2018, coal accounts for 27% of worldwide energy consumption and 38% of world electricity generation.

According to International Energy Agency's "Key World Energy Statistics 2018", in 1973, the share of coal in world Total Primary Energy Supply (TPES) was 1,496 million tons of equivalent oil (Mtoe), equaling to 24.5% and in 2016 the share of coal in world Total Primary Energy Supply was 3,731 million tons of equivalent oil, equaling to 27.1% (Figure 1-1). These numbers indicates that, despite the fact that the mentioned time period witnessing a rising environmental awareness, coal has maintained its traditional place in the energy picture (International Energy Agency, 2018).

World energy balance, 1973

(Mtoe)									
SUPPLY AND CONSUMPTION	Coal ¹	Crude oil	Oil products	Natural gas	Nuclear	Hydro	Biofuels and waste ²	Others ³	Total
Production	1 474.00	2 938.39	-	991.26	53.04	110.29	640.86	6.13	6 213.97
Imports	140.06	1 561.97	409.58	73.42	-	-	0.13	8.14	2 193.30
Exports	-130.35	-1 613.00	-443.04	-72.58	-	-	-0.19	-8.31	-2 267.47
Stock changes	12.49	-19.81	-16.39	-15.10	-	-	0.06	-	-38.75
TPES	1 496.20	2 867.55	-49.85	977.01	53.04	110.29	640.86	5.96	6 101.05

World energy balance, 2016

(Mtoe)									
SUPPLY AND CONSUMPTION	Coal ¹	Crude oil	Oil products	Natural gas	Nuclear	Hydro	Biofuels and waste ²	Others ³	Total
Production	3 657.19	4 473.27	-	3 032.41	679.65	349.22	1 344.87	227.39	13 763.99
Imports	795.23	2 379.32	1 329.40	915.52	-	-	23.92	62.11	5 505.50
Exports	-833.43	-2 354.63	-1 414.63	-932.53	-	-	-19.44	-62.25	-5 616.91
Stock changes	111.90	-15.32	-7.21	19.55	-	-	-0.06	-	108.86
TPES	3 730.89	4 482.63	-92.43	3 034.95	679.65	349.22	1 349.29	227.25	13 761.45

Figure 1-1 Simplified energy balances of 1973 and 2016 (International Energy Agency, 2018)

Coal is the most prominent fuel in the electricity generation sector. According to the 2016 year data of IEA, 38.4% of world electricity generation is supplied by coal, followed by natural gas with 23.2% as can be seen from Figure 1-2. Comparing with the 1976 data of 38.3%, coal seems to hold its share almost constant in the electricity generation, while the oil leaving its share to natural gas (International Energy Agency, 2018).

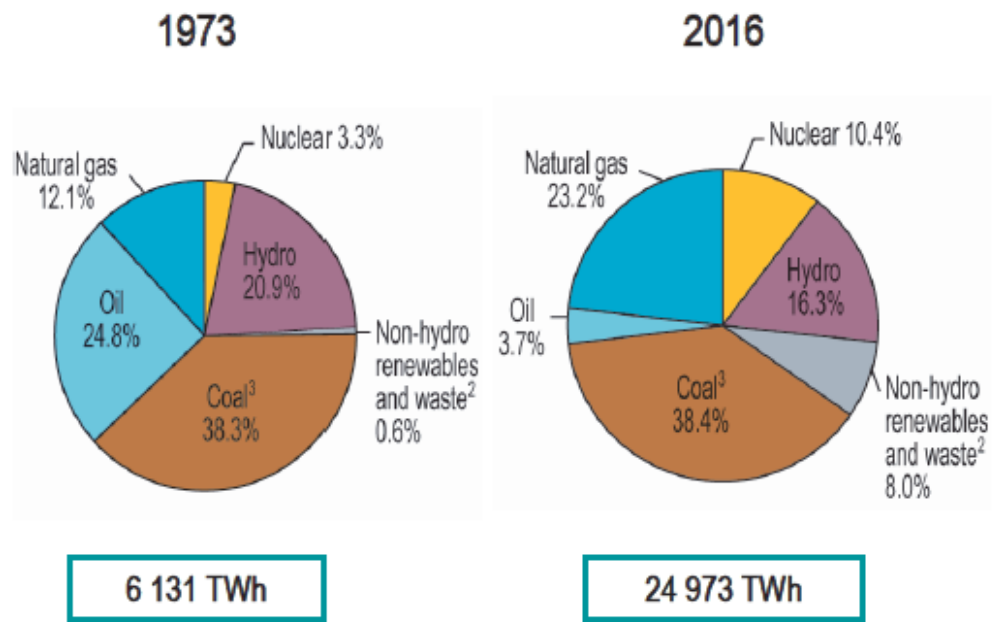


Figure 1-2 1973 and 2016 source shares of electricity generation (International Energy Agency, 2018)

While these figures show the total and long term trends of coal in energy supply, the usage of coal differs in various regions of the world. In Europe and North America, coal demand and production declined during the last decades, mainly due to environmental policies and development of renewable technologies. In all major European countries –France, Spain, Italy and the United Kingdom – most of the coal mines were closed (International Energy Agency, 2019b).

On the other hand, the demand for coal increased in Asian countries, mainly China, and India. The main reason for this increase is the increasing electricity demand in these countries.

As a result of these different regional trends, global coal demand declined slightly but then grew by 1% in 2017 since the global economic growth caused the industry sector and therefore the electricity usage to increase. Because of strong coal powered electricity generation in China and India, coal demand is expected to grow again in the following years (International Energy Agency, 2019b).

According to the Ministry of Energy and Natural Resources (MENR)'s "General Energy Balance Table 2017", the share of coal in Turkey in terms of Total Primary Energy Supply is close to the world percentages: By the end of 2017, Turkey supplied 145.3 Mtoe coal, thus the share of coal in the total primary energy supply was 27% (Ministry of Energy and Natural Resources, 2018).

In terms of the electricity generation percentages, in 2018 total 113,3 TWh electricity was generated from coal, which is 37.3% in total electricity generation (International Energy Agency, 2019a).

In terms of installed capacity, as of the end of 2018 the power plant capacity fueled by coal in Turkey was 18,997 MW, 21.5% of the total installed capacity (International Energy Agency, 2019a).

According to the MENR, Turkey is evaluated as being at medium levels in terms of the reserves and production amounts of lignite, and also at low levels in anthracite. Turkey has approximately 3.2% of the total world reserves of lignite coal. Since the grade of most lignite reserves is low, it is mainly used in thermal power plants.

Lignite coal fields are spread out among all regions of the country, and the grade of the lignite coal varies between 1000-5000 kcal/kg. Around 68% of the total lignite coal reserves are low calorie, with 23.5% between 2000-3000 kcal/kg, 5.1% between 3000-4000 kcal/kg, and 3.4% is above 4000 kcal/kg grading (International Energy Agency, 2019a).

MENR's energy policy emphasizes the importance of the domestic energy resources and tries to decrease the dependency on the imported energy resources. Thus, the energy policy contains the use of domestic lignite reserves instead of the imported natural gas in the power generation. The local lignite reserve areas which are suitable for the power generation are mainly used for electricity generation.

In this context, in the 2015-2019 Strategic Plan of the MENR, under the Goal of “Optimum Resource Diversity”, two of the objectives are related to the development of coal (Resources, 2017):

1. Electricity generation from domestic coal shall be increased to 60 billion kWh annually by the end of the plan period.
2. Transformation of existing domestic coal resources into electricity generation investments and exploration of new resources will be done.

All of these data, trends and policies indicate that coal will continue its prominent historical role in the global energy picture as being still the largest source of electricity and the second-largest source of primary energy. In the case of Turkey, the importance of coal is inevitable due to the scarcity of other domestic energy resources –except renewables. Thus, the demand of primary energy in Turkey is mainly met by imported energy.

Although the usage of coal in energy production will preserve its place, there are also inevitable environmental aspects that should be focused on. One of the most important environmental problems are the global warming and climate change.

Greenhouse gases prevent heat from escaping back to the Earth’s atmosphere. The industrialization and the growth in world population has increased the amount of greenhouse gases in the atmosphere. A large increase in the greenhouse gas levels in the atmosphere may result in an effect that too much heat is being captured by these gases and this increases the average temperature of the Earth. Finally, it may result in an inhabitable place.

One of the most important one of these greenhouse gases is CO₂ because the largest concentration of greenhouse gases in the atmosphere belongs to CO₂. The CO₂ concentration in the atmosphere shows an ever increasing trend since the industrial revolution after 1850’s. The latest CO₂ concentration measured in the atmosphere has

reached to 414 ppm as of May 2019 (Yeşil Ekonomi, 2019). This value will keep increasing since fossil fuel usage continues. Earth's ecosystem naturally emits carbon dioxide but humans also cause a significant carbon emission through their basic activities such as burning fossil fuels which is a more effective source than the natural sources. So technologies in carbon capture has rapidly gained interest in the last decades (Huang *et al.*, 2018). While the other emissions from combustion of fossil fuels can be stated as regional, CO₂ emissions are global in scale (Akpan and Akpan, 2012).

The United Nations Framework Convention on Climate Change (UNFCCC) signed in 1992 is the main international agreement on climate action regarding CO₂ emissions. The ultimate objective of it is to stabilize greenhouse gas concentrations at a level that would prevent dangerous anthropogenic interference with the climate system. It states that such a level should be achieved within a time-frame sufficient to allow ecosystems to adapt naturally to climate change, to ensure that food production is not threatened, and to enable economic development to proceed in a sustainable manner. In 1997, Kyoto Protocol is agreed on which introduced legally binding emission reduction targets for developed countries. The main weakness of the Kyoto Protocol is commented as that it only requires developed countries to take action. As the United States has never signed the Kyoto Protocol, some of the countries pulled out from the agreement. It also only applies to around 14% of the world's emissions. However, more than 70 developing and developed countries have made various non-binding commitments to reduce or limit their greenhouse gas emissions.

In 2016, Paris Agreement entered into force after the conditions for ratification by at least 55 countries accounting for at least 55% of global greenhouse gas emissions were met. All EU Countries ratified the Paris Agreement. All of these agreements are a way for countries to work together to limit global temperature increases and climate change.

One of the other hazardous emissions from fossil fuel combustion is sulfur dioxide (SO₂). SO₂ is an acidic and invisible gas that can form harmful compounds with other gases. Although it does not have a large place as CO₂ in the global warming problem, about 99% of SO₂ emission in the atmosphere is generated from anthropogenic sources (Australian Government Department of the Environment and Energy, 2005). An important result of SO₂ emission is forming **acid rain** in the atmosphere. NO_x emission is another problem due to combustion of fossil fuel and it also ends up forming **acid rain** in the atmosphere like SO₂.

Motivation for the study:

The aim of this study is to investigate the efficient and clean combustion of Turkish lignites by using oxy-combustion technology which uses oxygen enriched air for combustion. Thus, combustion efficiency gets higher and by circulation of the flue gas into the combustor the CO₂ concentration in the flue gas becomes rich. Therefore, CO₂ capture from the flue gas becomes feasible.

Since Turkish lignites have high sulfur content, the sulfur dioxide generated during combustion is captured by limestone. However, sulfur dioxide removal mechanism differs during oxy-combustion since carbon dioxide concentration in the oxidant gas mixture is high. In order to study these mechanisms, gas mixtures representing the oxy-combustion conditions are given to TGA to investigate the effects of different carbon dioxide concentrations on sulfur capture. Other parameters investigated during this study are temperature, sulfur dioxide concentration in the gas mixture, limestone particle size and limestone type.

In this study different characteristics of two indigenous Turkish lignite were investigated by Thermal Gravimetric Analysis (TGA). Pyrolysis studies were carried out first under both nitrogen and carbon dioxide atmosphere and combustion characteristics of lignites were also studied. Two types of limestone and one type of

dolomite were used to examine the characteristics of SO₂ capture in oxy-combustion conditions.

This thesis study was part of a TÜBİTAK Project “Oxy-Combustion of Lignite and Torrefied Biomass in a Circulating Fluidized Bed (OXYCOMBUSTION)”. The aim of the project is to reduce the country’s dependence on foreign energy sources and to enable the domestic lignites to be evaluated more effectively and to reduce the CO₂ emissions which causes Greenhouse Effect and Climate Change, by using oxygen-rich air in combustion process and by co-combusting lignite and torrefied biomass. The collaborators on this project were (Barzegar, 2019):

1. ITU, Department of Chemical Engineering,
2. METU, Departments of Mechanical and Environmental Engineering,
3. Marmara Research Center, Institute of Energy,
4. EGE University, Institute of Solar Energy,
5. Karabük University, Faculty of Technology.

The main objectives of this TUBITAK project were: designing an equipment for CO₂ capture, building a torrefied biomass production system, retrofitting a laboratory scale CFB to operate under oxy-fuel combustion conditions, conducting in-situ adsorption of SO₂ in the CFB, and conducting techno-economic and feasibility assessments. These objectives were categorized and each team was assigned to carry out a specific task on the project. The assigned sub-project for METU included the following tasks:

- Characterization of Lignite and Biomass Samples in a TGA under Oxygen-enriched and Oxy-fuel Combustion Conditions,
- Characterization of Limestone and Dolomite Samples in a TGA, and SO₂ Capture Kinetics
- SO₂ Capture in the CFB under Oxygen-enriched and Oxy-fuel Combustion Conditions.

The first and the last objectives were the subjects of a Ph.D. thesis, carried out at Mechanical Engineering Department, METU. The second objective was considered in this thesis as an M.Sc. study at Environmental Engineering Department, METU.

The first part of the thesis deals with pyrolysis of coal in nitrogen and carbon dioxide atmosphere. Usually pyrolysis of coal is done in N_2 atmosphere. However, there may be some situations where CO_2 can be used for pyrolysis of coal. Therefore, we have studied this case of CO_2 pyrolysis to see the difference between N_2 and CO_2 used as an inert gas (Barzegar, 2019).

The second part of the thesis deals with investigation of the effects of different carbon dioxide concentrations on sulfur capture, together with temperature and particle size.

CHAPTER 2

THEORETICAL BACKGROUND

2.1. Carbon Capture

The CO₂ concentration in the flue gas from a coal combustion power plant is approximately 10-15% by vol. whereas these values are lower in flue gas emissions from a natural gas power plant which is 5-10% by vol. In order to capture CO₂ from the flue gas, a high concentration of CO₂ in the flue gas should be obtained (Huang *et al.*, 2018). Then this CO₂ from the flue gas is captured by a suitable technology.

Three main CO₂ capture technologies are listed below:

- Post-combustion capture

In this technology, fuel is burned with normal air and CO₂ is separated from the flue gas after the combustion process. The CO₂ concentration in the flue gas of coal combustion power plant is approximately 10-15% by vol. The main advantage of this process is that it does not require any modifications in the existing combustion plants. The concentration of CO₂ in the flue gas in these systems is considered to be low for CO₂ capture. Separation of CO₂ from other emissions present in the flue gas like SO₂, NO_x, etc., are costly. CO₂ is generally scrubbed from the flue gas with chemical solvents (Nemitallah *et al.*, 2017).

- Pre-combustion capture

In these systems, an air separation unit (ASU) separates oxygen and nitrogen in the air and oxygen is used in the fuel gasification process. The gasification process results in a gas mixture mainly consisting of CO and H₂. This gas mixture is passed through a

water gas shift reactor to produce CO₂ from CO and then the produced high concentration CO₂ can be captured with solvents (Nemitallah *et al.*, 2017).

- Oxy-fuel combustion

Oxy-combustion technology uses pure oxygen or a mixture of oxygen and flue gas instead of air to burn the fuel. In this technology, using high oxygen concentrations results in high combustion efficiencies. Also, by re-introducing the flue gas back to the bed, a control over the gaseous emissions can be achieved (Chen, Yong and Ghoniem, 2012).

Figure 2-1 shows the schematic diagram of the three above mentioned carbon capture technologies. The effectiveness of each carbon capture technology mainly depends on the processes they are used. According to the review of Nemitallah *et al.* (2017) on the CO₂ capture technologies, the pre-combustion capture technology is most compatible with Integrated Gasification Combined Cycles (IGCC). However, this technique is costlier in comparison to the other capturing technologies due to the performed methane reforming and the conversion of CO to CO₂. Post-combustion and oxy-combustion technologies can be used effectively in pulverized coal (PC) combustion systems. All three methods can be applicable for the Natural Gas Combined Systems (NGCC). The authors concludes that overlooking the economic aspects, pre-combustion capture is preferable for IGCC systems, oxy-combustion is preferable in PC systems and post-combustion can be preferred in NGCC systems (Nemitallah *et al.*, 2017).

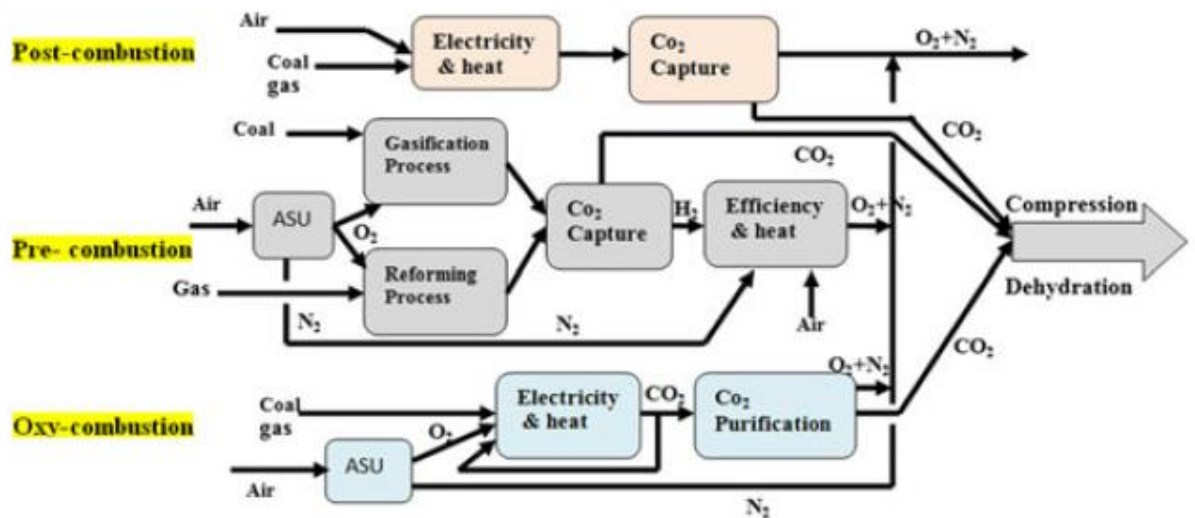


Figure 2-1 A schematic diagram showing the three carbon capture technologies (Nemitallah *et al.*, 2017)

2.2. Oxy-fuel Combustion

A flowchart of oxy-fuel combustion process for power generation is shown in Figure 2-2. In this process, oxygen is separated from air in a device called ASU which separates the oxygen through membranes. A large portion of the flue gas is re-introduced back into the furnace. This recycled flue gas is used to control the flame temperature and make up the volume of the missing nitrogen to ensure there is enough gas to carry the heat through the boiler (Duan *et al.*, 2009). As a result, the flue gas has high CO₂ and water vapor concentrations. The water vapor and ash in the flue gas can be removed in an ash remover and a condenser (Huang *et al.*, 2018).

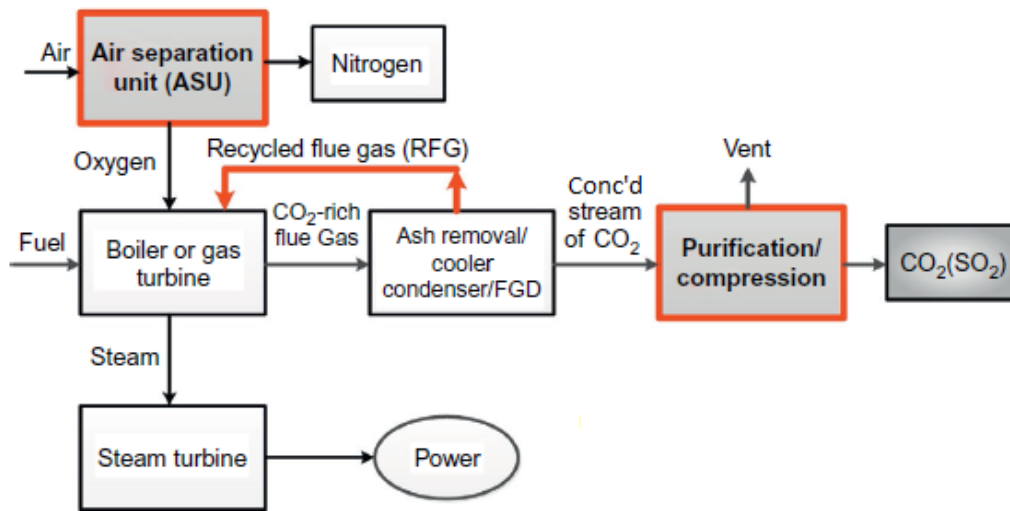


Figure 2-2 Flowchart of oxy-fuel combustion technology for power generation (Huang *et al.*, 2018)

Advantages of oxy-fuel combustion

The advantages of oxy-fuel combustion plants over air-fired plants are summarized below (Huang *et al.*, 2018).

- Reduced boiler heat losses

In an oxy-fuel combustion, typically two-thirds of the flue gas is recirculated back to the boiler. In air-fired combustion systems large amounts of nitrogen is heated in the combustion process and then released in the exhaust gas. But this exhaust gas mixture is cooled down before the release to the atmosphere. The temperature of the exhaust gas is higher than the ambient temperature. This temperature difference results in a heat loss approximately 10% for the air-fired boilers. In oxy-fuel combustion systems, this bulk nitrogen amount does not exist, therefore the volume of the flue gas is lower than the case of air-fired combustion. The heat loss through exhaust gas is reduced significantly.

- Compact boiler design

In oxy-fuel combustion systems, the retrofitting of existing PC boilers can be improved. In oxy-fuel combustion systems, a portion of flue gas is circulated back internally to the boiler to maintain the flame temperature at an acceptable level, so the volume of the recycled flue gas is decreased. This also results in a decrease in the boiler volume, heat dissipation and the electricity required for the flue gas recirculation.

Also, in oxy-fuel combustion systems, it is possible to control the combustion conditions and temperature distribution via adjusting the concentration and the position of the introduced oxygen.

Consequently, in general oxy-fuel combustion systems can have a more flexible design as compared to air-fired systems.

- Low emissions

In oxy-fuel combustion systems, since the nitrogen in the process is eliminated or the concentrations are reduced by increasing the oxygen concentration, NO_x emissions are also reduced significantly. This means that the separation of CO_2 is easier and the volume of equipment for flue gas desulphurization and NO_x removal process decreases. Therefore, the technology required for these processes will be more economical and more convenient when it is compared to the air-combustion systems.

However, oxy-combustion systems have technical and economical disadvantages, too. In order to overcome these disadvantages, more experimental studies should be carried out to determine the coal combustion and heat transfer characteristics under oxy-fuel combustion conditions. Also due to high oxygen concentrations required in the process, the system may have an economic challenge due to the high energy cost in terms of oxygen production (ASU unit) and CO_2 separation (Huang *et al.*, 2018).

Toftgaard et al. (2010) summarized many studies regarding the efficiency of oxy-fuel combustion systems and concluded that this system is the most energy efficient

and cost efficient carbon capture technology among the others. This conclusion is mainly based on the assumptions of greater boiler efficiency that caused by smaller flue gas volume and the reduced need for flue gas cleaning (reduced NO_x and SO₂ emissions). On the other hand the main disadvantage is the need for high oxygen concentrations during combustion which can be provided with an ASU system (Toftegaard *et al.*, 2010).

The oxy-fuel combustion plant configurations generally suggest a flue gas recirculation back to the combustion bed to be able to control the flame temperatures within the acceptable limits of the boiler materials. Circulating fluidized bed combustion (CFBC) systems are studied in recent years for the oxy-combustion system. One of the main advantages of this system is to be able to circulate solids with the recycle of flue gas and to be able to control combustion better. Another advantage of the system is to be able to add calcium based sorbents such as limestone to the boiler together with coal to capture SO₂ in the flue gas and reduce the emissions (Chen *et al.*, 2012).

2.3. Pyrolysis and Oxy-Fuel Combustion

A carbonaceous material such as coal can go through three processes: 1) pyrolysis of carbonaceous matter, 2) combustion, and 3) gasification of remaining char.

Pyrolysis (devolatilization) is the thermal degradation of an organic material in the absence of air to produce synthesis gases, char, etc. During this process volatilize matters are released from the coal and a char is produced. The main product of the coal pyrolysis is a solid carbonaceous matter called char.

The pyrolysis process of coal takes place by the following reaction:



Combustion process occurs as the volatile products and some of the char reacts with oxygen to form carbon dioxide and carbon monoxide, which releases heat.

Gasification is the decomposition of hydrocarbons into a synthesis gas by controlling the amount of oxygen present. So, in a coal gasification process, a limited amount of oxygen or air is introduced into the reactor to allow some of the organic material to be burned to produce carbon monoxide and energy, which drives a second reaction, gasification, that converts further organic material to hydrogen and additional carbon monoxide (Speight, 2011).

Duan et al., 2009, investigated the coal pyrolysis characteristics in CO₂ atmosphere to have a better understanding of the combustion characteristics and the SO₂/NO_x formation mechanisms of oxy-fuel combustion. The heating rates used were 10, 30, 50 and 70 °C/min. In their study, replacing N₂ with CO₂ does not influence the volatile matter release temperature significantly. At about 760 °C, N₂ and CO₂ atmospheres starts to differ from each other and different peaks were observed. In N₂ atmosphere calcite decomposition and in CO₂ atmosphere at 900 °C gasification of char is observed. Their sulfur release characteristics of pyrolysis study showed that in CO₂ atmosphere when temperature exceeds 800 °C the SO₂ release rate increases. They concluded that before temperature reaches 400 °C CO₂ behaves as an inert gas in coal pyrolysis however at 760 °C CO₂ concentration in the ambient prevents calcite from decomposing (Duan *et al.*, 2009).

2.4. Emissions from Oxy-fuel Combustion

The flue gas in oxy-fuel combustion systems mainly consists of water vapor and CO₂. The high CO₂ concentration in the flue gas results in more efficient CO₂ capture as mentioned above. Since the nitrogen in the process is eliminated or the concentrations are reduced by increasing the oxygen concentration, NO_x emissions are also reduced drastically (Nemitallah *et al.*, 2017).

The main difference between air combustion and oxy-fuel combustion is the high levels of CO₂ in the flue gas (more than 90% by vol.). However, due to the increased oxygen concentration and reduced nitrogen concentrations in the gas composition, and

also high CO₂ concentrations in the returned flue gas, the combustion characteristics of the coal and therefore the emissions differ from of the air combustion.

Nitric oxide is formed in the combustion process by three mechanisms: prompt NO_x, thermal NO_x and fuel nitrogen. Prompt NO_x is more important in gaseous hydrocarbon flames but thermal NO_x concentrations are reduced due to the effective removal of nitrogen from the oxidant. Fuel nitrogen mechanisms are also expected to occur and can give rise to a significant NO_x production if the fuel nitrogen content of the fuel is high (Chen *et al.*, 2012).

The formation of sulfur compounds is a significant complication in the combustion of coal in power plants. Most of the sulfur is oxidized into SO₂ but a small percentage can be further oxidized to SO₃. Although the amount of SO₃ is relatively small as compared to SO₂, SO₃ have a great affinity for water, producing sulfuric acid (H₂SO₄) which can result in the corrosion of the surfaces. The increased amount of oxygen in oxy-fuel combustion systems have an effect on the degree of oxidation of SO₂ to SO₃ (Ahn *et al.*, 2011).

Sulfur emissions in an oxy-combustion system is mainly dependent on the sulfur content of the coal. A study with two different coal types is reviewed; coal with 0.24 wt. % sulfur content (Highvale coal) and coal with 0.96 wt. % sulfur content (eastern bituminous). The researchers burned coal in air and in mixtures of O₂ and CO₂ and observed the NO_x and SO₂ emissions. The results showed that the air-fired and oxy-fired combustion systems did not have any significant difference on the SO₂ emissions but the difference lays in the sulfur content of the coals. SO₂ emission rate was weakly affected by the oxygen concentration in the gas mixture which was expected since sulfur conversion during coal combustion is not a kinetically controlled reaction rather controlled by equilibrium. Also for the NO_x emissions they observed higher oxygen concentrations result in higher flame temperature which leads to higher NO_x emission rates. For both coals combustion in air showed the highest NO_x emission rates. This

is explained by higher formation of thermal NO_x due to more molecular nitrogen present in the system (Croiset, Thambimuthu and Palmer, 2006).

Stanger and Wall (2011) also reviewed the **pilot-scale studies** for the sulfur speciation and impacts on oxy-combustion system. They stated that the SO₂ concentrations are higher in oxy-combustion systems as compared to air-fired systems (Stanger and Wall, 2011).

Emission control methods for SO₂ from coal combustion are listed below (IEA Coal Research., 1989):

- Use of low sulfur coal
- Pretreatment of coal to remove the sulfur
- Capture of sulfur during combustion
- Post-combustion treatment of flue gases
- Conversion of coal into liquid or gaseous form

The coal types that have low sulfur content which meets with the SO₂ emission standards are limited to specific geographical regions. Therefore the first method cannot be applied everywhere.

The pretreatment of coal to remove the sulfur content requires physically cleaning the coal with washing and gravity separation techniques but this method can result in an as much as 40% decrease in the yield of coal. Also a high portion of the sulfur can be associated with the organic part of the coal and cannot be removed.

One of the most effective methods for sulfur removal amongst the above mentioned methods is the “flue gas desulfurization (FGD)”. However, generally two or more flue gas scrubber systems are required to ensure the sufficient emission concentrations (more than 95% removal of SO₂). The cost of these FGD systems represents a significant portion of the coal fired power plant and it is expensive. The conversion of

coal into liquid or gaseous form is also economically impractical (IEA Coal Research., 1989).

The last method is to retain sulfur during the combustion process. The SO₂ formed during the combustion can be captured with a SO₂ acceptor such as calcium based sorbents, limestone or dolomite. The main application for injecting calcium based sorbents into the combustion bed together with the coal is used in fluidized bed combustors. Fluidization is the process of static solid particles to transform into dynamic liquid-like state through a suspension in a gas or liquid (Kunii and Levenspiel, 1991). The through mixing within the bed between the sorbent and the combustion gases ensures good contact.

2.5. Sulfur Retention with Limestone

Porosity and pore distribution of limestones designates the amount of calcium that can react with sulfur. Studies have shown that there is an average pore diameter value which is approximately 0.3 μm. Pores smaller than this diameter is blocked by the formation of calcium sulfate (CaSO₄) since it has larger molar volume than calcium carbonate (CaCO₃). Beyond this pore diameter, according to the studies, gaseous permeability increases but the effective surface area decreases (IEA Coal Research., 1989).

Increasing the calcium to sulfur ratio (Ca/S) by increasing the amount of limestone added to the boiler, increases the sulfur retained in the reactor. Ca/S mol ratio of 1 is required to reduce the SO₂ emissions to zero. This theoretical requirement means addition of 3.15 kg of limestone per kg of sulfur in coal. However, in practice the amount of sulfur removed varies depending on the properties of limestone and the conditions of the boiler (IEA Coal Research., 1989).

The SO₂ retention with limestone or dolomite addition can occur via two different sulfation reactions in the boiler (reactor) depending on whether the calcination of the limestone occurs: 1) Direct sulfation and 2) Indirect Sulfation



The calcination reaction of calcium is dependent on the CO_2 concentration in the boiler/reactor and the temperature. This calcination reaction is an endothermic reaction. The thermodynamic equilibrium curve of CaCO_3 calcination is shown in Figure 2-3. (De Diego *et al.*, 2011).

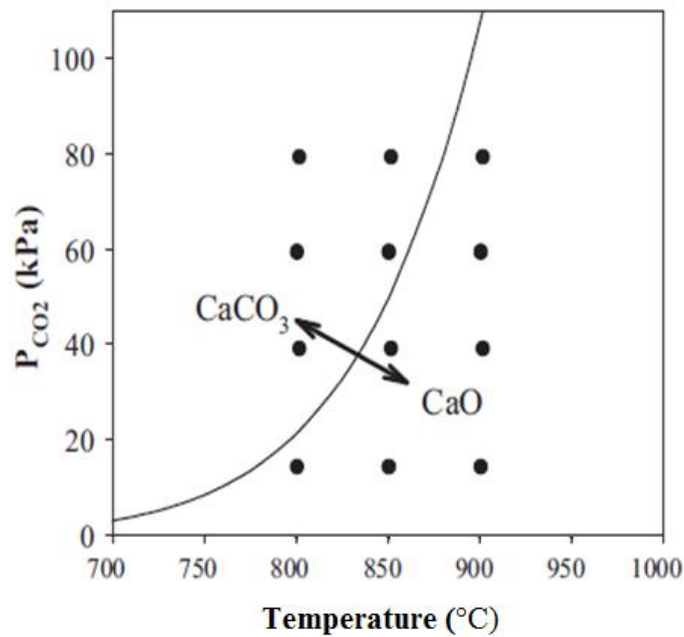


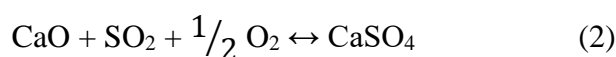
Figure 2-3 Thermodynamic equilibrium curve of CaCO_3 calcination (De Diego *et al.*, 2011)

As can be seen from Figure 2-3, CO_2 presence in the gas phase is an inhibiting factor for calcination reaction. Generally, if the temperature is high and CO_2 concentration is low, the calcination reaction shifts to the right and the products of the reaction is on the right side of the “Thermodynamic Equilibrium Curve” of CaCO_3 calcination. However, if the temperature is low and CO_2 concentration is high, the calcination reaction shifts to the left and the products of the reaction is on the left side of the “Thermodynamic Equilibrium Curve” of CaCO_3 calcination reaction.

At oxy-fuel conditions, with high operation temperatures and even with high CO₂ concentrations (up to 90% CO₂ in the flue gas), calcination reaction is expected to occur and the reaction shifts to CaO side.

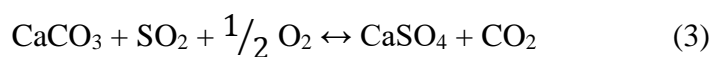
During air-fired combustion processes, high CO₂ concentrations (more than 20%) and temperatures about 800 °C result in uncalcining condition for the limestone (García-Labiano *et al.*, 2011) and CaCO₃ cannot calcine.

If the limestone is calcined, calcined limestone (CaO) reacts with the SO₂ emission from the coal combustion and forms CaSO₄:



This reaction is called **indirect sulfation**.

However, at oxy-fuel combustion conditions CO₂ concentration in the system is significantly higher than that of air-fired combustion. So the calcination reaction may not occur and SO₂ in the gas phase reacts directly with CaCO₃:



This reaction is called **direct sulfation** (García-Labiano *et al.*, 2011).

In this study, the characteristics of direct and indirect sulfation under various CO₂ concentrations and temperature are studied. Two different limestone was tested. The conditions are chosen in such a way that they represent the Oxy-fuel Combustion conditions. The experiments were conducted in a TGA.

Wang et al. (2015), studied the sulfation, calcination and carbonation behavior of 600 – 100 μm limestone samples in bubbling fluidized bed reactor. They studied both the air combustion and oxy-fuel combustion mechanisms. In oxy-fuel conditions, they concluded that the sulfation of limestone is highly dependent on the operating temperatures. At these conditions their studies showed direct sulfation results. On the

other hand, in their air-fueled combustion tests, indirect sulfation reactions occurred. They consolidated their studies with scanning electron microscopy (SEM) and observed a CaSO_4 product layer in air-fueled conditions which inhibited the gas transport into the pores of the compound significantly. But this specific layer was not observed in oxy-fuel conditions. The main limiting factor for reaction in air-fired combustion was the diffusion (Wang, Li and Eddings, 2015).

Jia et al. (2010), compared the SO_2 and NO_x emissions under air-fired and oxy-fuel combustion systems. They experimented on two bituminous coals and petroleum coke in a circulating fluidized bed. A series of tests showed that NO_x concentrations in the flue gas during oxy-fuel combustion was lower than the air-fired combustion at around $850\text{ }^\circ\text{C}$. For the sulfur capture experiments, coal and petroleum coke were burned with the addition of two different limestones. During coal experiments they observed that during oxy-fuel combustion, sulfur capture efficiency decreased slightly. At $850\text{ }^\circ\text{C}$, they observed direct sulfation which they concluded might be the reason for the lower sulfur capture efficiencies. In petroleum coke experiments, the bed temperature was kept at $850\text{ }^\circ\text{C}$ during air-firing and the first part of the oxy-combustion and then the combustion mode was switched to oxy-fuel combustion and the bed temperature was increased up to $950\text{ }^\circ\text{C}$. During oxy-fuel combustion, CO_2 has started rapidly increasing and stabilized at around 85% concentration. NO_x concentrations stayed steady however, SO_2 concentration increased significantly when the bed temperature increased. Sulfur capture was observed to be at 60% range during the oxy-fuel combustion at $850\text{ }^\circ\text{C}$ and when the temperature increased to $950\text{ }^\circ\text{C}$, the sulfur capture efficiency has also increased by 20%. They concluded that difference in sulfur capture efficiencies was due to the change from direct sulfation to indirect sulfation with the change in temperature (Jia, Tan and Anthony, 2010).

CHAPTER 3

MATERIALS AND METHODS

3.1. Experimental Setup

In this study a thermogravimetric analyzer (TGA) was used for the coal combustion and sulfur capture experiments. In order to simulate the flue gas compositions in the experiments, a gas mixing unit consisting of 4 different gases (N_2 , CO_2 , O_2 and 10% SO_2 + 90% by vol. CO_2 gas mixture) was used. The experimental set up consisted of a TGA and a gas mixing unit with 4 mass flow controllers (MFC) in order to carry out the experiments in different atmospheric conditions. The schematic diagram of the experimental set up is shown in Figure 3-1 and the photographs of the TGA device, gas mixing unit and the MFCs are shown in Figure 3-2 and Figure 3-3.

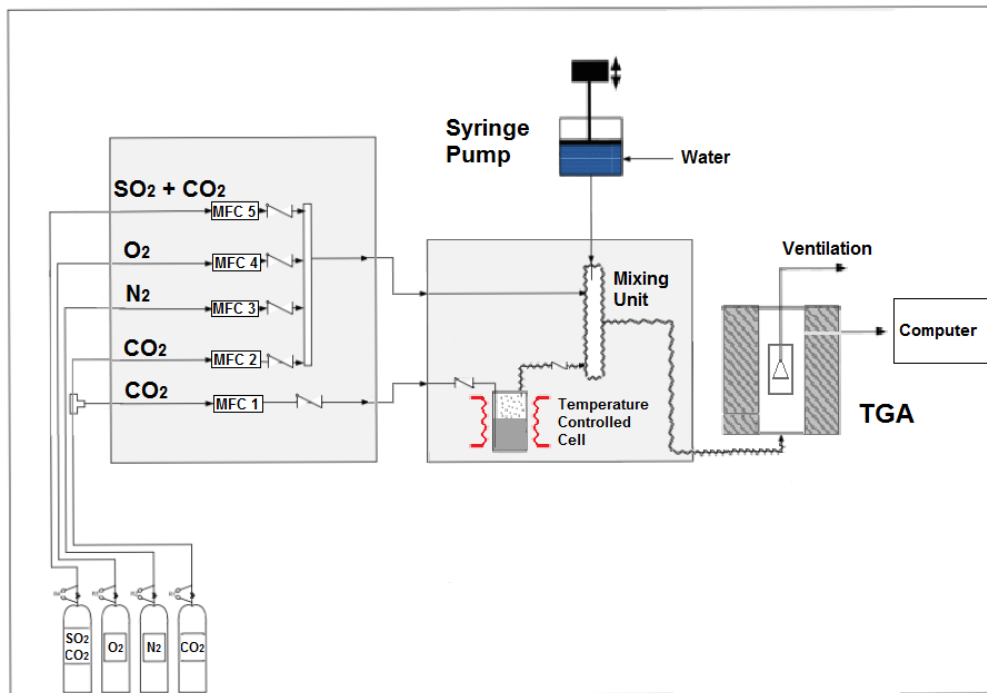


Figure 3-1 Schematic diagram of TGA and gas mixing unit



Figure 3-2 Thermogravimetric Analyzer (TGA)

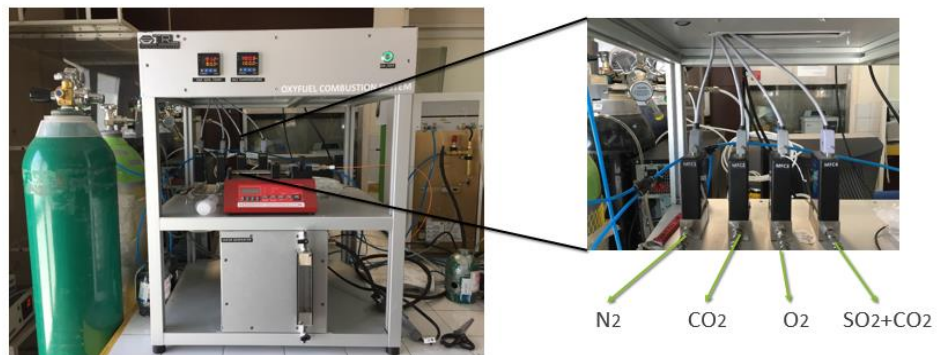


Figure 3-3 Gas mixing unit and the MFCs

The sample pan of TGA had a diameter of 8 mm and depth of 2 mm and made out of platinum. This pan was hanged to the high sensitive scale (± 0.001 mg) with a quartz hanger. The maximum temperature the furnace can reach was 1000°C and the heating

rate of TGA can increase from 0.1°C/min to 150°C/min. The precision of the furnace was $\pm 2^\circ\text{C}$.

In this study, PerkinElmer Pyris 1 model thermogravimetric analyzer was used. Technical properties of this system is shown in Table 3-1.

Table 3-1 Technical properties of PerkinElmer Pyris 1 model TGA

Temperature	Ambient - 1000°C
Heating rate range	0.1°C/min - 150°C/min
Temperature precision	$\pm 2.0^\circ\text{C}$
Balance capacity	1300 mg
Balance sensitivity	0.1 μg
Balance accuracy	Higher than 0.02%
Balance acuity	0.001%
Tare balance	Can be repeated up to $\pm 2 \mu\text{g}$
Sample pan capacity	0 – 60 μl
Cooling	From 1000°C to 40°C in 15 min.
Dimensions	67 x 28 x 60 cm
Weight	40 kg

In circulating fluidized bed combustors, the flue gas concentration depends on the gas composition returned back to the fluidized bed and the oxygen concentration. In oxy-combustion conditions, the sulfur capture efficiency of limestone is also affected by the gas concentration in the bed. In order to simulate the oxy-combustion conditions in the TGA system, nitrogen, carbon dioxide, oxygen and sulfur dioxide mixtures in different concentrations were fed to the system. A different MFC was used for each gas; nitrogen, carbon dioxide, oxygen and sulfur dioxide. Sulfur dioxide gas was used in a gas mixture of 10% SO_2 and 90% CO_2 by volume. The gas flow rates were measured by Teledyne Hastings Model HFC 202 Mass Flow Controllers. This simulation gas was fed to the TGA with a heated line. The temperature of this heated line can be between 40°C to 120°C. Technical details of the gas mixing unit is shown in Table 3-2. 100 mL/min flowrate of gas mixture was used in the experiments (except

the experiments investigating the effect of flow rate). 110mL/min purge nitrogen gas was also sent to the scale part of TGA to prevent any corrosion that may arise from the reaction of the gas mixture.

Table 3-2 Technical properties of gas mixing unit

Power requirements of the system	Voltage: 220 (VAC) Power: 1200 (VA)
Materials contacting the fluid	316 stainless steel or teflon
Heated line temperature range	40°C to 120°C
Heated line path length	2 meters
Steam generator temperature range	25°C to 90°C
Temperature precision	±1.0°C
Syringe pump	8.349 µl/hr – 607.6 µl/hr
Gas input and output	Teflon lines with 6 mm outer diameter
MFC 1 flowrate range	0 – 100 sccm CO ₂
MFC 2 flowrate range	0 – 30 sccm N ₂
MFC 3 flowrate range	0 – 50 sccm O ₂
MFC 4 flowrate range	0 – 20 sccm (10% CO ₂ + 90% CO ₂)
Total flowrate range	70 – 130 sccm
Dimensions	50 x 70 x 55 cm

System is designed to prepare the desired gas mixture and to react with limestone in TGA for SO₂ capture. The desired gas mixture is selected from the gas mixture software. Then, these gases are fed to the system from pressurized tubes and sent to the corresponding MFCs which are adjusted to 2 bar each. The gas mixture reaches the TGA system via heated line. The reaction between the gas mixture and the sample in the sample pan results in an increase or a decrease in the weight of the sample depending on the reactions, and these changes in the weight are recorded by the software of the TGA.

The heating rates used in this study were 5-10-15-20 °C/min according to the technical properties of TGA listed in Table 3-1. However, the heating rates in real combustors

are much higher e.g. about 100 °C/min. Under these heating rates the combustion reaction is much faster and combustion is completed in a shorter time.

3.2. Physical and Chemical Characteristics of Coal Samples

Two different Turkish lignites were selected for this study: Orhaneli lignite from Orhaneli-Bursa region and Soma lignite from Soma-Manisa region. These two lignites were selected due to their different sulfur content. Orhaneli lignite was selected to represent the high sulfur content, and Soma lignite to represent the low sulfur content coal. Sample were provided by TÜBİTAK-MAM Energy Institute. The samples were sieved into different particle sizes: 74-150 µm, 150-425 µm and 425-850 µm. They were dried at 105 °C for about 2 hours and then stored in air tight vials in order to avoid contact with moisture.

The proximate and ultimate analysis, calorific value determination tests (higher heating and lower heating values) of lignites and also X-ray fluorescence (XRF) analysis of lignite ashes were determined by TÜBİTAK-Marmara Research Center (MRC). The analysis of lignites were also conducted by the same Institute. The standard methods and the instrument used for these analysis of lignites and limestones are listed in Table 3-3.

Table 3-3 Methods and instruments used in the characterization of lignites and limestones

	Standard Method	Instrument
Proximate analysis	ASTM D 7582	LECO TGA 701 model thermogravimetric analyzer instrument
Ultimate analysis	ASTM D 5373 (C,H,N) ASTM D 4239 (S) ASTM D 3176 (O)	LECO Truspec CHN-S ultimate analysis instrument

Higher heating value /ASTM D 5868 ISO 1928 Lower heating value	LECO AC600
X-ray fluorescenceASTM D 7582 (XRF) analysis	Philips PW-2404 model X-ray fluorescence spectrometer (XRF)
BET surface analysis TS EN 459-2	ICP, BET surface area determination instrument (Quantachrome, Autosorb-1-C/MSS)
Thermogravimetric analysis (TGA)	Perkin Elmer Pyris-1

Table 3-4 shows the results of proximate and ultimate analysis and the calorific values of the lignites. When compared on dry basis, Orhaneli has a fixed carbon content of approximately 2 times higher than Soma. The ash content of Soma lignite is however 4 times higher than Orhaneli. These results also reflect on the calorific values of the lignites, Orhaneli lignite has a higher calorific value than Soma lignite.

Table 3-4 Proximate and ultimate analysis of the coal samples

	Orhaneli Lignite	Soma Lignite
<i>Proximate Analysis (% by wt., as received)</i>		
Moisture	24.83	6.42
Volatile Matter	37.63	35.67
Fixed Carbon	28.15	19.67
Sulfur	1.75	1.00

Ash	7.64	37.24
-----	------	-------

Proximate Analysis (%by wt., dry basis)

Volatile Matter	50.06	38.12
Fixed Carbon	37.69	21.01
Sulfur	2.33	1.07
Ash	9.92	39.80

Ultimate Analysis (%by wt., dry basis)

Carbon	55.31	28.57
Hydrogen	5.53	2.66
Nitrogen	0.98	0.63
Sulphur	2.33	1.07
Oxygen (by difference)	25.93	27.27
Ash	9.92	39.80

Calorific Values (kcal/kg, dry basis)

HHV	5920	3477
LHV	5718	3348

The ash content of both lignites were analyzed by the X-ray fluorescence spectrometer (XRF) and the results are shown in Table 3-5. Both lignites have about 20-22% by wt. CaO content in ash which can be effective in SO₂ capture.

Table 3-5 XRF analysis of lignite ashes

	Orhaneli Lignite	Soma Lignite
<i>Components (%by wt.)</i>		
Al ₂ O ₃	8.27	22.24
As ₂ O ₃	-	0.02
BaO	0.13	0.12
CaO	22.80	19.37
Cr ₂ O ₃	-	0.02
CuO	-	0.02
Fe ₂ O ₃	13.45	5.85
K ₂ O	0.03	1.95
MgO	3.69	2.08
MnO	0.18	0.07
Na ₂ O	0.29	0.24
NiO	-	0.01
P ₂ O ₅	0.2	0.25
SO ₃	25.87	6.793
SiO ₂	13.61	39.51
SrO	0.14	0.05
TiO ₂	0.26	1.14
V ₂ O ₃	0.01	0.14
ZnO	-	0.02
ZrO ₂	-	0.03

3.3. Physical and Chemical Characteristics of Sorbents - Limestone and Dolomite Samples

In this study two limestones, Çan from Çanakkale and Çumra from Konya and one dolomite, Eskişehir dolomite were used. XRF analysis of these samples are shown in Table 3-6 and Table 3-7. XRF analysis were performed in the Chemical Analysis Laboratory of the Central Analysis Laboratory of METU. Rigaku ZSX Primus II analyzer was used for the XRF analysis of the limestones and dolomite.

Table 3-6 XRF analysis of limestone samples

	Çan Limestone	Çumra Limestone
<i>Compound (%by wt., dry basis)</i>		
CaO	97.78	98.13
SiO ₃	0.99	0.65
Al ₂ O ₃	0.62	0.32
MgO	0.28	0.74
Fe ₂ O ₃	0.22	0.16
ZnO	0.04	-
SO ₃	0.04	0.07
MnO	0.04	-
P ₂ O ₅	0.02	-
K ₂ O	0.01	0.04
Cl	-	0.01
Loss on Ignition (LOI)	41.2	41.4

Calcium oxide (CaO) is the main chemical compound of the limestone which plays the main part in sulfur capture. Both limestone samples have high CaO percentages.

Results of the XRF analysis of Eskişehir dolomite can be seen in Table 3-7. The CaO percentage of dolomite is lower than limestones. MgO is another chemical compound which plays an important role in sulfur capture reactions.

Table 3-7 XRF analysis of dolomite sample

	Eskişehir Dolomite
<i>Compound (%by wt., dry basis)</i>	
CaO	75.77
MgO	24.01
SiO ₂	0.0714
Al ₂ O ₃	0.0503
SrO	0.0426
Fe ₂ O ₃	0.0261
Loss on Ignition (LOI)	45.1

The BET surface area analysis were done in TUBİTAK MAM Laboratory. The results are shown in Table 3-8.

Table 3-8 BET surface area analysis results of limestones and dolomite

	Çan Limestone	Çumra Limestone	Eskişehir Dolomite
Before calcination	0.5 m ² /g	1.13 m ² /g	1.5 m ² /g
After calcination (at 900 °C)	13.45 m ² /g	13.62 m ² /g	20.26 m ² /g

3.4. Experimental Procedures

3.4.1. Experimental Procedure for Pyrolysis and Combustion Tests

For the characterization of Orhaneli and Soma lignites, pyrolysis experiments in nitrogen and carbon dioxide atmospheres, and combustion experiments in dry-air were performed in TGA. In each experiment, 15 mg lignite sample was used and experiments were performed at 100 mL/min gas flowrate. For each experiment, four different heating rates were used: 5 °C/min, 10 °C/min, 15 °C/min and 20 °C/min. Experiments started from 50 °C and ended at 950 °C with a specified heating rate. Table 3-9 shows the list of experiments performed in the scope of lignite pyrolysis and combustion tests.

Table 3-9 List of experiments for Orhaneli and Soma lignites

Test No	Coal Type	Atmosphere	Heating Rate (°C/min)
Pyrolysis			
1	Orhaneli	N ₂	5 °C/min
2	Orhaneli	N ₂	10°C/min
3	Orhaneli	N ₂	15 °C/min
4	Orhaneli	N ₂	20 °C/min
5	Soma	N ₂	5 °C/min
6	Soma	N ₂	10°C/min
7	Soma	N ₂	15 °C/min
8	Soma	N ₂	20 °C/min
9	Orhaneli	CO ₂	5 °C/min
10	Orhaneli	CO ₂	10°C/min
11	Orhaneli	CO ₂	15 °C/min
12	Orhaneli	CO ₂	20 °C/min
13	Soma	CO ₂	5 °C/min
14	Soma	CO ₂	10°C/min
15	Soma	CO ₂	15 °C/min
16	Soma	CO ₂	20 °C/min
Combustion			
17	Orhaneli	Dry air	5 °C/min
18	Orhaneli	Dry air	10°C/min
19	Orhaneli	Dry air	15 °C/min
20	Orhaneli	Dry air	20 °C/min
21	Soma	Dry air	5 °C/min
22	Soma	Dry air	10°C/min
23	Soma	Dry air	15 °C/min
24	Soma	Dry air	20 °C/min

3.4.2. Methods Used for the Calculations of Kinetic Data

Different kinetic methods were studied for obtaining kinetic data of pyrolysis in nitrogen and carbon dioxide atmosphere, and combustion in dry air. There are two methods used to analyze nonisothermal solid-state kinetic data, which are “model fitting” and “model free” (isoconversional) methods. Model-fitting methods determine the kinetic triplet (model, frequency factor and activation energy) whereas isoconversional methods generate the activation energy as a function of reaction progress without modelistic assumption (Khawam, 2007). In this study, four different isoconversional methods were studied. Isoconversional methods calculate the kinetic parameters without trying to fit the data into a model. Instead of a modelistic approach, these methods use several curves obtained from different heating rates for selected conversion values (α). Activation energy (E_a) and pre-exponential factor (A) values are calculated for each conversion points resulting in a isoconversional plot of activation energies vs. conversion points (Khawam, 2007). Thus, these methods are also called as “isoconversional methods”. Selected models in this study are the isoconversional Flynn-Wall-Ozawa (FWO) and Kissinger-Akahira-Sunose (KAS) methods, the differential Friedman method and Miura-Maki integral method.

The pyrolysis process of coal takes place by the following reaction (Urych, 2014).



This reaction can be formulated in a single step equation:

$$\frac{d\alpha}{dt} = k(T) f(\alpha) \quad (1)$$

where α is the degree of conversion which is a measure of reaction progress as a function of time or temperature (Khawam, 2007). $f(\alpha)$ is the conversion function of

the reaction characterizing its mechanism and $k(T)$ is the rate constant at temperature T .

The degree of conversion represents the decomposed amount of the sample at time t and is defined as follows:

$$\alpha = \frac{(m_i - m_t)}{(m_i - m_f)} \quad (2)$$

where m_i is the initial mass of the sample, m_f is the final mass of the sample, and m_t is the sample mass at time t which are obtained by TGA for the selected region.

The rate constant $k(T)$ is found from the Arrhenius equation:

$$k(T) = Ae^{(-E_a/RT)} \quad (3)$$

where A is the pre-exponential factor, E_a is the activation energy, R is the universal gas constant and T is the absolute temperature.

In kinetic studies, one of the most used reaction models is the reaction order model which assumes the coal pyrolysis reaction is generally a first order reaction (Idris *et al.*, 2010). So, the conversion function is described as:

$$f(\alpha) = (1 - \alpha)^n \quad (4)$$

where n is the reaction order and α is the degree of conversion.

The change in the reaction rate can be described as a function of temperature by substitution of Eq. (3) and Eq. (4) into Eq. (1):

$$\frac{d\alpha}{dt} = Ae^{(-E_a/RT)} f(\alpha) \quad (5)$$

In the non-isothermal condition where the sample is heated at a constant heating rate (β), the temperature at time t can be described as:

$$T = T_0 + \beta t \quad (6)$$

where T_0 is the initial temperature, β is the constant heating rate. For non-isothermal data, the following mathematical relationship is used:

$$\frac{d\alpha}{dT} = \frac{d\alpha}{dt} \cdot \frac{dt}{dT} \quad (7)$$

where $d\alpha/dT$ is the non-isothermal reaction rate, $d\alpha/dt$ is the isothermal reaction rate and dT/dt is the heating rate, β .

So, by substituting Eq. (5) into Eq. (6), Eq. (8) is obtained.

$$\frac{d\alpha}{dT} = \frac{A}{\beta} e^{(-E_a/RT)} f(\alpha) \quad (8)$$

This equation is the differential form of the **non-isothermal rate law**.

Flynn-Wall-Ozawa Method

Flynn-Wall-Ozawa (FWO) method is one of the most commonly used non-isothermal isoconversional kinetic method. By integrating the non-isothermal rate law equation, Eq. (10) is obtained:

$$g(\alpha) = \frac{A}{\beta} \int_0^T e^{(-E_a/RT)} dT \quad (9)$$

which is the integral form of the non-isothermal rate law. It is also called temperature integral which has no analytical solution. So, in order to simplify the above integral, a variable is defined as (Brown, 2001):

$$x = \frac{E_a}{RT} \quad (10)$$

So, Eq. (9) becomes:

$$g(\alpha) = \frac{AE_a}{\beta R} \int_x^\infty \frac{e^{-x}}{x^2} dx \quad (11)$$

If $p(x)$ is defined as:

$$p(x) = \int_x^{\infty} \frac{e^{-x}}{x^2} dx \quad (12)$$

Then Eq. (11) becomes:

$$g(\alpha) = \frac{AE_a}{\beta R} p(x) \quad (13)$$

where $p(x)$ is the exponential integral which can be found by substituting Doyle's approximation (Biomedical Research Centre, 1994):

$$p(x) \cong e^{-1.0518x-5.331} \quad (14)$$

Doyle's temperature integral approximation is based on the observation that $\log p(x)$ is linear with respect to x over a short range of x values (Khawam, 2007).

For the FWO method, \ln of each side of Eq. (13), should be taken:

$$\ln g(\alpha) = \ln \frac{AE_a}{\beta R} + \ln p(x) \quad (15)$$

Substituting Doyle's approximation Eq. (14):

$$\ln g(\alpha) = \ln \frac{AE_a}{\beta R} - 5.331 - 1.0518x \quad (16)$$

Then, substituting $\frac{E_a}{RT}$ for x and rearranging, Eq. (17) is obtained:

$$\ln \beta = \ln \frac{AE_a}{g(\alpha)R} - 5.331 - 1.052 \frac{E_a}{RT} \quad (17)$$

FWO method is based on this mathematical equation.

For this method, a plot of $\ln \beta$ vs. $1/T$ is drawn for each conversion value and the kinetic parameters are calculated from the slope and the intercept values.

KAS Method

For the KAS method, coal pyrolysis reaction is assumed as a first order reaction (Idris *et al.*, 2010). So, the conversion function is described as:

$$f(\alpha) = (1 - \alpha)^n \quad (4)$$

The method is based on taking the derivative of Eq. (8) and generating ($d^2 \alpha / dT^2$). According to KAS method, the maximum reaction rate occurs when the second derivative is zero from which the following equation can be obtained:

$$\frac{Ea \beta}{R T^2} = A (n(1 - \alpha)^{n-1}) e^{-\frac{Ea}{RT}} \quad (18)$$

Taking the ln of both sides and rearranging;

$$\ln \frac{\beta}{T^2} = \ln \left(\frac{AR}{Ea g(\alpha)} \right) - \frac{Ea}{RT} \quad (19)$$

In this method the activation energy is obtained by plotting $\ln(\beta/T^2)$ vs. $1/T$ (Khawam, 2007).

Miura-Maki Method

In Miura-Maki method, the approximation is the same as KAS method, by rearranging Eq. (19) and substituting Eq. (20), Eq. (21) is obtained.

$$g(\alpha) = -\ln(1 - \alpha) \quad (20)$$

$$\ln \frac{\beta}{T^2} = \ln \left(\frac{AR}{Ea} \right) + 0.6075 - \frac{Ea}{RT} \quad (21)$$

In this method the activation energy is obtained by plotting $\ln(\beta/T^2)$ vs. $1/T$ (Jiang and Wei, 2018).

Friedman Method

Friedman method is a temperature differential method. This method is a differential method calculated by taking the ln of Eq. (5) and rearranging with substituting Eq. (7),

$$\ln \beta \left(\frac{d\alpha}{dt} \right) = (\ln(A f(\alpha))) - \frac{Ea}{RT} \quad (22)$$

The plot of $\ln \beta \left(\frac{d\alpha}{dT} \right)$ vs. $1/T$, the slope will give the activation energy (Jiang and Wei, 2018)

3.4.3. Experimental Procedure for Limestone Sulfation Tests

As mentioned before, sulfur capture experiments were performed with two different procedures depending on the conditions. Table 3-10 shows the list of sulfation experiments.

In **indirect sulfation**, firstly calcination reaction of the limestone must occur. In order to sustain calcination reaction conditions, a gas mixture without SO_2 is fed into the system. The calcination gas mixture consists of specified percentages of CO_2 , 4% O_2 , and N_2 as the rest. 10 mg limestone sample is heated from 50 °C to the desired temperature with a heating rate of 100 °C/min. At this temperature, the complete calcination of the limestone occurs. When the calcination reaction ends and weight stabilizes, SO_2 is introduced into the gas mixture to start sulfation. (García-Labiano *et al.*, 2011):

$$X_{S,I}(t) = \frac{W(t) - W_0}{W_{CaSO_4} - W_{CaO}}$$

$$W_{CaSO_4} = W_{CaCO_3} \cdot \frac{M_{CaSO_4}}{M_{CaCO_3}} = 1.36 * W_{CaCO_3}$$

$$W_{CaO} = W_{CaCO_3} \cdot \frac{M_{CaO}}{M_{CaCO_3}} = 0.56 \cdot W_{CaCO_3}$$

$$W_{CaCO_3} = W_{sample} \cdot (1 - x_{inert})$$

$W(t)$	mass of the sample at time t
W_0	initial mass of the sample after calcination
W_{CaO}	initial mass of CaO
W_{CaCO_3}	initial mass of CaCO ₃
W_{CaSO_4}	mass of the sample assuming total conversion of CaO to CaSO ₄
x_{inert}	fraction of inerts in the sample
W_{sample}	initial mass of sample

In **direct sulfation**, a gas mixture with specified percentages of CO₂, 4% O₂, 3000 ppm SO₂ and N₂ as the rest, is fed directly into the system. TGA, containing 10 mg of limestone was heated from 50 °C to the desired temperature with a heating rate of 100 °C/min. When TGA reaches the desired temperature, it is kept at that temperature for at least 5 hours. In **direct sulfation** conditions, since calcination does not occur, not the weight loss but weight gain is observed.

The equation for determining the conversion due to direct sulfation is stated below:

$$X_{S,D}(t) = \frac{W(t) - W_0}{W_{CaSO_4} - W_{CaCO_3}}$$

$W(t)$	mass of the sample at time t,
W_0	initial mass of the sample
W_{CaCO_3}	initial mass of CaCO ₃

W_{CaSO_4} mass of the sample assuming a total conversion to $CaSO_4$

The experiments regarding the limestone and dolomite samples are listed in Table 3-10. The range of parameters were: temperature (between 800-900 °C, CO_2 conc. (between 15-80% by vol.), SO_2 conc. (1500-4500 ppm), particle size (75-106 μm).

Table 3-10 List of limestone sulfation experiments

Test No	Limestone Type	Temperature (°C)	CO_2 Conc. (vol.%)	SO_2 Conc. (ppm)	Particle Size (μm)
1	Çan limestone	800 °C	15%	3000 ppm	75 - 106
2	Çan limestone	800 °C	40%	3000 ppm	75 - 106
3	Çan limestone	800 °C	60%	3000 ppm	75 - 106
4	Çan limestone	800 °C	80%	3000 ppm	75 - 106
5	Çan limestone	850 °C	15%	3000 ppm	75 - 106
6	Çan limestone	850 °C	40%	3000 ppm	75 - 106
7	Çan limestone	850 °C	60%	3000 ppm	75 - 106
8	Çan limestone	850 °C	80%	3000 ppm	75 - 106
9	Çan limestone	900 °C	15%	3000 ppm	75 - 106
10	Çan limestone	900 °C	40%	3000 ppm	75 - 106
11	Çan limestone	900 °C	60%	3000 ppm	75 - 106
12	Çan limestone	900 °C	80%	3000 ppm	75 - 106
13	Çan limestone	800 °C	60%	3000 ppm	75 - 106

14	Çan limestone	800 °C	60%	3000 ppm	180-250
15	Çan limestone	800 °C	60%	3000 ppm	300-425
16	Çan limestone	900 °C	60%	3000 ppm	75 - 106
17	Çan limestone	900 °C	60%	3000 ppm	180-250
18	Çan limestone	800 °C	60%	1500 ppm	75 - 106
19	Çan limestone	800 °C	60%	3000 ppm	75 - 106
20	Çan limestone	800 °C	60%	4500 ppm	75 - 106
21	Çan limestone	900 °C	60%	1500 ppm	75 - 106
22	Çan limestone	900 °C	60%	3000 ppm	75 - 106
23	Çan limestone	900 °C	60%	4500 ppm	75 - 106
24	Çumra limestone	800 °C	15%	3000 ppm	75 - 106
25	Çumra limestone	800 °C	40%	3000 ppm	75 - 106
26	Çumra limestone	800 °C	60%	3000 ppm	75 - 106
27	Çumra limestone	850 °C	15%	3000 ppm	75 - 106
28	Çumra limestone	850 °C	40%	3000 ppm	75 - 106
29	Çumra limestone	850 °C	60%	3000 ppm	75 - 106
30	Çumra limestone	900 °C	40%	3000 ppm	75 - 106
31	Çumra limestone	900 °C	60%	3000 ppm	75 - 106

32	Eskişehir dolomite	800 °C	15%	3000 ppm	75 - 106
33	Eskişehir dolomite	800 °C	40%	3000 ppm	75 - 106
34	Eskişehir dolomite	800 °C	60%	3000 ppm	75 - 106
35	Eskişehir dolomite	800 °C	80%	3000 ppm	75 - 106
36	Eskişehir dolomite	850 °C	15%	3000 ppm	75 - 106
37	Eskişehir dolomite	850 °C	40%	3000 ppm	75 - 106
38	Eskişehir dolomite	850 °C	60%	3000 ppm	75 - 106
39	Eskişehir dolomite	850 °C	80%	3000 ppm	75 - 106
40	Eskişehir dolomite	900 °C	15%	3000 ppm	75 - 106
41	Eskişehir dolomite	900 °C	40%	3000 ppm	75 - 106
42	Eskişehir dolomite	900 °C	60%	3000 ppm	75 - 106
43	Eskişehir dolomite	900 °C	60%	1500 ppm	75 - 106
44	Eskişehir dolomite	900 °C	60%	3000 ppm	75 - 106
45	Eskişehir dolomite	900 °C	60%	4500 ppm	75 - 106

CHAPTER 4

RESULTS AND DISCUSSION

4.1. Thermogravimetric Analysis of Lignites

Two lignite types were studied for the pyrolysis and combustion experiments; Orhaneli and Some lignites. The physical and chemical characteristics of these lignites and the properties and the working principle of the TGA instrument are described in Chapter 3 in details.

During the TGA experiments, temperature and weight loss values of samples are continuously recorded with a software in a computer attached to the TGA. In a TGA graph, x-axis shows the temperature or time and y-axis shows the weight loss/gain. In TGA experiments, when the sample undergoes a physical and/or chemical transformation, the sample weight differs as compared to the initial weight (Mohalik, Lester and Lowndes, 2017).

A sample graph lignite combustion with air is shown in Figure 4-1 for general representation of TGA results. In this figure the solid line shows the % weight change in the sample as the temperature increases. It starts with 100% of the weight of the sample and as the combustion reaction proceeds, the sample weight decreases. The derivative thermogravimetry (DTG) graph which is represented with a dashed line, shows the rate of change in weight of the sample with respect to temperature or time, which is the reaction rate.

During the lignite combustion, three main reaction regions in DTG curve are observed. These regions are determined according to the start and end points of the DTG peaks. The first temperature region (the first peak), which occurs below 200 °C corresponds to the release of moisture content and very high volatile matter of the sample. The

second region (the second peak) which is between 200-700 °C shows the release of volatile matter and the burning of heterogeneous organic matter. The main weight loss has occurred in this region for the sample. The third region (the third peak) is the oxidation of char remaining after devolatilization between 700-900 °C (Yorulmaz and Atimtay, 2011). These regions can be seen in Figure 4-1.

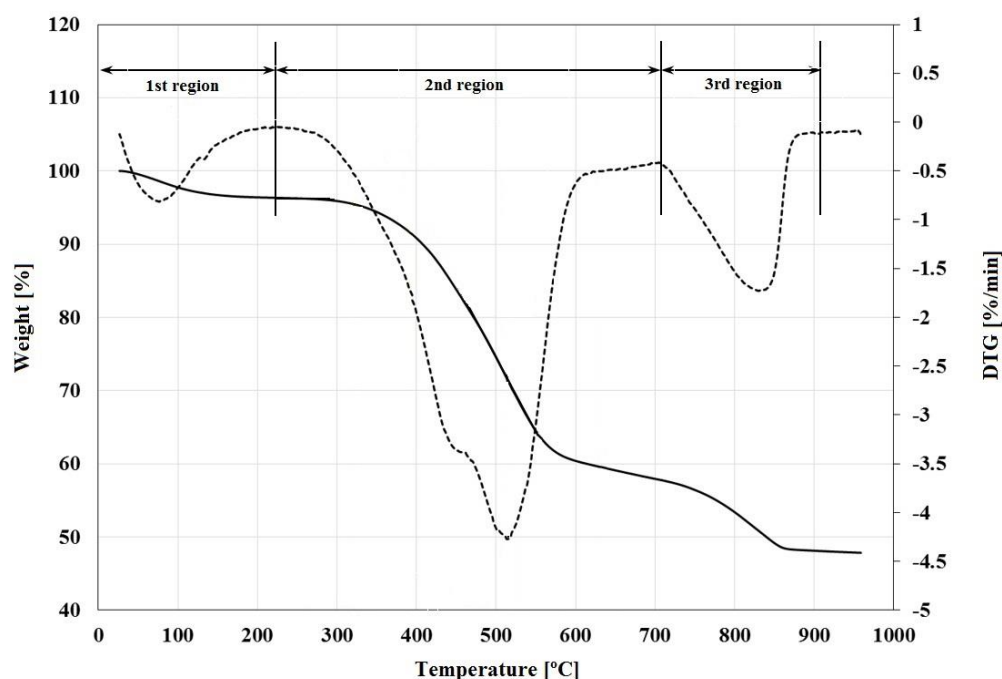


Figure 4-1 TGA and DTG curves showing the characteristic temperatures and weight loss regions for a coal sample

In this section, characterization of lignite samples used in this study are reported. For the lignite pyrolysis and combustion experiments, particle size was selected as 74-150 μm and sample weight was adjusted as 15 mg. In the experiments, temperature of TGA was increased from room temperature up to 980 °C with different heating rates. The flowrate of gas was kept at 100 sccm.

4.1.1. Thermogravimetric Analysis Results of Coal Pyrolysis

The pyrolysis tests of Orhaneli and Soma lignites were conducted in nitrogen and carbon dioxide atmospheres in four heating rates, 5, 10, 15, and 20 °C/min. The

pyrolysis results of Orhaneli lignite in both nitrogen and carbon dioxide atmosphere are shown in Figure 4-2 and for Soma lignite in Figure 4-3.

As can be seen from DTG curve in Figure 4-2, three peaks are observed in Orhaneli lignite in nitrogen and carbon dioxide atmospheres. The first peak represents the moisture release which takes place between room temperature and about 220 °C. The second peak is the volatile matter release that starts at approximately 220 °C and goes up to 650 °C. During this process, Orhaneli lignite loses about 30% of its initial weight. At this stage, the evolving species are mainly CH₄, CO₂, light aliphatic gases, H₂O, tar, CO, and H₂ (Abbasi-Atibeh and Yozgatligil, 2014). Up to 700 °C, the pyrolysis behavior of Orhaneli lignite in nitrogen and carbon dioxide atmospheres was nearly the same. This indicates that at lower temperature zones, carbon dioxide acts as an inert gas in lignite pyrolysis (Yuzbasi and Seluk, 2012). At 650 °C the third region which is the char formation region starts. At this point, the curve of the carbon dioxide atmosphere starts to deviate from the nitrogen atmosphere.

In nitrogen atmosphere, at about 650 °C a third peak starts to form. This peak can be attributed to calcite decomposition reaction which releases CO₂ as a product:



The quantity of CaCO₃ in the sample can easily be calculated from Table 3-5. It is approximately 4% of the sample weight. Decomposition of the CaCO₃ causes the release of CO₂ by about 2% of the total weight.

In carbon dioxide atmosphere, the high partial pressure of CO₂ prevents the calcite decomposition process. Instead, at this atmosphere, char gasification reaction takes place: $C(s) + CO_2 (g) \rightarrow 2CO (g)$ (Toftegaard *et al.*, 2010). The gasification process starts at about 700 °C. During this process, the Orhaneli lignite loses about 40% of its total weight which is close to the amount of its fixed carbon content (Table 3-4).

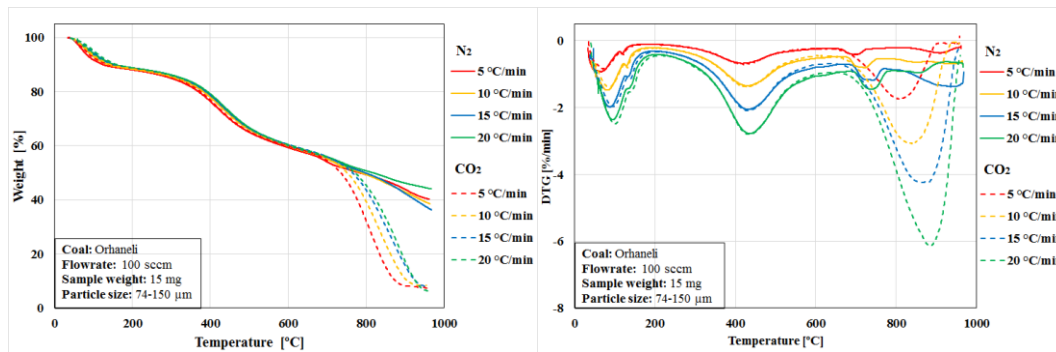


Figure 4-2 TGA and DTG graphs of pyrolysis of Orhaneli lignite in N_2 and CO_2 atmospheres

In Figure 4-3, pyrolysis results of Soma lignite in nitrogen and carbon dioxide atmospheres are shown. In these graphs again three reaction regions are observed. The first peak from room temperature up to 200 °C shows the moisture release and the second peak from 200 °C to 650 °C represents the release of volatile matter. At this point, Soma lignite loses 20% of its initial weight which is lower than that of Orhaneli lignite which confirms the low volatile matter content of Soma lignite as shown in Table 3-4.

Up to 650 °C, nitrogen and carbon dioxide atmospheres show the same pyrolysis results, they do not differ in any significant way. The third region which is the char combustion, starts when the temperature reaches to 650 °C and continues with increasing temperature. At this temperature the result of two atmospheres starts to differ from each other. In nitrogen atmosphere, calcite decomposition is observed which is about 13.3% of the initial weight of Soma lignite. When two lignites are compared, it is apparent that this peak in Soma is more pronounced than Orhaneli which is due to the higher ash content of Soma.

In carbon dioxide atmosphere, char gasification reaction takes place at approximately 700 °C. This reaction takes place between the fixed carbon content of the coal and CO_2 . About 20% of the weight loss in this region can be attributed to this process. However, in carbon dioxide atmosphere at about 870 °C another reaction starts to

occur because of calcite decomposition. This process takes place at high temperatures (Hyatt, Cutler and Wadsworth, 1955). The rest of the weight loss is attributed to this calcination reaction (about 8% weight loss).

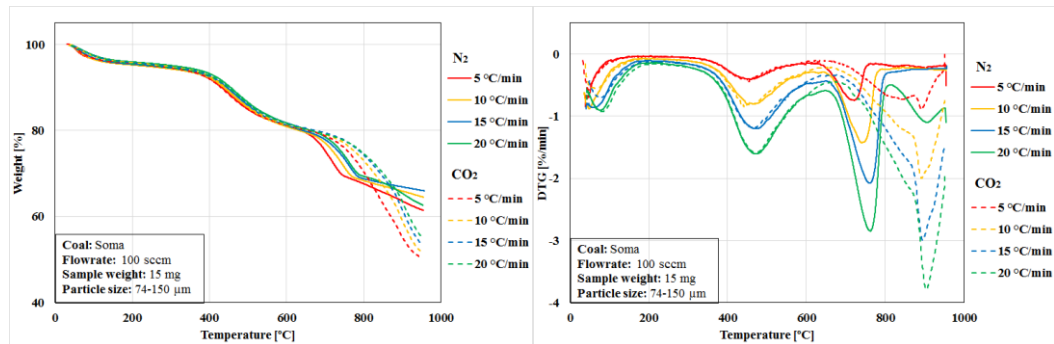


Figure 4-3 TGA and DTG graphs of Soma lignite in N_2 and CO_2 atmospheres

4.1.2. Kinetic Results of Coal Pyrolysis

The kinetic analysis of coal pyrolysis when N_2 is replaced with CO_2 is the first attempt in research toward oxy-fuel combustion technology (Meng *et al.*, 2013). In this section, pyrolysis kinetics of Orhaneli and Soma lignites in nitrogen and carbon dioxide atmospheres were studied at the devolatilization and char formation regions. In order to calculate the kinetic parameters, four different heating rates were studied: 5, 10, 15 and 20°C/min. For the calculation of the pyrolysis kinetics, four different methods were mentioned in Chapter 3 were used: FWO, KAS, Friedman and Miura-Maki integral method. For each method, conversion values ranging from 0.1 to 0.9 were used. All the methods have different y-axis values however, they all have the same x-axis values which is $1/T$ ($1000/T$ for the simplifications). Y-axes are as follows: for FWO method $\ln\beta$, for KAS and Miura-Maki methods $\ln(\beta/T_2)$, and for the Friedman method $\ln \beta (d\alpha/dT)$. The activation energies were calculated from the slopes of the linear regression lines and the pre-exponential factors were calculated

from the intercept points (Barzegar *et al.*, 2018). The calculated kinetic results for each method for Orhaneli and Soma lignites for the devolatilization and the char formation regions and R^2 values are shown in Appendix A.

In order to understand the relationship and the differences between the kinetic methods of pyrolysis, Figure 4-4 and Figure 4-5 were plotted using the activation energies calculated from the slopes of the isoconversional plots. As mentioned earlier, the activation energy values of KAS and Miura-Maki methods are the same due to the same slope, but their pre-exponential factors are different.

In Figure 4-4, both for nitrogen and carbon dioxide atmospheres, the activation energy values change with the conversion factor due to the complicated multi step nature of pyrolysis reaction (Sommariva *et al.*, 2010). In Orhaneli lignite, at devolatilization region, the activation energy starts from 197.0 kJ/mol for nitrogen and 228.7 kJ/mol for carbon dioxide atmospheres. Up to 0.6 conversion, the values are nearly constant at about 170 kJ/mol, and then decreases to about 100 kJ/mol for both nitrogen and carbon dioxide atmospheres.

In the char formation region, the activation energy values are approximately uniform with the increase of conversion factor. On the other hand, the activation energy values decrease from 388.7 kJ/mol to 218.6 kJ/mol as conversion advances at carbon dioxide atmosphere and stays constant from there on. The activation energies in the char formation region are higher than the devolatilization region showing that the reactions in the char formation region are more energy intense.

Another important point that can be deduced from these graphs is that FWO, KAS and Miura-Maki kinetic methods are in good agreement for Orhaneli lignite as shown in Figure 4-4. However, the activation energies calculated with Friedman method differ from the other three methods. The isoconversional integral methods assumes a constant activation energy for the whole integral interval. (Vyazovkin and Sbirrazzuoli, 2006).

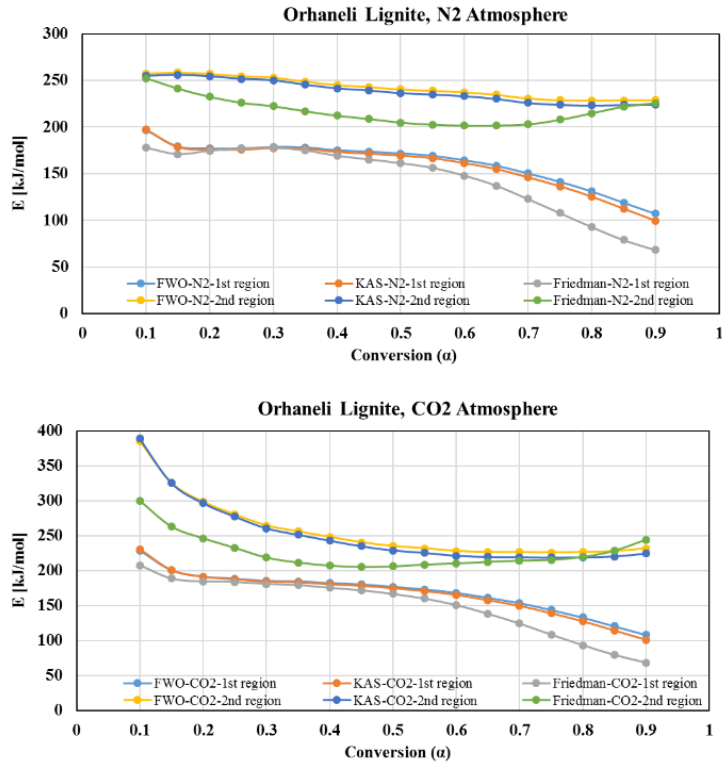


Figure 4-4 Activation energy values as a function of conversion factor in different isoconversional methods for Orhaneli lignite under N₂ and CO₂ atmospheres

In Soma lignite, in devolatilization region, the activation energy value starts from 292.8 kJ/mol for nitrogen and decreases to 250 kJ/mol and stays constant. In carbon dioxide atmosphere, the activation energy value starts from 408.7 kJ/mol and decreases with a steep decline. In char formation region, in nitrogen atmosphere, Soma lignite stays constant for the low conversion factors and starts to decrease at high conversion factors. However, in carbon dioxide atmosphere an increase is observed in the activation energy at 0.5 conversion rate, which can be attributed to CaCO₃ decomposition reaction. This increase results in a peak at 280.6 kJ/mol in nitrogen and at 353.1 kJ/mol for carbon dioxide atmosphere. The activation energies in the char formation region are higher than that of devolatilization region.

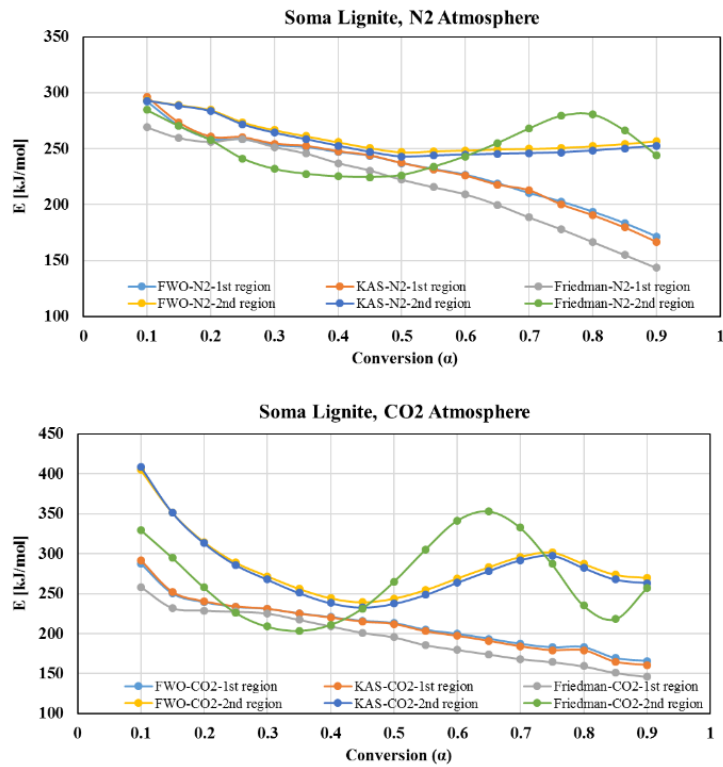


Figure 4-5 Activation energy values as a function of conversion factor in different isoconversional methods for Soma lignite under N₂ and CO₂ atmospheres

The Orhaneli and Soma lignites activation energies are shown in in Table 4-1 and Table 4-2 and pre-exponential factor values are shown in Table 4-3 and Table 4-4 for Orhaneli and Soma lignites for each atmosphere.

Table 4-1 Activation energies for Orhaneli lignite in N₂ and CO₂ atmospheres

Method	E _{a, max} [kJ/mol]		E _{a, avg} [kJ/mol]		E _{a, min} [kJ/mol]	
	N ₂	CO ₂	N ₂	CO ₂	N ₂	CO ₂
Devolatilization Region						
FWO	197.0	228.7	161.7	169.5	107.0	108.5
Miura-Maki	197.5	230.8	158.6	166.8	99.5	101.1
KAS	197.5	230.8	158.6	166.8	99.5	101.1
Friedman	177.9	207.9	144.8	150.8	68.2	68.6
Char Formation Region						
FWO	258.5	385.3	242.0	256.4	228.1	225.8
Miura-Maki	255.9	388.7	238.2	251.5	223.2	218.6
KAS	255.9	388.7	238.2	251.5	223.2	218.6
Friedman	252.3	300.0	217.5	226.2	201.8	205.4

Table 4-2 Activation energies for Soma lignite in N₂ and CO₂ atmospheres

Method	E _{a, max} [kJ/mol]		E _{a, avg} [kJ/mol]		E _{a, min} [kJ/mol]	
	N ₂	CO ₂	N ₂	CO ₂	N ₂	CO ₂
Devolatilization Region						
FWO	292.2	287.7	232.4	211.9	171.5	165.7
Miura-Maki	296.6	291.8	232.5	210.7	166.8	160.8
KAS	296.6	291.8	232.5	210.7	166.8	160.8
Friedman	269.0	258.3	216.9	195.5	143.5	146.1
Char Formation Region						
FWO	293.2	404.8	260.6	285.2	246.8	239.2
Miura-Maki	292.8	408.7	257.7	281.2	243.1	232.9
KAS	292.8	408.7	257.7	281.2	243.1	232.9
Friedman	284.7	353.1	250.6	268.2	224.5	203.7

Table 4-3 Pre-exponential factors for Orhaneli lignite in N₂ and CO₂ atmospheres

Method	A _{max} (min ⁻¹)		A _{min} (min ⁻¹)	
	N ₂	CO ₂	N ₂	CO ₂
Devolatilization Region				
FWO	2.13 10 ¹⁹	1.59 10 ²²	1.23 10 ¹⁰	1.58 10 ¹⁰
Miura-Maki	1.19 10 ¹⁴	1.18 10 ¹⁷	4.75 10 ²	6.32 10 ²
KAS	2.25 10 ¹³	2.28 10 ¹⁶	1.67 10 ⁴	2.67 10 ³
Friedman	1.30 10 ¹⁴	5.65 10 ¹⁶	1.16 10 ⁴	1.22 10 ⁴
Char Formation Region				
FWO	6.14 10 ¹⁵	6.16 10 ²¹	3.40 10 ¹⁴	8.86 10 ¹²
Miura-Maki	1.38 10 ¹⁰	4.49 10 ¹⁶	4.90 10 ⁷	1.06 10 ⁶
KAS	3.42 10 ¹⁰	8.68 10 ¹⁵	1.35 10 ⁹	3.21 10 ⁶
Friedman	6.99 10 ¹²	9.33 10 ¹³	1.57 10 ¹⁰	7.44 10 ⁸

Table 4-4 Pre-exponential factors for Soma lignite in N₂ and CO₂ atmospheres

Method	A _{max} (min ⁻¹)		A _{min} (min ⁻¹)	
	N ₂	CO ₂	N ₂	CO ₂
Devolatilization Region				
FWO	2.63 10 ²⁵	1.22 10 ²⁵	8.65 10 ¹³	3.74 10 ¹³
Miura-Maki	2.62 10 ²⁰	1.19 10 ²⁰	8.35 10 ⁶	3.37 10 ⁶
KAS	5.08 10 ¹⁹	2.29 10 ¹⁹	3.53 10 ⁷	1.42 10 ⁷
Friedman	8.96 10 ¹⁹	1.37 10 ¹⁹	5.26 10 ⁸	8.13 10 ⁸
Char Formation Region				
FWO	7.08 10 ¹⁷	1.50 10 ²²	1.77 10 ¹⁵	1.82 10 ¹³
Miura-Maki	3.35 10 ¹²	1.14 10 ¹⁷	6.43 10 ⁸	6.87 10 ⁶
KAS	6.48 10 ¹¹	2.21 10 ¹⁶	1.01 10 ⁹	7.54 10 ⁶
Friedman	2.33 10 ¹⁴	1.23 10 ¹⁵	1.09 10 ¹¹	2.60 10 ⁸

As can be seen from the Table 4-1 and Table 4-2, activation energies found with all methods except the Friedman method are close to each other for Orhaneli lignite. Average activation energy, $E_{a, \max}$ (kJ/mol), for N_2 atmosphere in the **devolatilization region** is 197.5 and for CO_2 atmosphere is 230.1 kJ/mol for the first three methods. Activation energies for CO_2 atmosphere is higher than N_2 atmosphere. However, the average activation energies, $E_{a, \max}$ (kJ/mol), in the **char formation region** for N_2 atmosphere is 256.7 and for CO_2 atmosphere is 387.5 kJ/mol for the first three methods. Here, the results obtained with Friedman method is far from average values.

For Soma lignite the average activation energy, $E_{a, \max}$ (kJ/mol), for N_2 atmosphere in the **devolatilization region** is 295.1 and for CO_2 atmosphere is 290.4 kJ/mol for the first three methods. Activation energies for CO_2 atmosphere here is close to the value in N_2 atmosphere. However, the average activation energy, $E_{a, \max}$ (kJ/mol), in the **char formation region** for N_2 atmosphere is 292.9 kJ/mol and for CO_2 atmosphere is 407.4 kJ/mol for the first three methods. Here the results obtained with Friedman method is also far from average values with the first three methods.

As for the pre-exponential factors range from $4.75E+02$ to $1.59E+22$ for Orhaneli lignite and $3.37E+06$ to $2.63E+25$ for Soma lignite.

4.1.3. Thermogravimetric Analysis Results of Coal Combustion

The combustion tests of Orhaneli and Soma lignites were conducted in dry air for four different heating rates, 5, 10, 15, and 20 °C/min. 74-150 μm particle size was used and the sample weight was 15 mg for the combustion tests.

The combustion results of Orhaneli and Soma lignite in dry air are shown in Figure 4-6 and Figure 4-7. For both lignite samples, the first region on the DTG curve is associated with the moisture release in the sample. The second peak is the oxidation and removal of volatile matter. The main weight loss is observed in this region. The third peak is associated with the oxidation of char remaining in the sample (Abbasi-Atibeh and Yozgatligil, 2014).

Both for the Orhaneli and Soma lignites, when the heating rates are increased, the duration of the combustion reactions shortens and the maximum weight loss rates are increased with increasing heating rates. The rate of loss becomes higher when the heating rate is increased due to the combustion process proceeding faster at higher heating rates. Increasing the heating rates results in a shift in combustion profiles to higher temperatures.

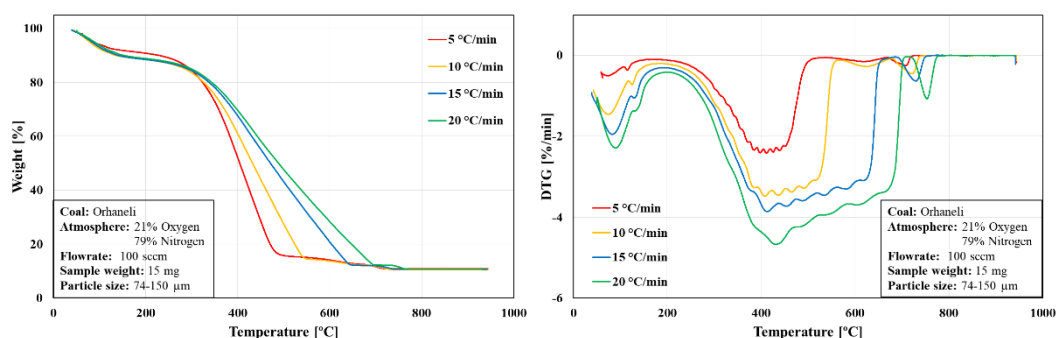


Figure 4-6 TGA and DTG graphs of combustion of Orhaneli lignite in dry air

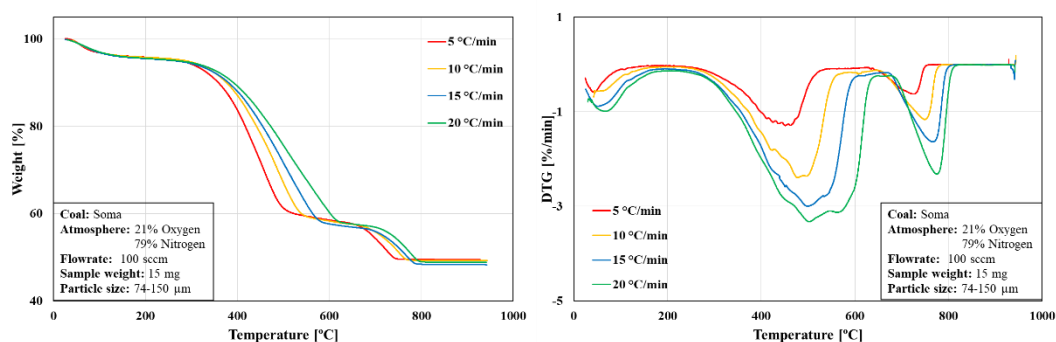


Figure 4-7 TGA and DTG graphs of combustion of Soma lignite in dry air

Figure 4-8 shows the comparison of both lignites at 20 °C/min heating rate. The difference between the second and the third peaks can be seen more distinctly. The second peak of Orhaneli lignite starts at 315 °C and for Soma lignite 400 °C. Due to the higher volatile matter content of Orhaneli lignite, the second peak starts earlier than Soma and with a steeper rate. Orhaneli lignite’s combustion reaction starts at

earlier temperatures compared to Soma lignite thus, the temperature corresponding to the maximum weight loss is lower.

The third peak which represents the oxidation of char which is relatively small in Orhaneli lignite. The ash amount of Orhaneli lignite (9.92% by wt., dry basis) is lower than of Soma lignite (39.8% by wt., dry basis), resulting in a smaller peak. This region starts at approximately 640 °C for Soma lignite and is more distinct.

The total weight loss of Orhaneli lignite is 90% and of Soma is 52%.

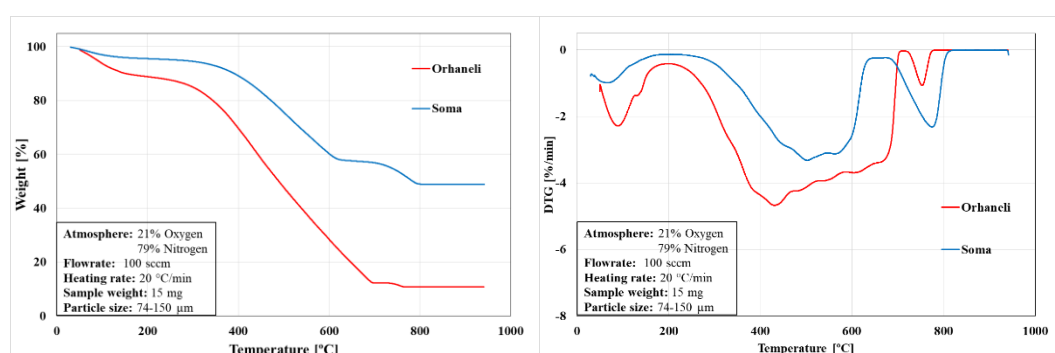


Figure 4-8 Comparison of Orhaneli and Soma lignites at 20 °C/min in dry air

4.2. Thermogravimetric Analysis of Limestones and Dolomite

Calcium based compound such as limestone and dolomite are used in SO₂ capture at high temperatures. The sulfation reaction can take place in two different ways depending on the temperature and CO₂ concentration in the gas phase: **direct sulfation** and **indirect sulfation**.

In this study, these two different reactions of SO₂ capture of limestone was studied. The thermographs of sulfation reactions differ from of the coal combustion reaction. In coal combustion the sample burns and the sample weight decreases. However, in sulfation the molecular weight of the final product is higher than that of the reactants so, instead of a weight loss, the sample shows a weight gain.

1. Direct sulfation: The limestone or dolomite sample reacts with the gas mixture containing SO₂. No weight loss, but an increase in weight of the sample is observed.
2. Indirect sulfation: The limestone or dolomite sample first goes into calcination reaction. The sample weight decreases, and then it reacts with SO₂ with increase in the sample weight.

For the indirect sulfation studies (calcination), different gas mixtures consisting of CO₂, O₂ and as a balance gas N₂ was fed to the system. The flowrate of gas mixture was kept at 100 sccm. The temperature of TGA was increased from room temperature up to the desired temperature with a heating rate of 100 °C/min. The samples were kept at the desired temperatures until the calcination reaction is finalized and the weight of the sample is stabilized. At this point, SO₂ is added to the same gas mixture and sulfation reactions start.

4.2.1. Thermogravimetric Analysis Results of Çan Limestone

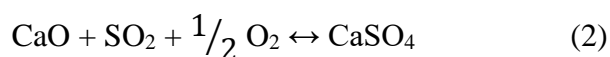
In this section calcination and sulfation results of Çan limestone under different CO₂ concentrations are examined. The effect of temperature, carbon dioxide concentration and particle size were investigated for both reactions.

4.2.1.1. Calcination of Çan Limestone in Indirect Sulfation

The calcination reaction which is the first step of **indirect sulfation** is discussed in this section. In **indirect sulfation**, calcination reaction occurs first:



The weight of the sample decreases by the amount of “loss on ignition” value of the limestone sample. When the sample weight stabilizes, SO₂ is added into the gas mixture for the sulfation reaction to start:



The weight of the sample increases by the amount of CaSO₄ formation.

This study shows that the results do not follow the thermodynamic equilibrium curve of CaCO_3 calcination (Figure 2-3) for every condition, instead the curve shows a slight shift to the right. TGA results of Çan limestone at 800 °C, 850 °C and 900 °C temperatures with different carbon dioxide concentrations are shown in Figure 4-9, Figure 4-10 and Figure 4-11 respectively.

According to the thermodynamic curve on Figure 2-3, at 800 °C, for the three high CO_2 concentrations, namely; 40%, 60% and 80% CO_2 , direct sulfation occurs. For 15% CO_2 concentration, indirect sulfation occurs. However, the experimental results showed that at 800 °C, for all four CO_2 concentrations **direct sulfation** reaction occurs and the calcination reaction does not take place. The sulfation results of Çan limestone at 800 °C for all four CO_2 concentrations are shown in Figure 4-9. At 850 °C according to the thermodynamic curve, at 60% and 80% CO_2 concentrations **direct sulfation** occurs and for 15% and 40% CO_2 concentrations **indirect sulfation** takes place. However, our experiments showed that for 15% CO_2 concentration, as expected, **indirect sulfation** takes place, and for 40%, 60% and 80% CO_2 concentrations, **direct sulfation** reaction occurs. Experimental results of Çan limestone at 850 °C are shown in Figure 4-10. At 900 °C, thermodynamic curve shows **indirect sulfation** at all four CO_2 concentrations. The results at 900 °C are shown in Figure 4-11. However, according to our experimental results obtained from the sulfation of Çan limestone, only at 80% CO_2 concentration **direct sulfation** occurs. For all the other CO_2 concentrations **indirect sulfation** takes place.

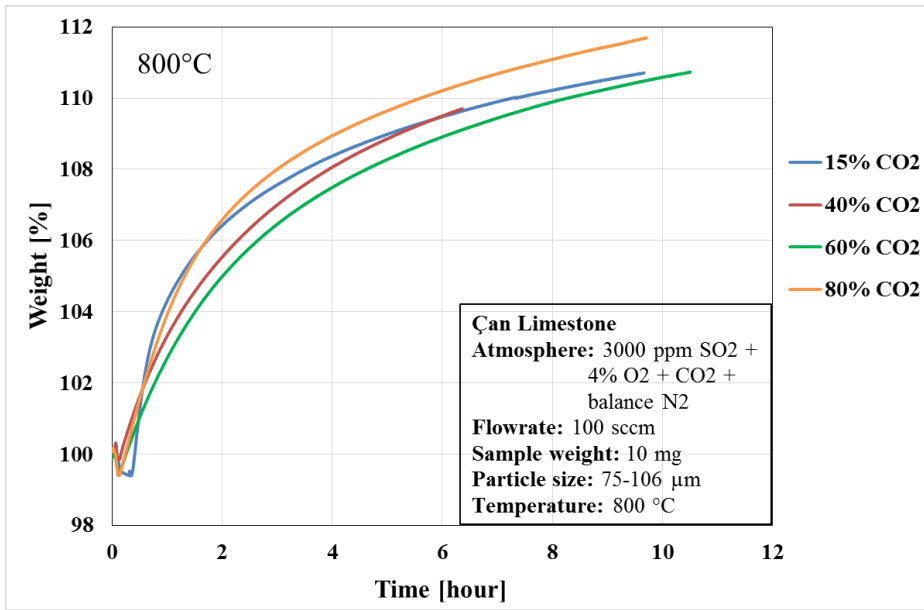


Figure 4-9 TGA results of Çan limestone at 800 °C

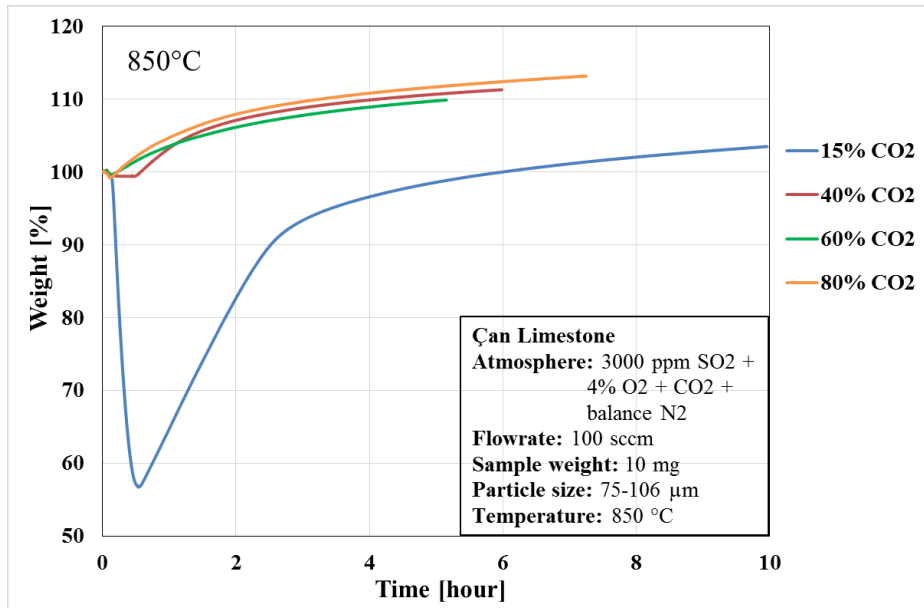


Figure 4-10 TGA results of Çan limestone at 850 °C

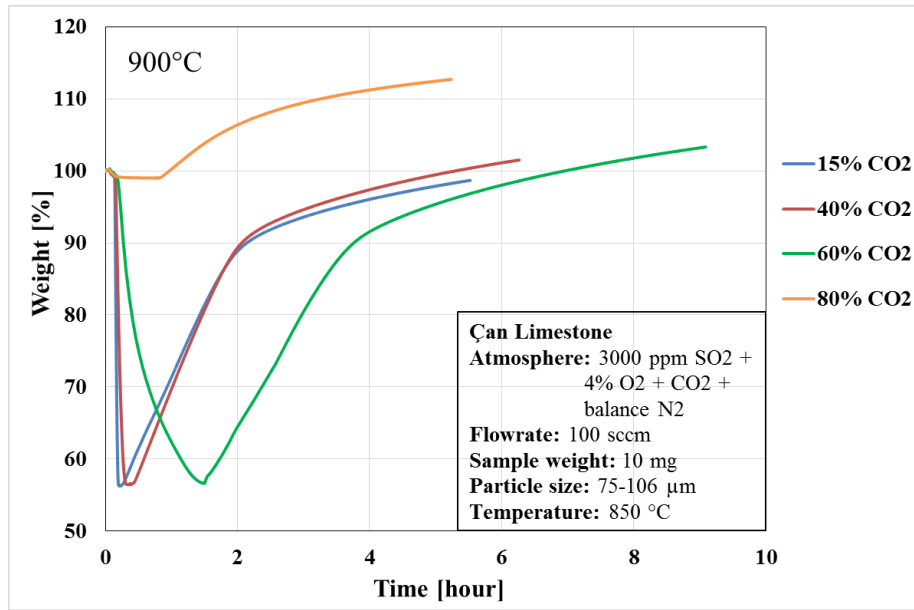


Figure 4-11 TGA results of Çan limestone at 900 °C

The calcium carbonate thermodynamic equilibrium curve shown in Figure 2-3 is calculated from the equation given below (Barin, 1989).

$$P_{\text{CO}_2} \text{ (Pa)} = 4.137 * 10^{12} \exp \left(-\frac{20474}{T(K)} \right) \quad (23)$$

Based on the results of the experiments with limestone in this study, a new thermodynamic equilibrium curve can be drawn with the experimental data which is shown with a dashed line in Figure 4-12. The solid line shows the theoretical calculations. This is a novel result for this study. The experimental curve is also confirmed by the studies of De Diego et al. (2011), they have ended up with the same thermodynamic equilibrium curve by conducting a series of experiments on sulfur retention with limestone at different temperatures and CO₂ concentrations.

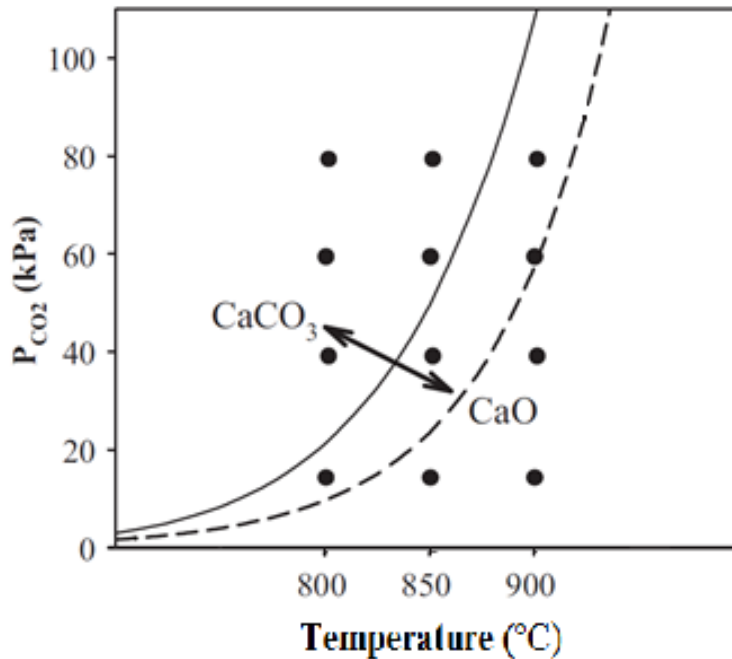


Figure 4-12 CaCO_3 - CaO calcination thermodynamic curve (solid line) and the curve obtained from the experimental results (dashed line) (De Diego et al., 2011)

Effect of Temperature

In **indirect sulfation** reactions, calcination period may vary slightly depending on temperature, carbon dioxide concentration and particle size. Figure 4-13 shows the effect of temperature on the calcination period in 15% CO_2 concentration at 850 °C and 900 °C. At 800 °C temperature cannot be used in these figures since in all four CO_2 concentrations at this temperature direct sulfation was observed.

Due to the fact that calcination reaction is an endothermic reaction (Stanmore and Gilot, 2005), lowering the calcination temperature resulted in a slightly longer calcination time. Calcination at 900 °C showed a steeper decrease in weight as compared to 850 °C and calcination is completed in a shorter time.

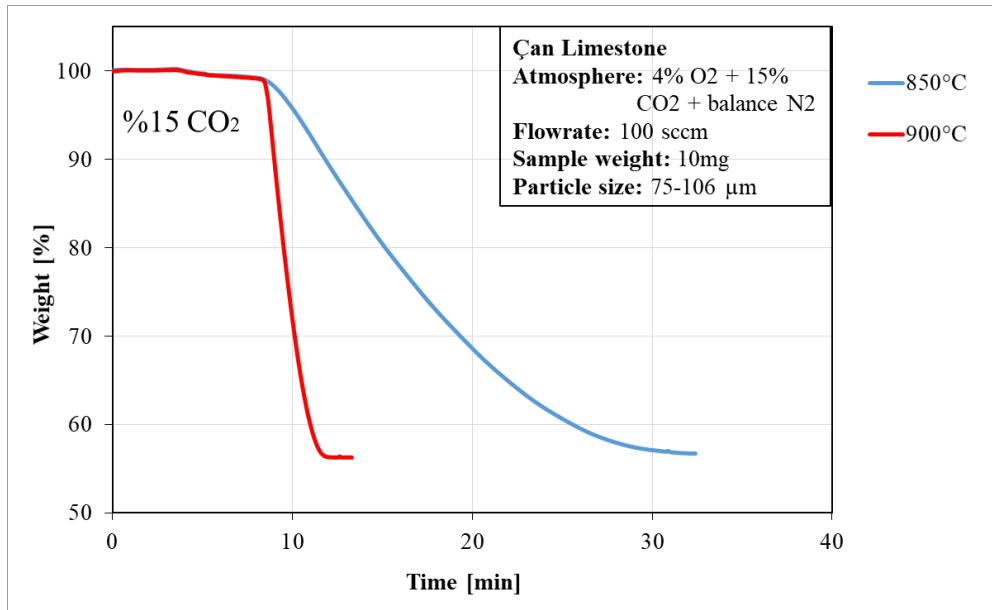


Figure 4-13 Calcination of Çan limestone at 15% CO₂ concentration

Effect of CO₂ Concentration

In Figure 4-14, the effect of carbon dioxide concentration on calcination reaction is observed at 15%, 40% and 60% carbon dioxide concentrations at 900 °C. At higher CO₂ concentrations, the reverse reaction of calcination reaction accelerates, thus the calcination takes longer to complete.

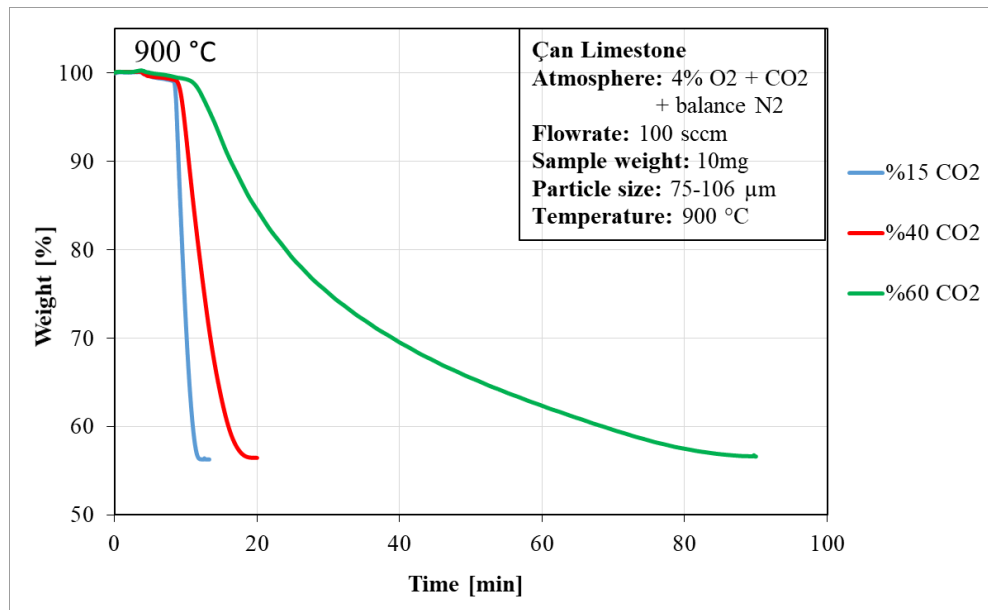


Figure 4-14 Calcination of Çan limestone at 900 °C

Effect of Particle Size

In Figure 4-15, the effect of different particle sizes on calcination time is shown. As can be seen in Figure 4-15, longer time is needed for the calcination to be completed for the larger particles (Ray *et al.*, 1996).

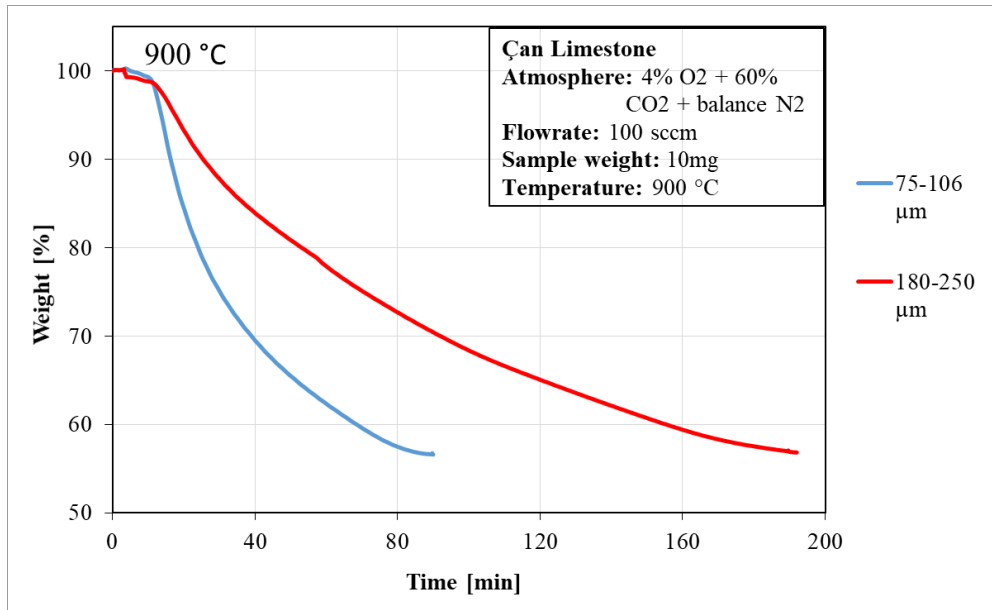


Figure 4-15 Calcination of Çan limestone at different particle sizes

SO₂ first reacts on the surface of the particles and around the pores. At this stage, the reaction is mainly kinetically controlled, thus the reaction occurs rapidly. Afterwards, SO₂ penetrates into the particles by diffusion to perform the sulfation reaction. Since the molar volume of CaSO₄ is greater than the molar volumes of CaO and CaCO₃, the formed CaSO₄ causes clogging of the pores. As a result of this clogging, the reaction slows down and the sulfation of the center of the particle cannot occur (Wang, Li and Eddings, 2015).

In **direct sulfation** reaction, the first step of the sulfation reaction proceeds more slowly compared to the **indirect sulfation** since calcination does not occur and therefore the particle pores are clogged. Thus, **direct sulfation** conversion is much lower as compared to the **indirect sulfation**. For these reasons, it is necessary to carry out the sulfation reaction under conditions that allow **indirect sulfation** to occur and adjust the reaction temperature according to the CO₂ concentration in the atmosphere. Thus, the limestone added to the medium to retain SO₂ will be used more effectively.

4.2.1.2. Sulfation of Çan Limestone

In sulfation reactions, sulfur dioxide starts to react with CaO formed due to the calcination at the surface of the particles and around the pores. This part of the reaction advances rapidly since it is controlled with chemical reaction and/or diffusion mechanisms (Wang, Li and Eddings, 2015). After this part, sulfur dioxide penetrates the particles with diffusion and the sulfation reaction continues. Due to the fact that the molar volume of CaSO₄ is higher than that of CaCO₃ and CaO, the new formed CaSO₄ clogs the pores at the surface of the particles as the reaction advances. Because of the clogged pores, reaction starts to slow down and the sulfation of the particles stop and the core of the particles stays as CaCO₃.

Conversion of Çan Limestone at Different Temperatures

The effect of different temperatures on sulfation of Çan limestone for different CO₂ concentrations are given in this section. TGA results obtained are converted into sulfur conversion values. The sulfur conversion of Çan limestone at 15%, 40%, 60% and 80% CO₂ concentration are shown in Figure 4-16, Figure 4-17, Figure 4-18 and Figure 4-19, respectively.

As mentioned before, sulfation of limestone can occur either in **direct sulfation** or **indirect sulfation** depending on temperature and CO₂ concentration in the gas phase. The sulfur conversion value at three temperatures, 800 °C, 850 °C and 900 °C, for 15% CO₂ concentration are shown in Figure 4-16. For 15% CO₂ concentration, at 800 °C **direct sulfation** reaction takes place and at 850 °C and 900 °C temperatures, **indirect sulfation** reactions occur.

In indirect sulfation at 850 and 900 °C, for the first two hours the sulfation conversion occurs rapidly. However, after the first two hours, indirect sulfation reactions occurs with same slope as direct sulfation (800 °C). When the temperatures resulting in the

indirect sulfation are compared, it can be seen that the increase in the temperature appears not to have any effect on the sulfur conversion in indirect sulfation conditions. At the end of eight-hour period, the sulfur conversion of **direct sulfation** at 800 °C was 30%. However, for the **indirect sulfation** sulfur conversion was 58%. This result showed that for 15% CO₂, sulfur conversion *doubles* at higher temperatures due to calcination and **indirect sulfation** of limestone.

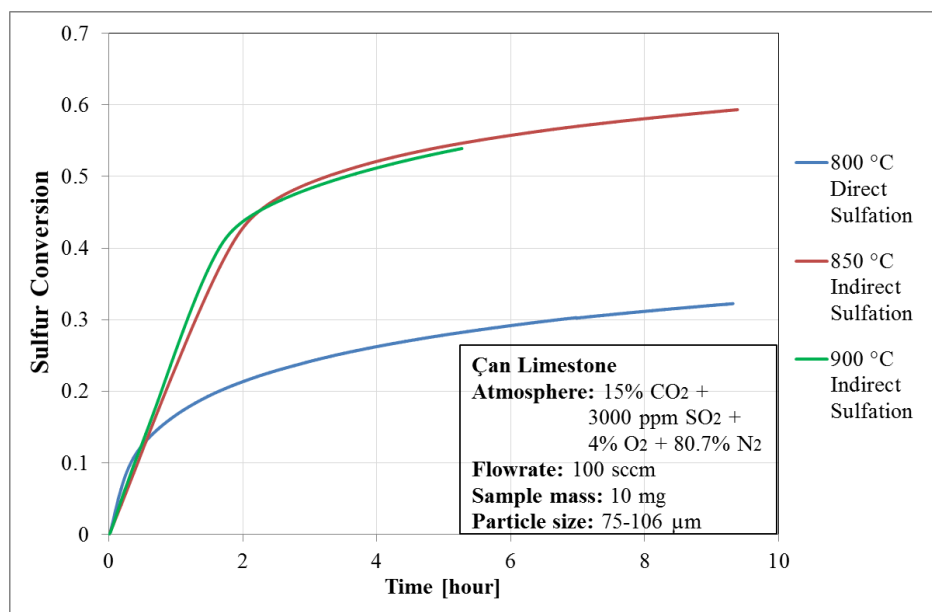


Figure 4-16 Sulfur conversion of Çan limestone at 15% CO₂ concentration

At Figure 4-17 and Figure 4-18, sulfur conversions at 40% and 60% CO₂ concentrations at different temperatures are shown. For both concentrations, at 800 °C and 850 °C, **direct sulfation** takes place and at 900 °C **indirect sulfation** occurs. In the direct sulfation, when the temperature is increased from 800 °C to 850 °C, an increase in the sulfur conversion is observed. At the end of a six-hour period, sulfur conversion was 28% at 800 °C, while it was 35% at 850 °C. **However, indirect**

sulfation conversion results were still higher than direct sulfation conversion results and reached to 58% for 900 °C.

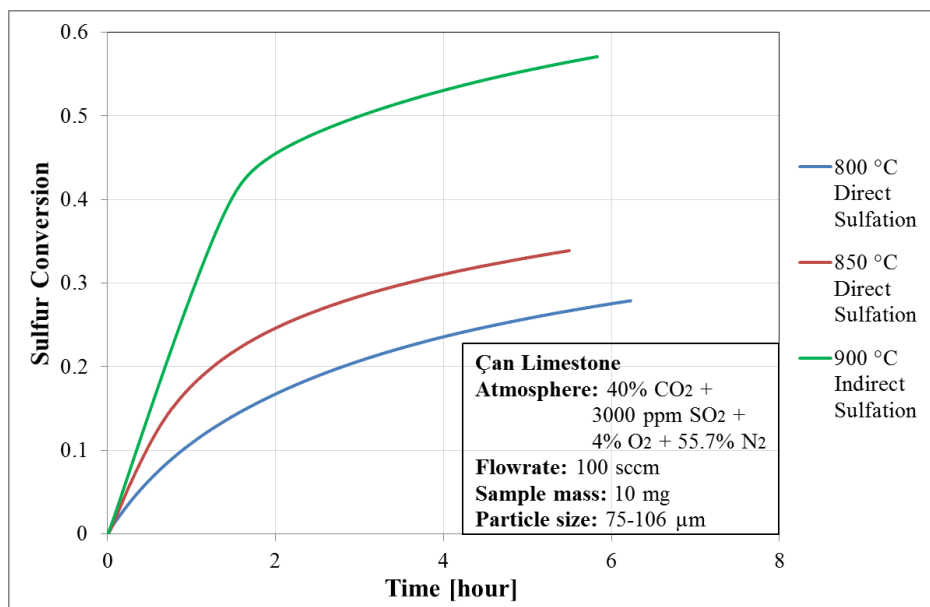


Figure 4-17 Sulfur conversion of Çan limestone at 40% CO₂ concentration

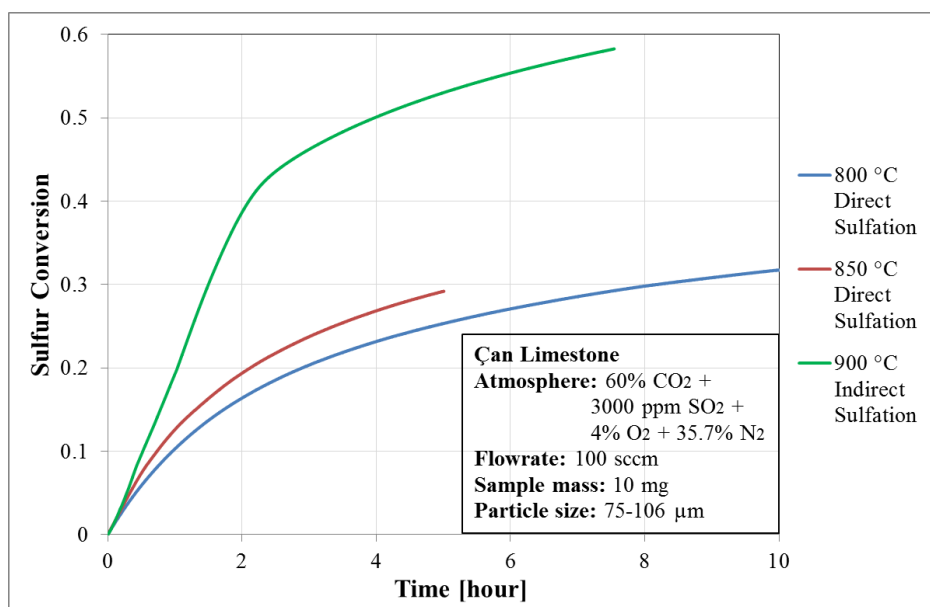


Figure 4-18 Sulfur conversion of Çan limestone at 60% CO₂ concentration

Sulfur conversions for 80% CO₂ concentration at different temperatures are shown in Figure 4-19. For 80% CO₂ concentration, **direct sulfation** is observed at all three temperatures. The increase in sulfur conversion with the increasing temperature can be seen properly in this figure. For a time period of six hours, sulfur conversion at 800 °C, 850 °C and 900 °C was about 32%, 38% and 43%, respectively.

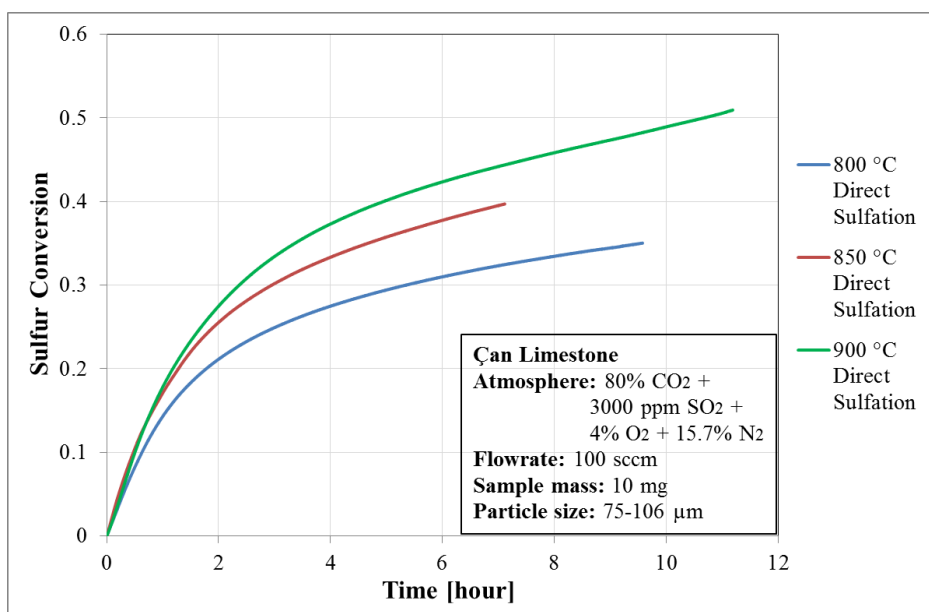


Figure 4-19 Sulfur conversion of Çan limestone at 80% CO₂ concentration

Conversion Results of Çan Limestone for Different CO₂ Concentrations

The effect of CO₂ concentrations on sulfation results at different temperatures are given in this section. The sulfur conversion of Çan limestone at 800 °C and 900 °C are shown in Figure 4-20 and Figure 4-21 and the comparison of these two temperatures are shown in Figure 4-22. At 800 °C temperature, at all four CO₂ concentrations, **direct sulfation** occurs. When the results are compared, it can be seen that there is not much difference between the different concentrations. At 900 °C direct

sulfation takes place at 80% CO₂ concentration while at other three CO₂ concentrations, **indirect sulfation** takes place. In **indirect sulfation**, not much difference can be observed between the different CO₂ concentrations.

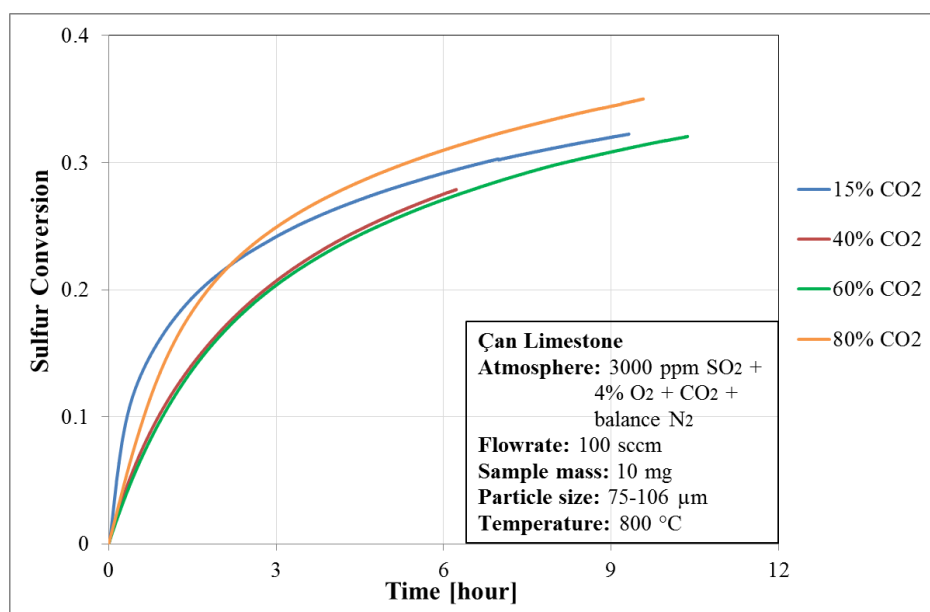


Figure 4-20 Sulfur conversion of Çan limestone at 800 °C

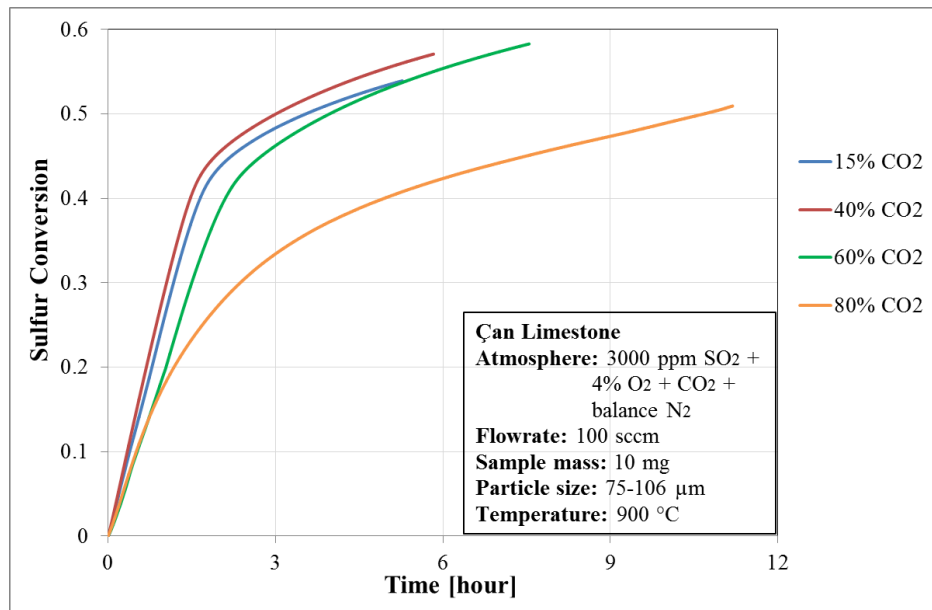


Figure 4-21 Sulfur conversion of Çan limestone at 900 °C

When Figure 4-22 is examined, it can be seen that the CO₂ concentration does determine the sulfation reaction to be either **direct** or **indirect sulfation** at the same temperature so therefore affecting the conversion percentage in that way since **indirect sulfation** has higher conversion results than **direct sulfation**. This derivation has been confirmed in literature studies by De Diego et al. (2011) and Wang et al. (2015). In an eight-hour reaction period, **conversion stays at 30-35% for direct sulfation and the conversion increases to 45-60% for indirect sulfation.**

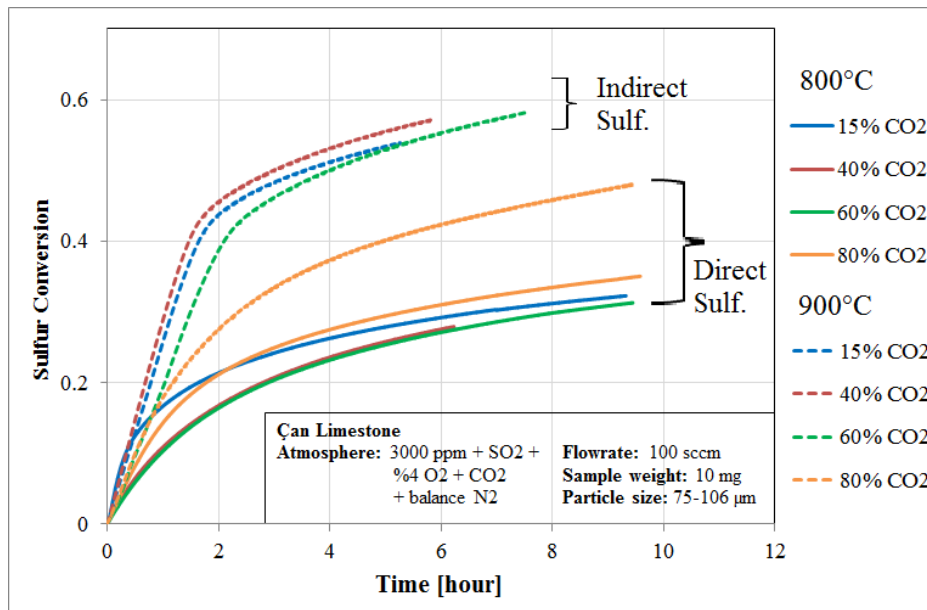


Figure 4-22 Comparison of sulfur conversion for Çan limestone at 800 °C and 900°C at different CO₂ concentrations

In **indirect sulfation**, SO₂ rapidly reacts at the surface of the particle with CaO forming CaSO₄. The formation of CaSO₄ clogs the pores after some time and inhibits the sulfation of the center of the particle, thus the sulfation reaction slows down but sulfur conversion rate is high. However, in **direct sulfation**, since the pores are clogged due to calcination not occurring, a more uniform and steady sulfation occurs however, with a lower sulfur conversion rate (Wang, Li and Eddings, 2015).

Conversion Results of Çan Limestone for Different Particle Sizes

The effect of particle size on the sulfation conversion was studied at both direct and indirect sulfation conditions. For comparison, CO₂ concentration is selected as 60%, therefore at 800 °C **direct sulfation** and at 900 °C **indirect sulfation** occurs. Figure 4-23 and Figure 4-24 shows the sulfation conversions of 75-106 µm, 180-250 µm and 300-425 µm particle sizes at two different temperatures. In order to sustain a certain level of sample thickness in the sample pan, different sample weights were used; 10, 15 and 20 mg respectively.

Particle size is an important factor in sulfation reactions. Small particle sizes have a larger surface area for reactions to occur. The sulfation reaction starts from the surface of the particle. CaSO_4 is a large molecule which clogs the pores as sulfation reaction progresses. This results in a decrease in the reaction surface area. So, it is expected to have higher sulfation conversions in smaller particle sizes than larger particles due to their high surface areas.

In **direct sulfation**, calcination reaction does not take place, so the pores of the particle are clogged at the beginning of the sulfation reaction. This results in sulfation reaction mainly to occur on the surface of the particles.

In larger particle sizes, total surface areas are lower, thus the sulfation conversions are lower than the smaller particle sizes. In Figure 4-23, the difference between the particle sizes can be seen. In an eight hour time period, for both 180-250 μm and 300-425 μm particles, sulfation conversion stays at 5% and but for 75-106 μm particles, at the same time period, sulfation conversion increases up to 30%.

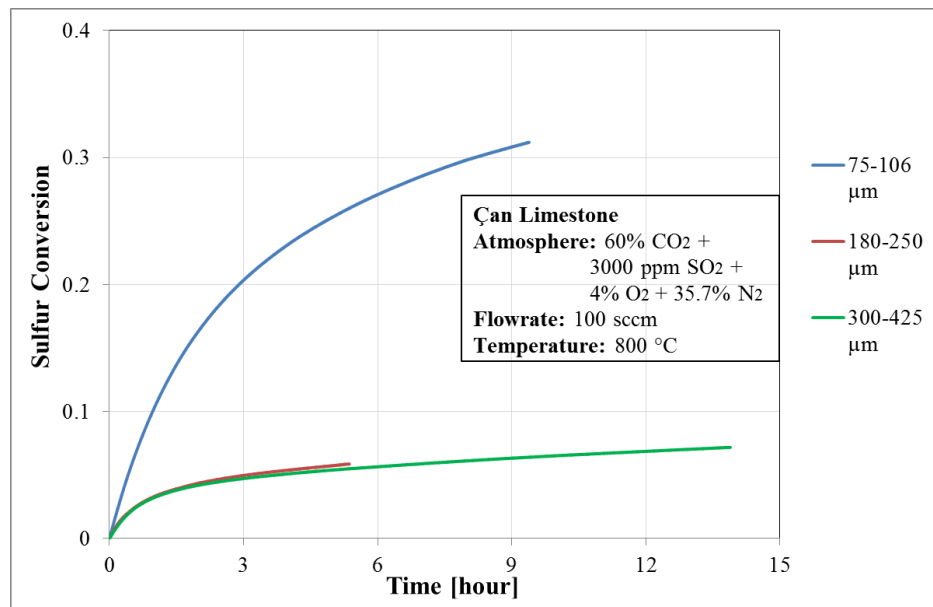


Figure 4-23 Sulfur conversion of Çan limestone for different particle sizes at 800 °C and 60% CO₂ concentration

Figure 4-24 shows the **indirect sulfation** of two particle sizes, 75-106 μm and 180-250 μm , at 900 °C. The sulfur conversion rates for the two particles are nearly the same for the first 1.5 hours. With smaller particle size, higher sulfation conversion rate is achieved due to greater surface area for SO_2 to react. In an eight hour time period, with 75-106 μm particle size 60% conversion is achieved whereas for 180-250 μm particle size only 30% conversion is achieved.

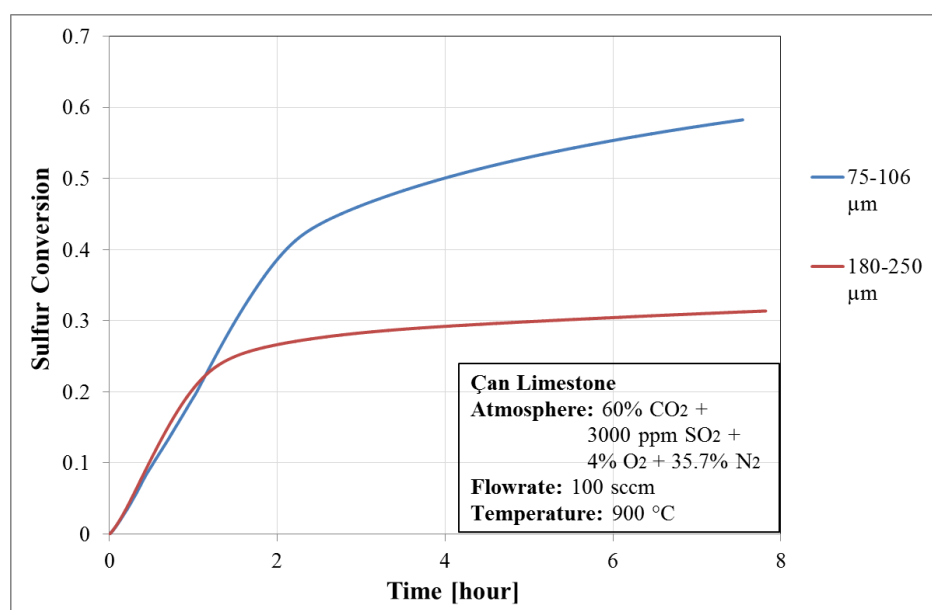


Figure 4-24 Sulfur conversion of Çan limestone for different particle sizes at 900 °C and 60% CO_2 concentration

Conversion Results of Çan Limestone with Different SO_2 Concentrations

Sulfur conversion of Çan limestone with different SO_2 concentrations are shown in this section. Again, in order to both investigate direct and indirect sulfation, 800 °C and 900 °C temperatures were selected with a 60% CO_2 concentration (Figure 4-25). As expected with increased SO_2 concentration, sulfation conversion rates increased. In **direct sulfation**, this increase is not so much. After a six-hour time period, sulfation conversion values vary between 25-30%. However, the effect of increased SO_2 concentration can be seen more clearly in **indirect sulfation**, sulfur conversion rates were 50% for the 1500 ppm and 63% for the 4500 ppm after a six-hour time period.

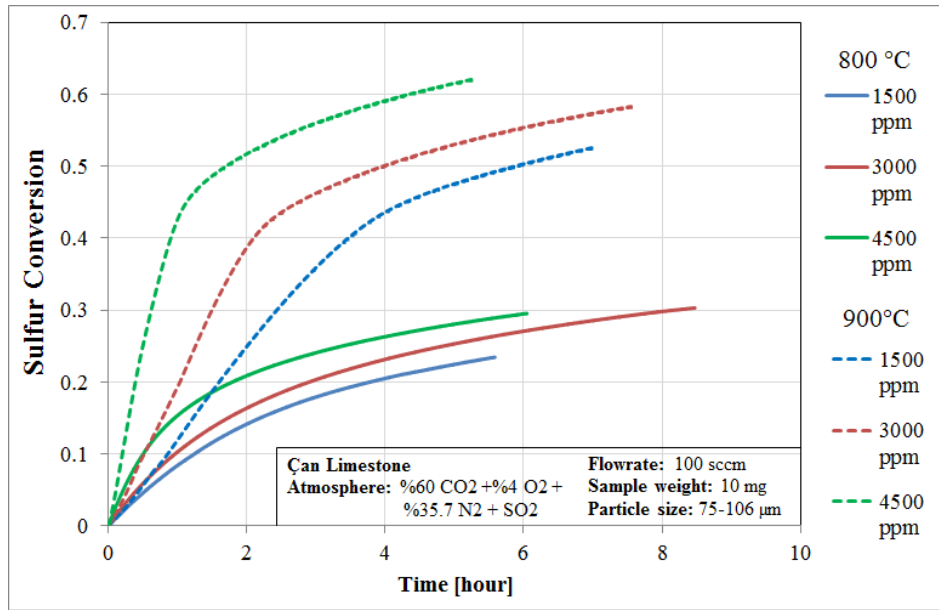


Figure 4-25 Comparison of sulfur conversion for Çan limestone at 800 °C and 900°C at different SO₂ concentrations

4.2.2. Thermogravimetric Analysis Results of Çumra Limestone

In this section calcination and sulfation results of Çumra limestone under different CO₂ concentrations and temperatures are examined. The effect of temperature and carbon dioxide concentration were investigated for both reactions.

Studies on Çumra limestone focused on the experimental thermodynamic curve obtained by De Diego et al. (2011) and the results of Çan limestone. The Çumra limestone sulfation experiments are carried out according to Table 3-10, only operation conditions close to or in-between thermodynamic equilibrium curves (theoretical curve and experimental) are studied. The results obtained from Çumra limestone showed compatibility with the Çan limestone studies, the obtained results followed the experimental thermodynamic equilibrium curve shown in Figure 4-12.

4.2.2.1. Calcination of Çumra Limestone in Indirect Sulfation

The TGA results of Çumra limestone at 800 °C, 850 °C and 900 °C temperatures with different carbon dioxide concentrations are shown in Figure 4-26, Figure 4-27 and Figure 4-28, respectively. At 800°C, for 15%, 40% and 60% CO₂ concentrations were studied. According to the results shown in Figure 4-26, at this temperature, for all three CO₂ concentrations, **direct sulfation** reaction occurs. Figure 4-27 shows the results at 850 °C, for 15% CO₂ concentration **indirect sulfation** and for 60 % CO₂ concentration **direct sulfation** occurs. And in Figure 4-28 at 900 °C, for 40% and 60% CO₂ concentrations, **indirect sulfation** is observed.

For Çan limestone, in **direct sulfation** experiments, weight loss was not observed, the limestone directly reacts with SO₂ and the weight of the sample increases. However, in Çumra limestone experiments, a weight loss of 5% is observed between 300-500 °C temperatures. After this weight loss, the weight stabilizes, and then when the temperature reaches the desired temperature, SO₂ is introduced into the gas mix and sulfation reaction starts.

In **indirect sulfation**, the 5% weight loss is again observed at temperatures between 300-500 °C. After this weight loss the calcination of calcium carbonate occurs and then the weight stabilizes. The sample weight decreases by the amount of loss on ignition value. Then SO₂ is introduced into the gas mix and sulfation reaction starts.

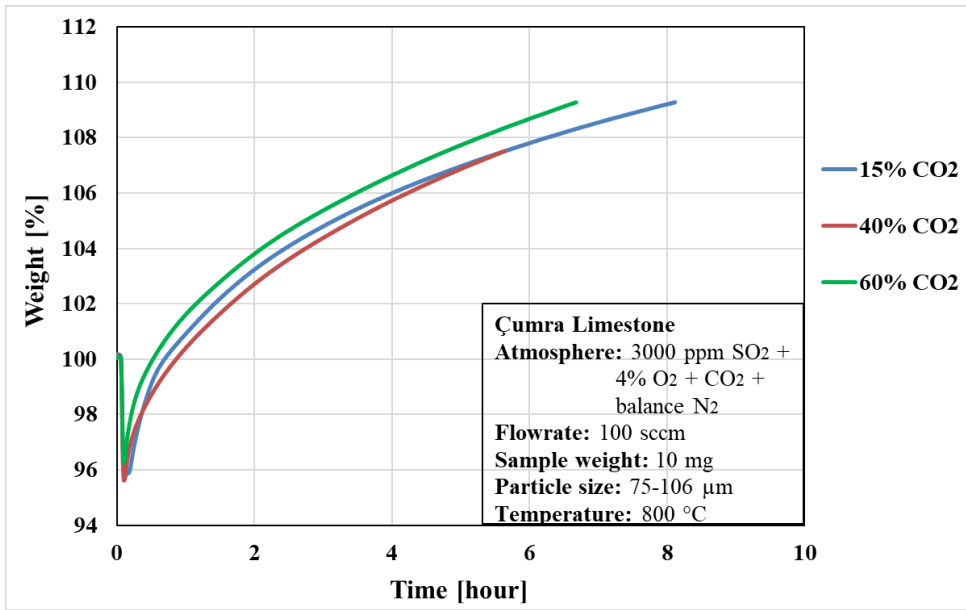


Figure 4-26 TGA results of Çumra limestone at 800 °C

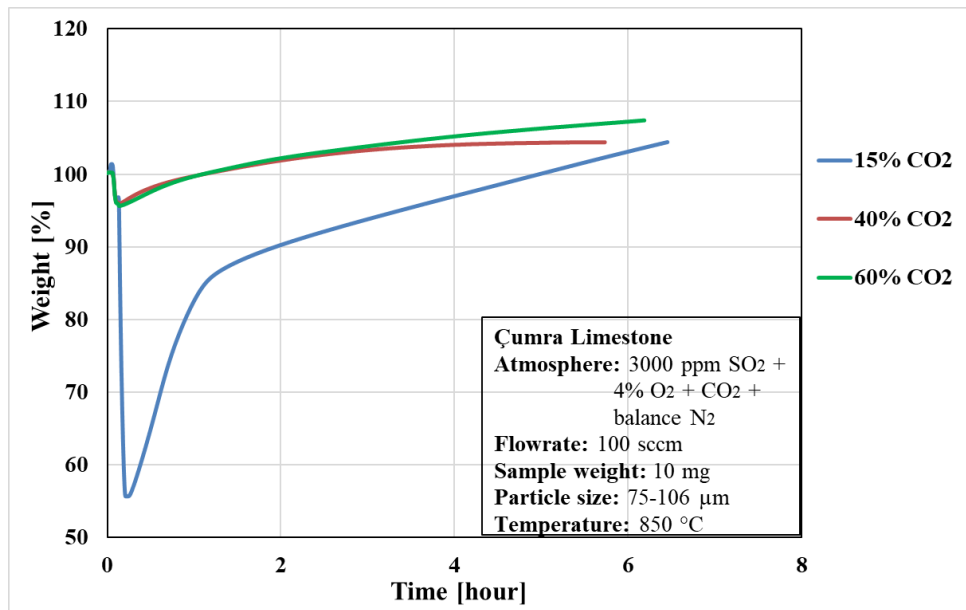


Figure 4-27 TGA results of Çumra limestone at 850 °C

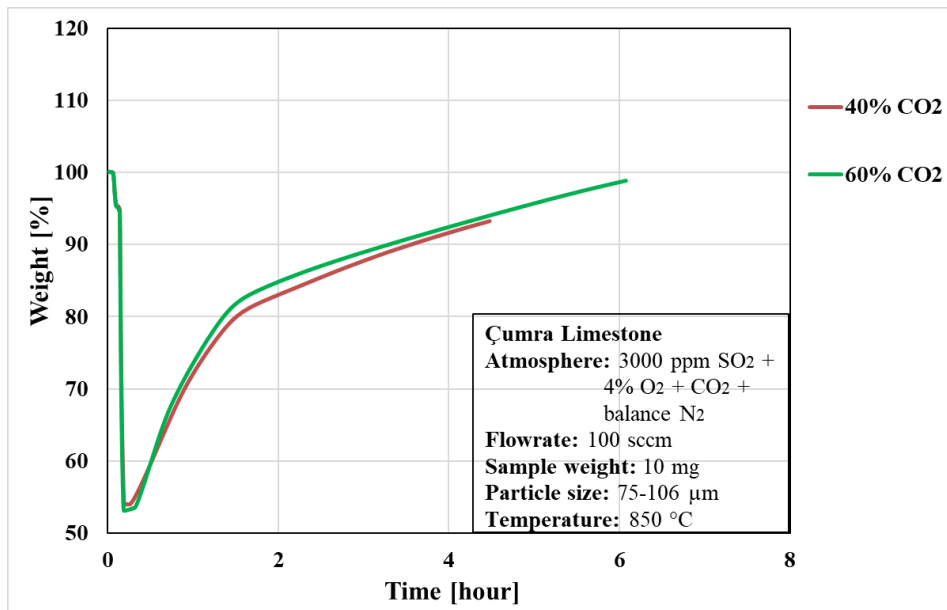


Figure 4-28 TGA results of Çumra limestone at 900 °C

4.2.2.2. Sulfation of Çumra Limestone

Conversion of Çumra Limestone at Different Temperatures

The effect of temperature on sulfation of Çumra limestone for different CO₂ concentrations are shown in Figure 4-29, Figure 4-30 and Figure 4-31. For 15% CO₂ concentration according to the experimental thermodynamic equilibrium curve, at 800 °C **direct sulfation** occurs and at 850 °C **indirect sulfation** occurs. The sulfation conversion value for **indirect sulfation** occurs rapidly at first and then slows down due the clogging of the pores. After an hour, the slopes of the two curves, **direct sulfation** at 800 °C and **indirect sulfation** at 850 °C, is approximately the same. At the end of six hour, the sulfur conversion for direct sulfation at 800 °C was 35% and for the indirect sulfation at 850 °C was 61%.

40% and 60% CO₂ concentrations at three different temperatures are shown in Figure 4-30 and Figure 4-31. For both of the CO₂ concentrations, at 800 °C and 850 °C, **direct sulfation** occurs and at 900 °C **indirect sulfation** occurs.

At both concentrations, in **direct sulfation**, when the temperatures increases, the sulfation conversion decreases. At the end of six hour time period, for 40% CO₂ concentration, the sulfation conversion is 35% at 800 °C and 25% at 850 °C. For the same time period, for 60% CO₂ concentration, the sulfation conversion is 36% at 800 °C and 34% at 850 °C. However, at 900 °C in **indirect sulfation**, the sulfation conversion rate increases.

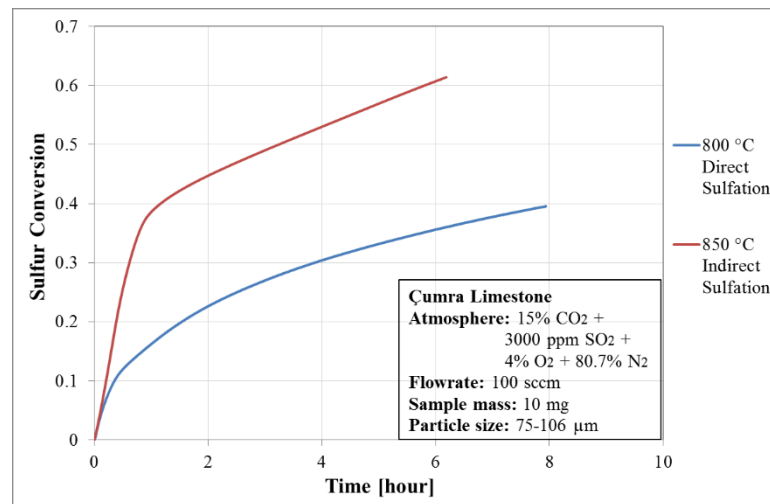


Figure 4-29 Sulfur conversion of Çumra limestone at 15% CO₂ concentration

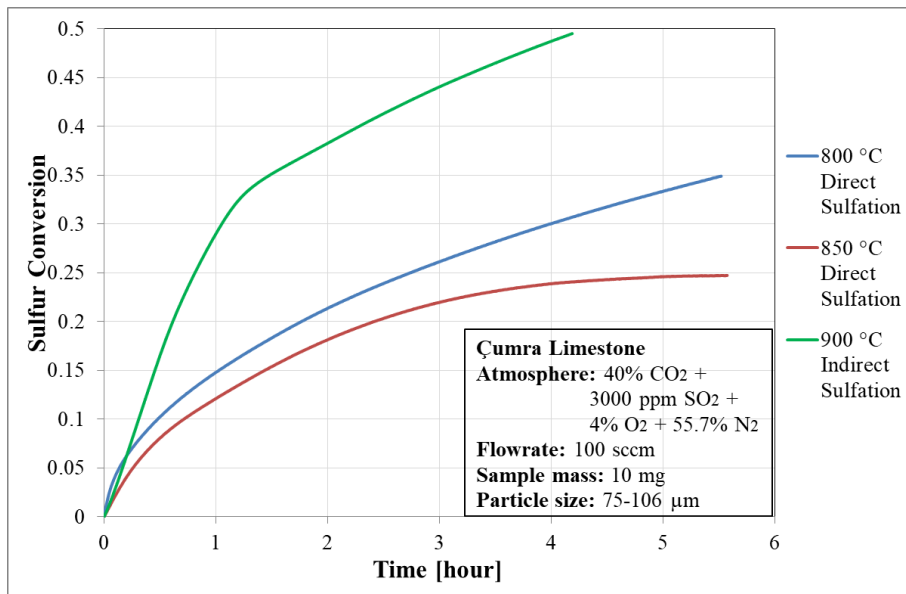


Figure 4-30 Sulfur conversion of Çumra limestone at 40% CO₂ concentration

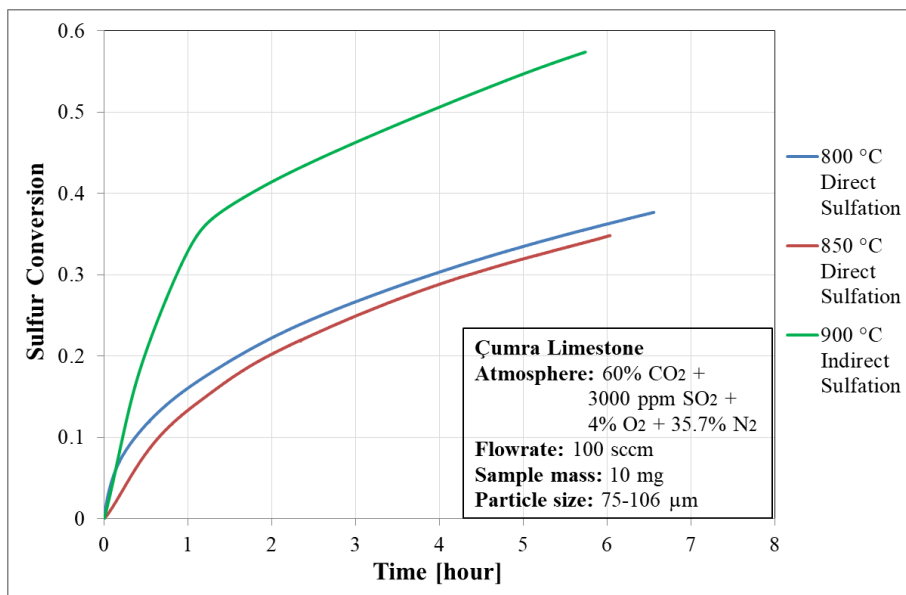


Figure 4-31 Sulfur conversion of Çumra limestone at 60% CO₂ concentration

Conversion Results of Çumra Limestone for Different CO₂ Concentrations

The effect of CO₂ concentrations on sulfation results of Çumra limestone are shown in Figure 4-32 and Figure 4-33. At 800 °C, direct sulfation reaction occurs, thus not much difference is observed between different CO₂ concentrations. At 900 °C, indirect sulfation occurs for 40% and 60% CO₂ concentrations and a slight difference can be seen between the different concentrations.

In Figure 4-34 the comparison of the two temperatures can be seen more clearly. According to these results, CO₂ concentration's main effect is to determine whether the direct or indirect sulfation will take place at the same temperature.

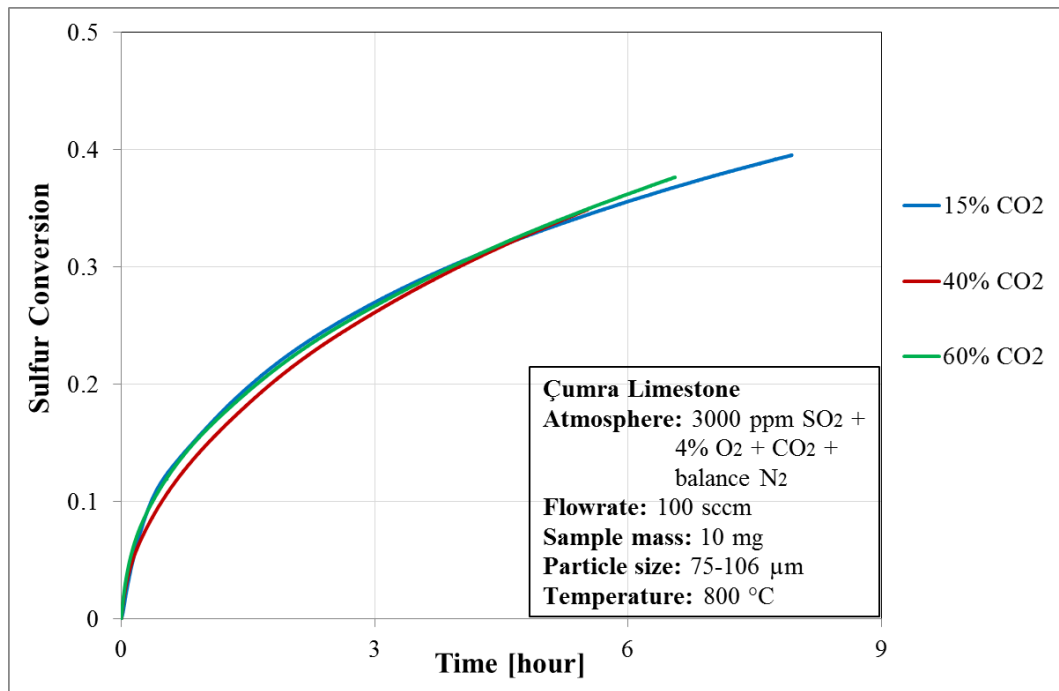


Figure 4-32 Sulfur conversion of Çumra limestone at 800 °C

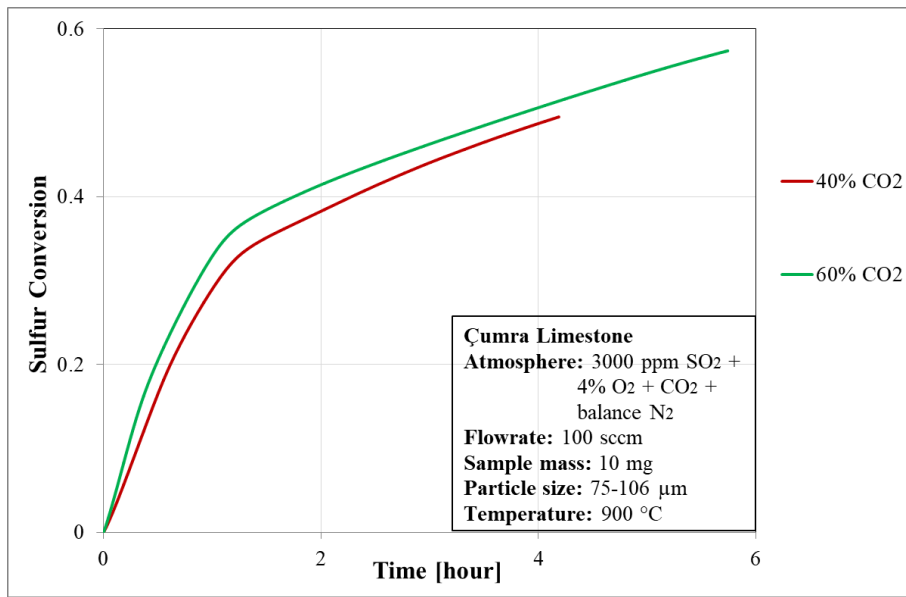


Figure 4-33 Sulfur conversion of Çumra limestone at 900 °C

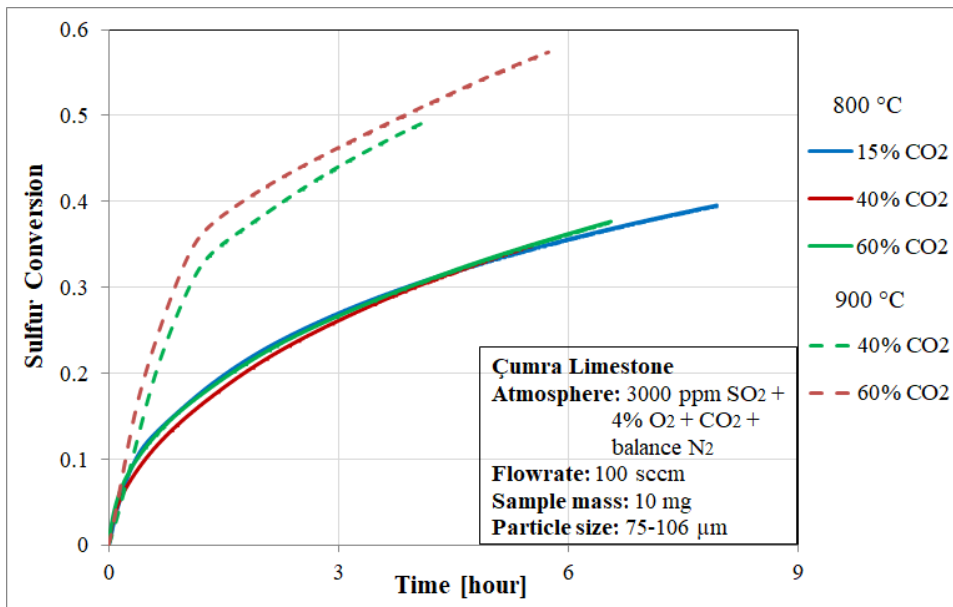
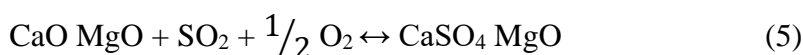


Figure 4-34 Comparison of sulfur conversion for Çumra limestone at 800 °C and 900 °C at different CO₂ concentrations

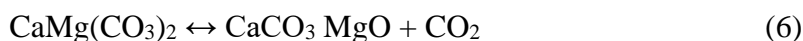
4.2.3. Thermogravimetric Analysis Results of Eskişehir Dolomite

In this section calcination and sulfation results of Eskişehir dolomite under different CO₂ concentrations are examined. The effect of temperature and carbon dioxide concentration were investigated for both reactions.

Table 3-7 shows the XRF analysis of Eskişehir dolomite. The main difference between the dolomite and limestone is the magnesium carbonate presence in dolomite together with calcium carbonate. In **indirect sulfation**, the magnesium carbonate forms magnesium oxide at temperatures between 300-500 °C and after the temperature reaches 800 °C, the calcination reaction of calcium carbonate starts. During the sulfation, magnesium oxide does not react with sulfur dioxide (Fuertes *et al.*, 1995).



In **direct sulfation**, again at temperatures between 300-500 °C magnesium carbonate forms magnesium oxide and sulfur dioxide react with calcium carbonate.



4.2.3.1. Calcination of Eskişehir Dolomite in Indirect Sulfation

The TGA results of Eskişehir dolomite at 800 °C, 850 °C and 900 °C temperatures with different carbon dioxide concentrations are shown in Figure 4-35, Figure 4-36 and Figure 4-37, respectively.

In dolomite samples, at temperatures between 300-500 °C, a weight loss is observed due to the formation of magnesium oxide from magnesium carbonate content of the dolomite sample. The second weight loss is the calcination of calcium carbonate. When the sample weight stabilizes, sulfur dioxide is added into the gas mixture for

the sulfation reaction to start. According to the results, at 800 °C for the 60% and 80% CO₂ concentrations, **direct sulfation** occurs and in all other conditions, **indirect sulfation** takes place.

The direct or indirect sulfation of dolomite is determined by whether the calcium carbonate is calcined or not. At both cases the magnesium carbonate reacts at temperatures between 300-500 °C. In Figure 4-35, at 800 °C, for 15% and 40% CO₂ concentrations, **indirect sulfation** reaction occurs and for 60% and 80% CO₂ concentrations, **direct sulfation** reaction occurs. At 800 °C for 60% and 80% CO₂ concentrations, the partial pressure of the CO₂ prevents the calcination reaction. Also, calcination reaction rate is not high at this temperature, thus **direct sulfation** occurs.

In Figure 4-36 and Figure 4-37, TGA graphs of dolomite sample at 850 °C and 900 °C are shown. For all CO₂ concentrations, indirect sulfation takes place for these temperatures. This is due to temperature being high enough for the calcination reaction to occur and the sulfation reaction rate at these temperatures is more dominant than the CO₂ present in the ambient.

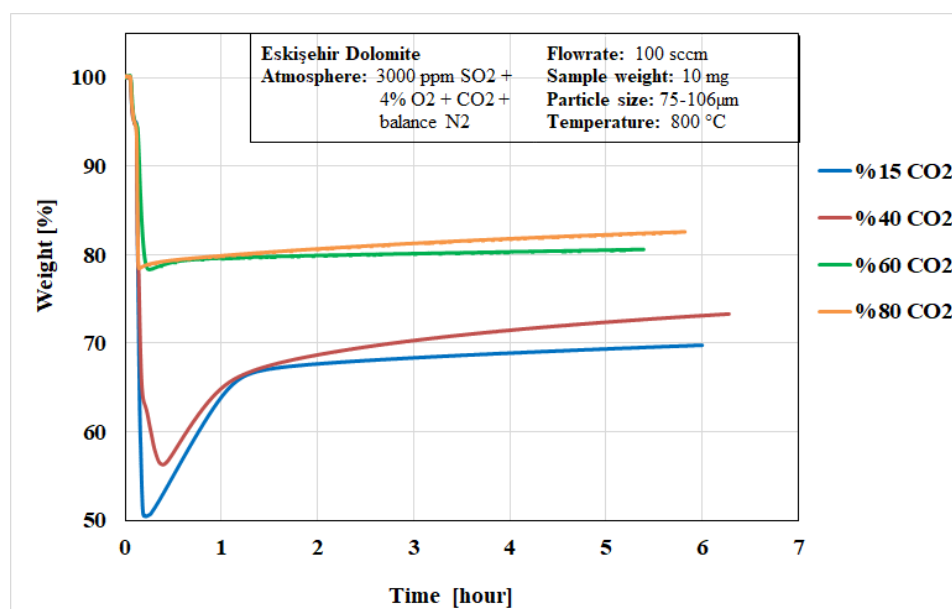


Figure 4-35 TGA results of Eskişehir dolomite at 800 °C

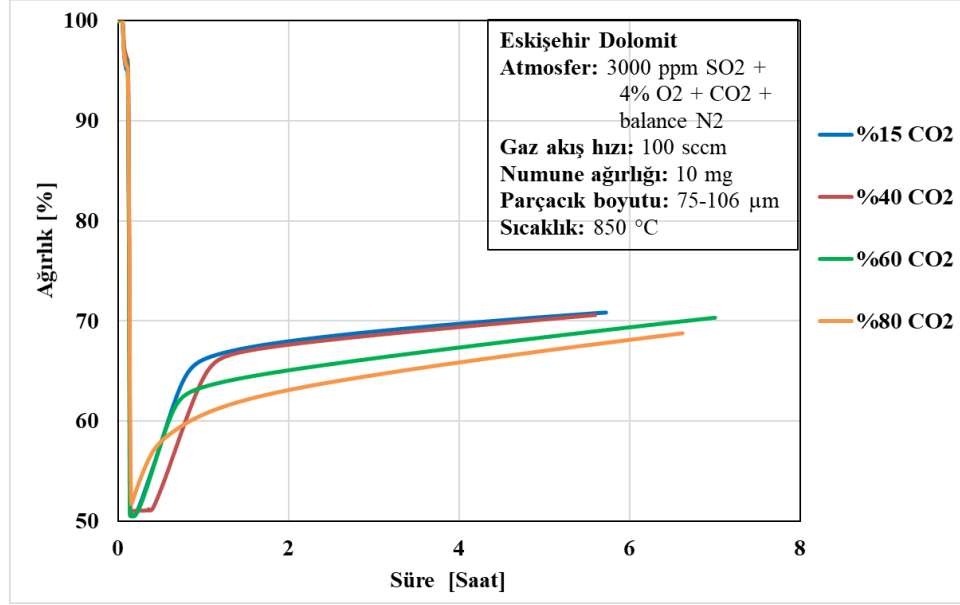


Figure 4-36 TGA results of Eskişehir dolomite at 850 °C

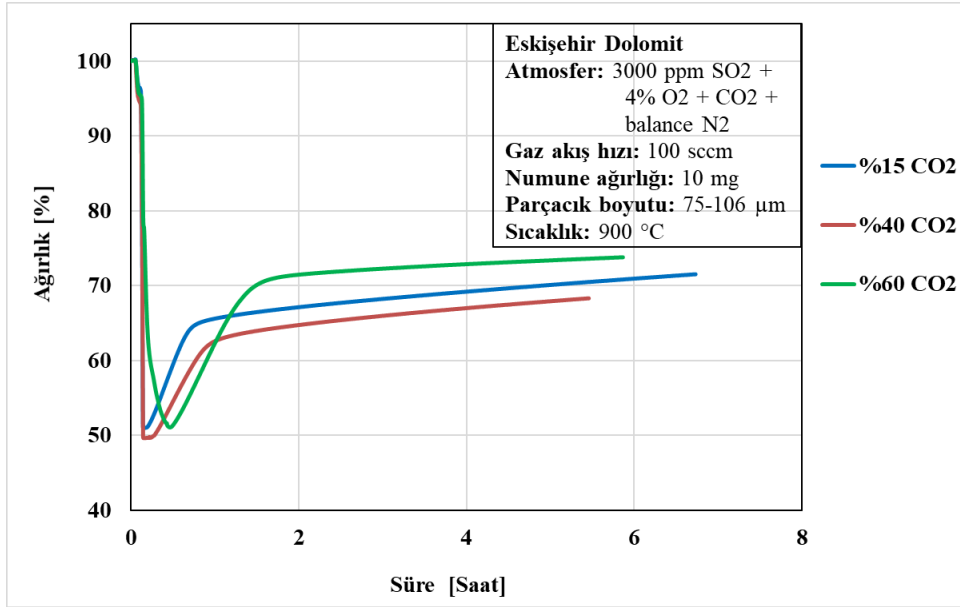


Figure 4-37 TGA results of Eskişehir dolomite at 900 °C

4.2.3.2. Sulfation of Eskişehir Dolomite

Conversion of Eskişehir Dolomite at Different Temperatures

The sulfur conversion of Eskişehir dolomite at 15%, 40%, 60% and 80% CO₂ concentration are shown in Figure 4-38, Figure 4-39, Figure 4-40 and Figure 4-41, respectively.

For 15% and 40% CO₂ concentrations, at all temperatures, **indirect sulfation** reaction takes place. In 15% CO₂ condition, the partial pressure of the carbon dioxide cannot prevent the calcination reaction to occur and **indirect sulfation** takes place. The sulfur conversion rates at this concentration for all three temperatures are approximately 35%. The sulfation reaction is rapid in the first hour and then due to the clogging of the pores, reaction slows down and the slope decreases.

For 40% CO₂ concentration, a higher sulfur conversion is obtained at 850 °C. At the end of five hour period, at 800°C is 27%, at 850 °C 32% and at 900 °C 30% sulfur conversion are obtained. The reaction rate is high during the first stage of the indirect sulfation (within the first 45 minutes). Then the reaction slows down and progresses with a lower rate as the pores of the sample gradually getting clogged.

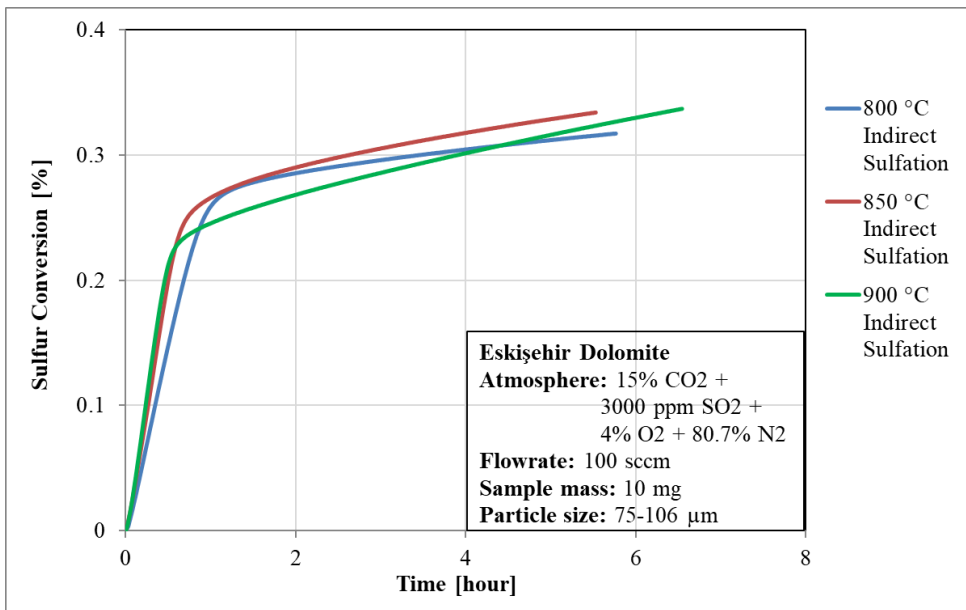


Figure 4-38 Sulfur conversion of Eskişehir dolomite at 15% CO₂ concentration

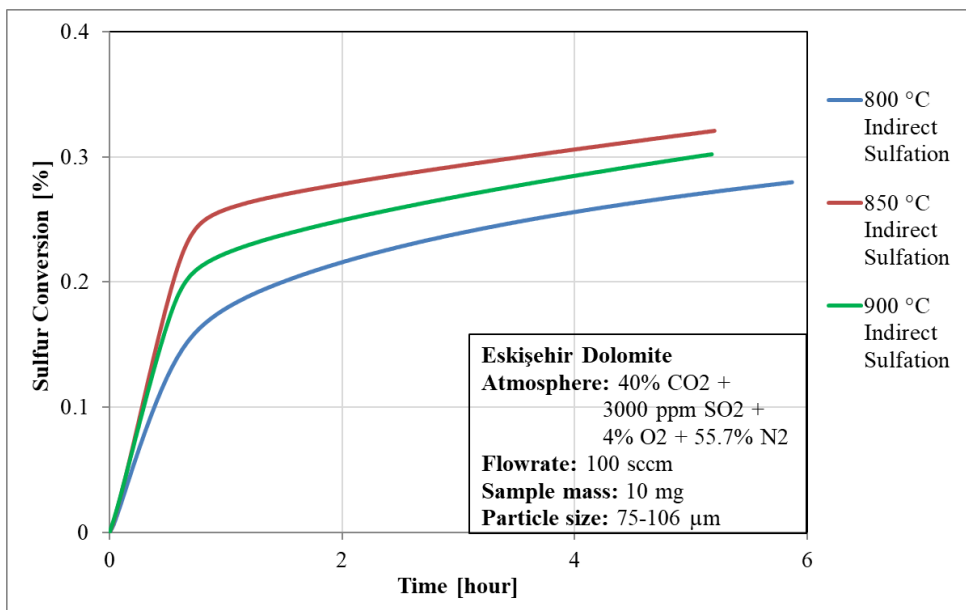


Figure 4-39 Sulfur conversion of Eskişehir dolomite at 40% CO₂ concentration

In Figure 4-40 and Figure 4-41, sulfation conversions for 60% and 80% CO₂ concentrations at different temperatures are shown. At 60% CO₂ concentration, at 800 °C **direct sulfation** occurs and at 850 °C and 900 °C **indirect sulfation** occurs. At 800 °C the partial pressure of CO₂ is high however the calcination rate is low; the calcination of dolomite sample cannot occur. In dolomite sample, the **direct sulfation** yields low conversion values. At the end of five-hour period, the sulfur conversion in direct sulfation was 8%. In **indirect sulfation**, the starting rates of the reactions within the first half hour are the same, then the reactions slow down as the pores gradually clo. The sulfation conversion value obtained after five hours at 900 °C is about 37%. The highest conversion is achieved at 900 °C.

In 80% CO₂ concentration, at 800 °C direct sulfation, at 850 °C indirect sulfation occurs. After five hours, at 800 °C the conversion is about 13%, which is low as compared to other experiments and at 900 °C it is about 26%. High CO₂ concentration (high CO₂ partial pressure) reduced the conversion efficiency.

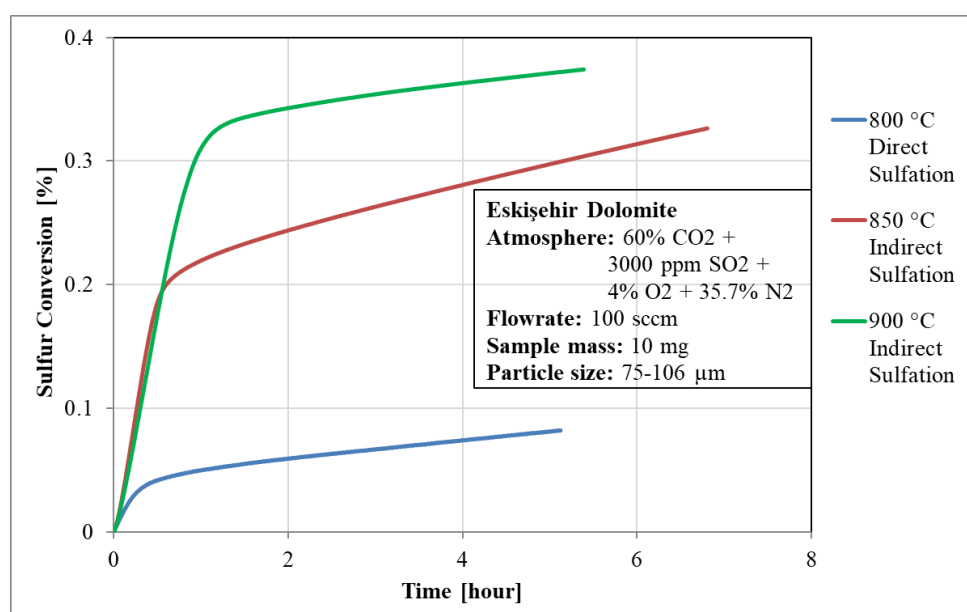


Figure 4-40 Sulfur conversion of Eskişehir dolomite at 60% CO₂ concentration

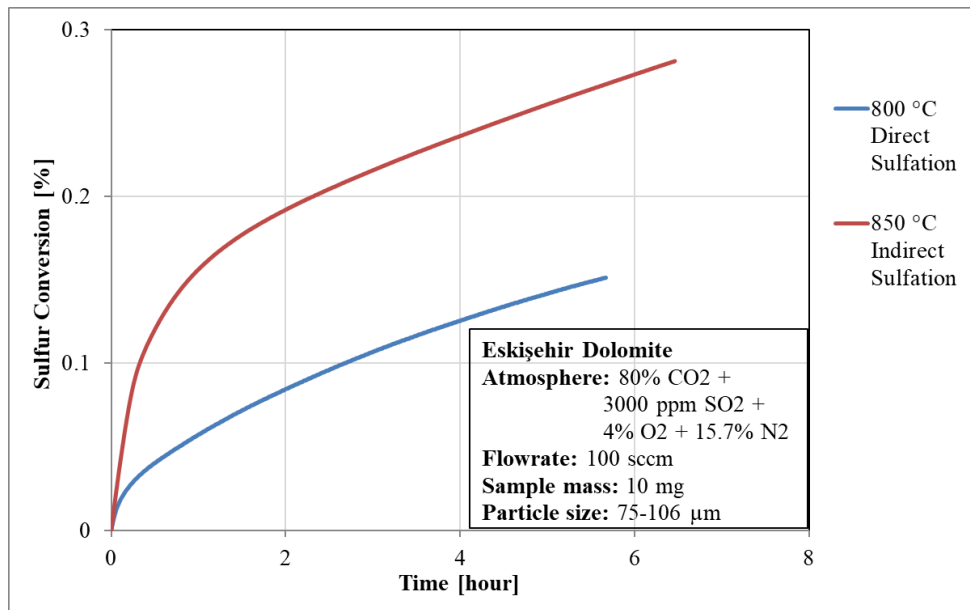


Figure 4-41 Sulfur conversion of Eskişehir dolomite at 80% CO₂ concentration

Conversion Results of Eskişehir Dolomite at Different CO₂ Concentrations

The sulfation conversion results of Eskişehir dolomite at different CO₂ concentrations are shown in Figure 4-42 and Figure 4-43 and the comparison of these two temperatures are shown in Figure 4-44. At 800 °C temperature in 15% and 40% CO₂ concentrations indirect sulfation, and in 60% and 80% CO₂ concentrations direct sulfation occurs. The CO₂ concentration in the gas mixture causes the reaction to be either direct or indirect, thus affecting the sulfation conversion. When CO₂ concentration increases in direct sulfation, the conversion increases and in indirect sulfation the increase in CO₂ concentration decreases the conversion value.

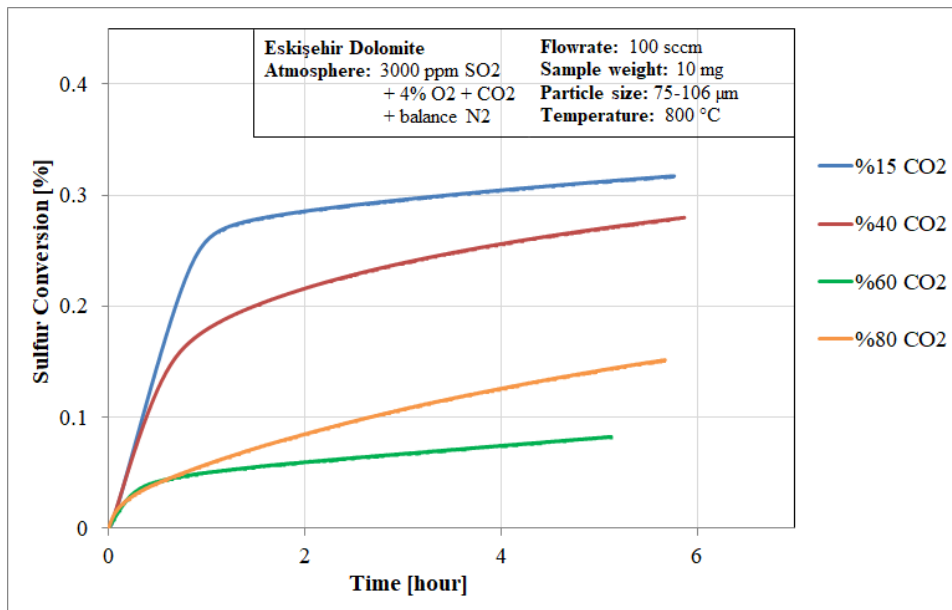


Figure 4-42 Sulfur conversion of Eskişehir dolomite at 800 °C

At 900 °C for all CO₂ concentrations indirect sulfation occurs. At this temperature, for 15% and 40% CO₂ concentrations, the obtained sulfur conversion results are very close. The sulfur conversion was 37% at 60% CO₂ concentration at the end of five-hour period.

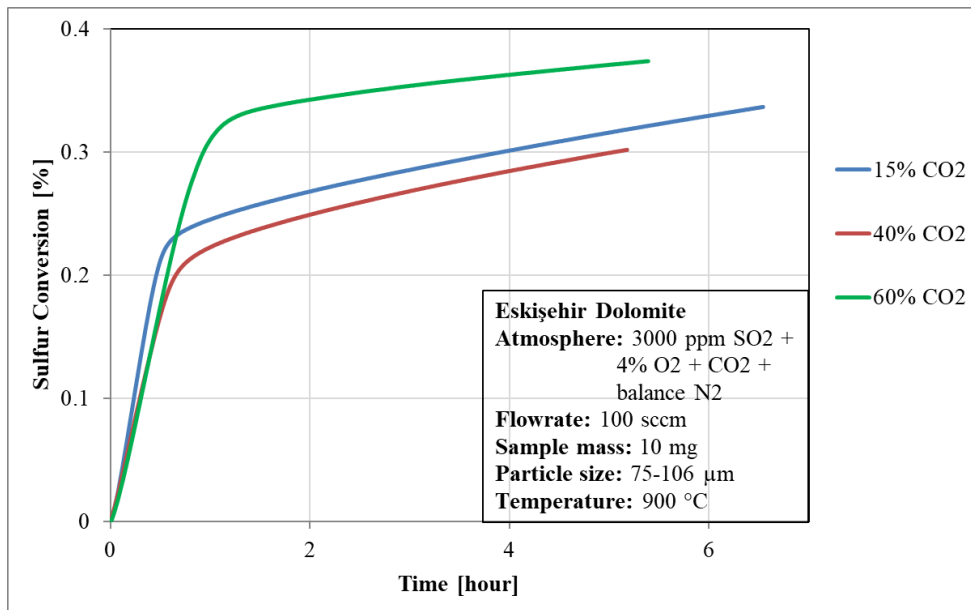


Figure 4-43 Sulfur conversion of Eskişehir dolomite at 900 °C

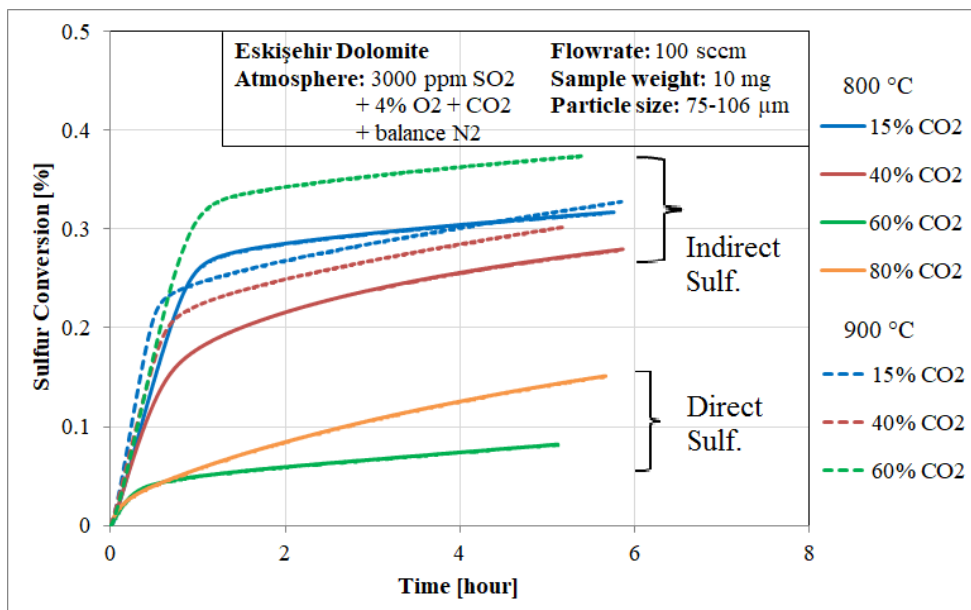


Figure 4-44 Comparison of sulfur conversion comparison for Eskişehir dolomite at 800 °C and 900°C at different CO₂ concentrations

Conversion Results of Eskişehir Dolomite with Different SO₂ Concentrations

Sulfur conversion of Eskişehir dolomite at 900 °C in 60% CO₂ concentrations with different SO₂ concentrations are shown in Figure 4-45. As expected, with increased SO₂ concentration, the sulfur conversion increases. After a five-hour period, with 1500 ppm, 3000 ppm and 4500 ppm SO₂ concentrations, 30%, 37% and 42% sulfur conversions are achieved, respectively.

The conversion efficiency is directly proportional to the SO₂ concentration. When SO₂ concentration is high, the first part of the reaction also occurs more rapidly. As the reaction progresses, with clogging of the dolomite samples pores, the reaction begins to slow down for all three SO₂ concentrations.

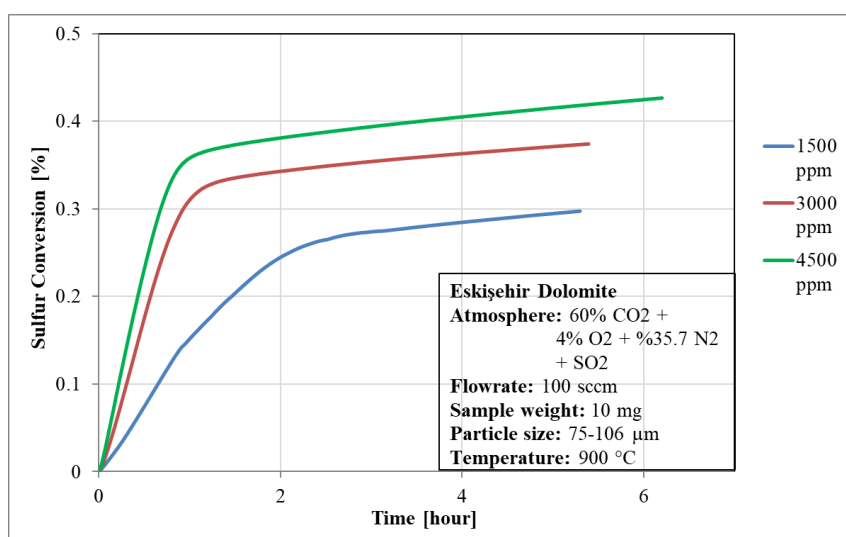


Figure 4-45 Sulfur conversion of Eskişehir dolomite at 900°C at different SO₂ concentrations

CHAPTER 5

CONCLUSION

CO₂ has the largest concentration of greenhouse gases in the atmosphere. In an oxy-combustion system, the resulting combustion gases will mainly consist of CO₂ and water vapor, making it easier to retain CO₂ in the flue gas. When the flue gas is mixed with certain amounts of combustion air and fed back to the system, the amount of CO₂ in the combustion gases increases, although the total amount of CO₂ produced is reduced. This provides a significant advantage in CO₂ sequestration and control in the flue gas.

NO_x emissions in a coal combustion system is another highly important issue. Due to the reduction in the amount of nitrogen fed to the system in oxy-combustion systems, NO_x emission will also be reduced.

The oxy-combustion system as its advantages and disadvantages all discussed in the introduction part of the thesis. The economic feasibility of the system in real life situations can differ depending on various aspects. This system provides an advantage in CO₂ sequestration and reduces the NO_x emissions however, formation of SO₂ is also a significant complication in the combustion of coal in power plants. SO₂ emissions react with water vapor in combustion and oxy-combustion conditions to form H₂SO₄ which can result in corrosion.

The aim of this study was to investigate the efficient and clean combustion of Turkish lignites by using oxy-combustion technology, to examine the characteristics of SO₂ capture with limestone in oxy-combustion conditions.

In pyrolysis of lignite samples in carbon dioxide atmosphere, the pyrolysis behavior of lignite in nitrogen and carbon dioxide atmospheres was nearly the same up to 650-

700 °C, due to carbon dioxide acting as an inert gas. The third peak of the DTG curve in nitrogen atmosphere is the calcite decomposition reaction which releases carbon dioxide as a product. In carbon dioxide atmosphere, the partial pressure of carbon dioxide prevented the calcite decomposition and char gasification reaction occurred instead. In Soma lignite, char gasification reaction between the fixed carbon and carbon dioxide starts at approximately 700 °C. However, at about 870 °C, another reaction starts in Soma lignite in carbon dioxide atmosphere due to calcite decomposition.

For both lignites activation energies were calculated using different kinetic methods in both nitrogen and carbon dioxide atmospheres. When the kinetic models are compared, the Friedman method resulted in activation energy values different from these isoconversional integral methods. The other three methods which gave similar results, assume a constant activation energy for the whole integral interval. Friedman method is a differential method and this assumption is not applied in the calculations.

In the combustion experiments of Orhaneli and Soma lignite in dry air, the first region of the DTG curve showed the moisture release and the second region the removal of volatile matter. The third peak in the combustion thermographs represents the oxidation of char. The high volatile matter content and low ash content of Orhaneli lignite makes it a better coal than Soma lignite. However, Orhaneli lignite has higher sulfur content than Soma lignite, thus limestone as an adsorbent to retain sulfur dioxide emission is necessary to use.

The retention of sulfur dioxide emission resulting from the oxy-combustion of lignite were studied with calcium based sorbents such as limestone and dolomite. For sulfur dioxide capture, two different reactions were studied: direct sulfation and indirect sulfation with two different limestones; Çan and Çumra limestone and Eskişehir dolomite.

The limestone experiments were done at three temperatures and for four different CO₂ concentrations. The studies in this thesis showed a slight shift in the calcium carbonate thermodynamic equilibrium curve (Figure 4-12). The novel result of this study is this shift in thermodynamic equilibrium curve from the theoretical curve which is supported by the De Diego et al. (2011). At the same conditions, they also concluded the same results (indirect or direct sulfation). However, due to different limestones being used, different sulfur conversion values were achieved.

When the calcination results in this study are examined, it is concluded that indirect sulfation will result in better sulfur conversion and limestone is more effective than dolomite to capture sulfur dioxide. In sulfation experiments, the effect of temperature was examined. In indirect sulfation, increase in temperature did not cause an increase in the sulfur conversion values. However, by increasing the temperature at the same CO₂ concentration, the reaction shifts to indirect sulfation, thus resulting in higher sulfation conversion values.

When the effect of CO₂ concentrations was examined, it is concluded that the main effect of CO₂ concentration is to determine whether the sulfation reaction will go to calcination (indirect sulfation) or not (direct sulfation) at the same temperature.

When the two limestones, Çan and Çumra, were compared, a shift in the theoretical thermodynamic curve was observed for both samples. This was very interesting for this study. The effects of temperature and CO₂ concentrations were both the same. However, Çan limestone revealed higher sulfur conversion values (about 60%) due to higher surface area.

In dolomite sample, the calcination results were different than limestone results. The effect of studied parameters (temperature, CO₂ concentration and SO₂ concentration) were the same as limestone in both direct and indirect sulfation reactions. However, in general, dolomite resulted in lower sulfur conversions (about 12% at 800 °C, and 28-37% at 900 °C) when compared to limestone samples.

As a future study, the oxygen-enhanced combustion and oxy-combustion of lignite samples and their kinetic studies with different methods should be studied. Regarding the studies about the sulfur dioxide capture in oxy-combustion conditions, the effect of water vapor on sulfur conversion should be investigated. The water vapor produced during the combustion process can influence the limestone sulfurization, some studies showed that water vapor can accelerate the solid state diffusion. This point is worth investigation in more detail in order to increase the limestone usage and sulfur conversion efficiency.

REFERENCES

- Abbasi-Atibeh, E. and Yozgatligil, A. (2014) ‘A study on the effects of catalysts on pyrolysis and combustion characteristics of Turkish lignite in oxy-fuel conditions’, *Fuel*. Elsevier Ltd, 115, pp. 841–849. doi: 10.1016/j.fuel.2013.01.073.
- Ahn, J., Okerlund, RÇ, Fry, A. and Eddings, E.G. (2011) ‘Sulfur trioxide formation during oxy-coal combustion’, *International Journal of Greenhouse Gas Control*, 5(SUPPL. 1). doi: 10.1016/j.ijggc.2011.05.009.
- Akpan, U. F. and Akpan, G. E. (2012) ‘The contribution of energy consumption to climate change: A Feasible policy Direction’, *International Journal of Energy Economics and Policy*, 2(1), pp. 21–33.
- Australian Government Department of the Environment and Energy (2005) *Sulfur dioxide (SO₂) - Air quality fact sheet*. Available at: <https://www.environment.gov.au/protection/publications/factsheet-sulfur-dioxide-so2> (Accessed: 28 July 2019).
- Barin, I. (1989) ‘Thermochemical Data of Pure Substances’, *VCH, Weinheim*, p. 8249.
- Barzegar, R., Avsaroglu, S., Yozgatligil, A. and Atimtay. A. (2018) ‘Pyrolysis characteristics of Turkish lignites in N₂ and CO₂ environments’, *Energy Sources, Part A: Recovery, Utilization and Environmental Effects*. Taylor & Francis, 40(20), pp. 2467–2475. doi: 10.1080/15567036.2018.1502845.
- Barzegar, R. (2019) *Investigation of Combustion of Lignite and Torrefied Biomass in a Thermogravimetric Analyzer (TGA) and in a Circulating Fluidized Bed (CFB) under Oxy-fuel Combustion Conditions*. Middle East Technical University.
- Biomedical Research Centre (1994) ‘Kinetic Analysis’, *Enzyme*, 401(September), pp. 395–401.
- Brown, M. E. (2001) *Introduction to Thermal Analysis: Techniques and Applications*,

Statewide Agricultural Land Use Baseline 2015. doi: 10.1017/CBO9781107415324.004.

Chen, L., Yong, S. Z. and Ghoniem, A. F. (2012) ‘Oxy-fuel combustion of pulverized coal: Characterization, fundamentals, stabilization and CFD modeling’, *Progress in Energy and Combustion Science*, 38(2), pp. 156–214. doi: 10.1016/j.peecs.2011.09.003.

Chen, W. Y., Seiner, J., Suzuki, T. and Lckner M. (2012) ‘Handbook of climate change mitigation’, *Handbook of Climate Change Mitigation*, 1–4, pp. 1–2130. doi: 10.1007/978-1-4419-7991-9.

Croiset, E., Thambimuthu, K. and Palmer, A. (2006) ‘Compared with Air’, 78(April 2000), pp. 402–407.

De Diego, L. F., Obras-Loscertales, M., Garcia-Labiano, F., Rufas, A., Abad, A., Gayan, P and Adanez J. (2011) ‘Characterization of a limestone in a batch fluidized bed reactor for sulfur retention under oxy-fuel operating conditions’, *International Journal of Greenhouse Gas Control*. Elsevier Ltd, 5(5), pp. 1190–1198. doi: 10.1016/j.ijggc.2011.05.032.

Duan, L., Zhao, C., Zhou, W., Qu, C. and Chen, X. (2009) ‘Investigation on Coal Pyrolysis in CO₂ Atmosphere’, *Energy & Fuels*, 23(7), pp. 3826–3830. doi: 10.1021/ef9002473.

Fuertes, A. B., Velasco, G., Alvarez T. and Fernandez M. J. (1995) ‘Sulfation of dolomite particles at high CO₂ partial pressures’, *Thermochimica Acta*, 254(C), pp. 63–78. doi: 10.1016/0040-6031(94)02067-X.

García-Labiano, F., Rufas, A., Diego, L. F., Obras-Loscertales, M. Gayan, P, Abad, A. and Adanez, J. (2011) ‘Calcium-based sorbents behaviour during sulphation at oxy-fuel fluidised bed combustion conditions’, *Fuel*, 90(10), pp. 3100–3108. doi: 10.1016/j.fuel.2011.05.001.

Huang, X., Guo, J., Liu, Z. nad Zheng, C. (2018) ‘Opportunities and Challenges of

Oxy-fuel Combustion’, pp. 1–12.

Hyatt, E. P., Cutler, I. B. and Wadsworth, M. E. (1955) ‘Carbon Dioxide Atmosphere’, *Journal of the American Ceramic Society*, 61(1943), pp. 70–74.

Idris, S. S., Rahman, N. A., Ismail, K. Alias, A. B., Rashid, Z.A. and Aris, M. J. (2010) ‘Investigation on thermochemical behaviour of low rank Malaysian coal, oil palm biomass and their blends during pyrolysis via thermogravimetric analysis (TGA)’, *Bioresource Technology*. Elsevier Ltd, 101(12), pp. 4584–4592. doi: 10.1016/j.biortech.2010.01.059.

IEA Coal Research. (1989) *The Problems of Sulphur*. Published by Butterworths on behalf of IEA Coal Research. Available at: <https://books.google.com.tr/books?id=ua4aAwAAQBAJ&printsec=frontcover&hl=tr#v=onepage&q&f=false> (Accessed: 28 July 2019).

International Energy Agency (2018) ‘Key World Energy Statistics 2018’. doi: 10.1787/key_energ_stat-2018-en.

International Energy Agency (2019a) *Coal Report, IEA Coal Research*. Available at: <https://www.enerji.gov.tr/en-US/Pages/Coal> (Accessed: 29 July 2019).

International Energy Agency (2019b) ‘Global Energy & CO₂ Status Report: Emissions’, *Iea.org*, p. 14. Available at: <https://www.iea.org/geco/emissions/>.

Jia, L., Tan, Y. and Anthony, E. J. (2010) ‘Emissions of SO₂ and NO_x during Oxy - Fuel CFB Combustion Tests in a Mini-Circulating Fluidized Bed Combustion Reactor’, (x), pp. 910–915. doi: 10.1021/ef901076g.

Jiang, G. and Wei, L. (2018) ‘Analysis of Pyrolysis Kinetic Model for Processing of Thermogravimetric Analysis Data’. doi: 10.5772/intechopen.79226.

Khawam, A. (2007) ‘Application of solid-state kinetics to desolvation reactions’, pp. xxiii, 321. doi: 10.1017/CBO9781107415324.004.

Kunii, D. and Levenspiel, O. (1991) *Fluidization Engineering, Porous Media*. doi:

10.1016/b978-0-7506-9236-6.50001-9.

Meng, F., Yu, J., Tahmasebi, A. and Han, Y. (2013) ‘Pyrolysis and combustion behavior of coal gangue in O₂/CO₂ and O₂/N₂ mixtures using thermogravimetric analysis and a drop tube furnace’, *Energy and Fuels*, 27(6), pp. 2923–2932. doi: 10.1021/ef400411w.

Ministry of Energy and Natural Resources. (2017) ‘2015-2019 Stratejik Planı’.

Ministry of Energy and Natural Resources (2018) ‘2017 Yılı Genel Enerji Denge Tablosu’.

Moffat, W. and Walmsley, M. R. W. (1996) ‘Understanding lime calcination’, *Current Anthropology*, 37(4), pp. 803–810. doi: <http://dx.doi.org/10.1179/009346988791974501>

Mohalik, N. K., Lester, E. and Lowndes, I. S. (2017) ‘Review of experimental methods to determine spontaneous combustion susceptibility of coal–Indian context’, *International Journal of Mining, Reclamation and Environment*. Taylor & Francis, 31(5), pp. 301–332. doi: 10.1080/17480930.2016.1232334.

Nemitallah, M. A., Habib, M. A., Badr, H. M., Said, S. A., Jamal, A., Ben-Mansour, R., Mokheimer, E. M. A. and Mezghani, K. (2017) ‘Oxy-fuel combustion technology: current status, applications, and trends’, *International Journal of Energy Research*. doi: 10.1002/er.3722.

Sommariva, S., Maffei, T., Migliavacca, G., Faravelli, T and Ranzi, E. (2010) ‘A predictive multi-step kinetic model of coal devolatilization’, *Fuel*. Elsevier Ltd, 89(2), pp. 318–328. doi: 10.1016/j.fuel.2009.07.023.

Speight, J. G. (2011) *Hydrocarbons from Synthesis Gas*. doi: 10.1016/B978-0-7506-8632-7.10008-8.

Stanger, R. and Wall, T. (2011) ‘Sulphur impacts during pulverised coal combustion

in oxy-fuel technology for carbon capture and storage’, *Progress in Energy and Combustion Science*, 37(1), pp. 69–88. doi: 10.1016/j.pecs.2010.04.001.

Stanmore, B. R. and Gilot, P. (2005) ‘Review-calcination and carbonation of limestone during thermal cycling for CO₂ sequestration’, *Fuel Processing Technology*, 86(16), pp. 1707–1743. doi: 10.1016/j.fuproc.2005.01.023.

Toftegaard, M. B., Brix, J., Jensen, P. A., Glarborg, P and Jensen, A. D. (2010) ‘Oxy-fuel combustion of solid fuels’, *Progress in Energy and Combustion Science*. Elsevier Ltd, 36(5), pp. 581–625. doi: 10.1016/j.pecs.2010.02.001.

Urych, B. (2014) ‘Determination of Kinetic Parameters of Coal Pyrolysis to Simulate the Process of Underground Coal Gasification (UCG)’, *Journal of Sustainable Mining*. Elsevier Masson SAS, 13(1), pp. 3–9. doi: 10.7424/jsm140102.

Vyazovkin, S. and Sbirrazzuoli, N. (2006) ‘Isoconversional kinetic analysis of thermally stimulated processes in polymers’, *Macromolecular Rapid Communications*, 27(18), pp. 1515–1532. doi: 10.1002/marc.200600404.

Wang, L., Li, S. and Eddings, E. G. (2015) ‘Fundamental study of indirect vs direct sulfation under fluidized bed conditions’, *Industrial and Engineering Chemistry Research*, 54(14), pp. 3548–3555. doi: 10.1021/ie504774r.

Yeşil Ekonomi (2019) *Karbondioksit yoğunluğu geçen ay 413,92 ppm oldu : Yeşil Ekonomi*. Available at: https://yesilekonomi.com/karbondioksit-yogunlugu-gecen-ay-41392-ppm-oldu/?utm_source=newsletter&utm_medium=email&utm_campaign=gecen_haftani_n_oene_cikan_haberleri&utm_term=2019-09-01 (Accessed: 4 August 2019).

Yorulmaz, S. Y. and Atımtay, A. (2011) ‘Investigation of combustion kinetics of five waste wood samples with thermogravimetric analysis’, *Environmental Earth Sciences*. Elsevier B.V., 90(7–8), pp. 511–520. doi: 10.1007/978-3-540-95991-5-46.

Yuzbasi, N. S. and Selcuk, N. (2012) ‘Air and oxy-fuel combustion behaviour of petcoke/lignite blends’, *Fuel*. Elsevier Ltd, 92(1), pp. 137–144. doi:

10.1016/j.fuel.2011.08.026.

APPENDICES

APPENDIX A Isoconversional Plots for Coal Pyrolysis

Isoconversional plots of FWO, KAS and Friedman methods for Orhaneli lignite in the first region (devolatilization region)

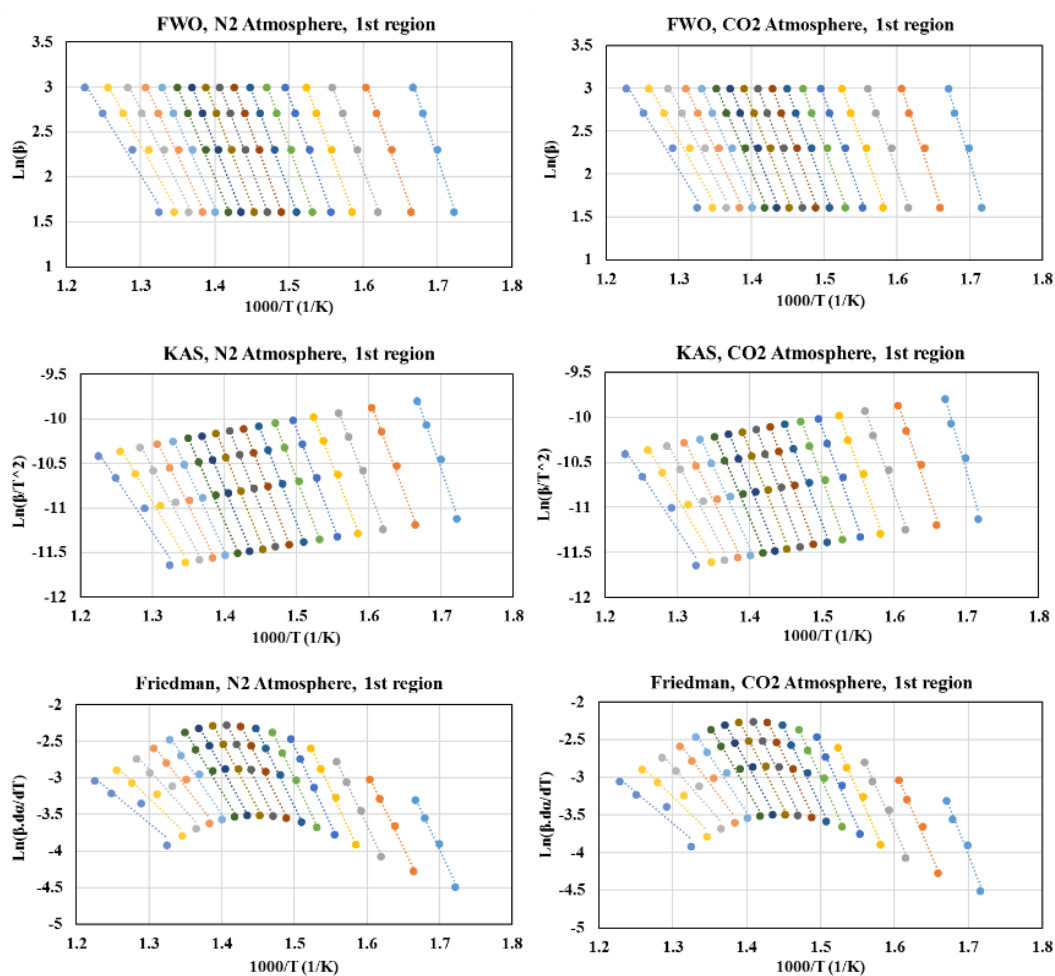


Figure A 1 Isoconversional plots of FWO, KAS and Friedman methods for *Orhaneli lignite* at different conversion values under N₂ and CO₂ atmospheres in the first region (devolatilization region)

Isoconversional plots of FWO, KAS and Friedman methods for Orhaneli lignite in the second region (char formation region)

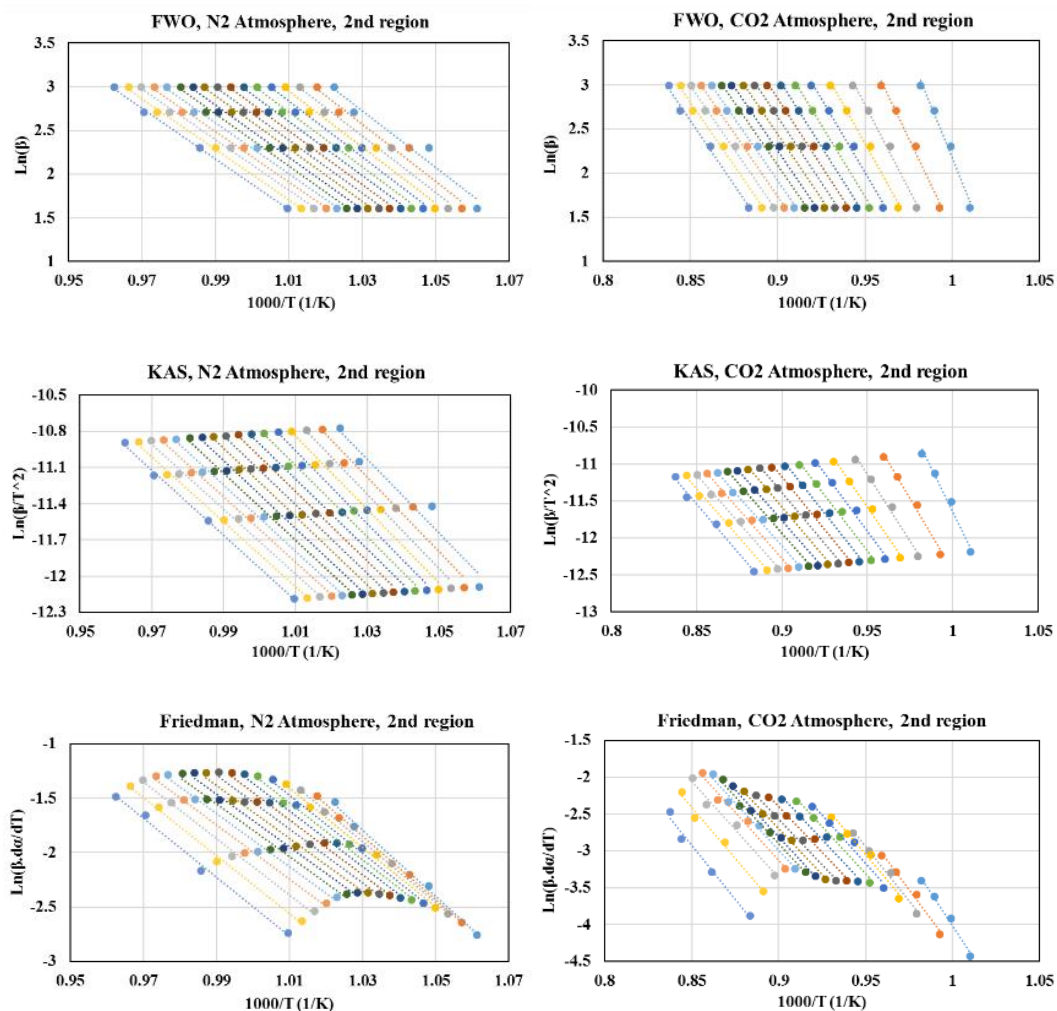


Figure A- 2 Isoconversional plots of FWO, KAS and Friedman methods for Orhaneli lignite at different conversion values under N₂ and CO₂ atmospheres in the first region (char formation region)

Table A- 1 R² values for Orhaneli lignite in N₂ and CO₂ atmospheres

Conversion values	FWO		KAS		Friedman	
	N ₂	CO ₂	N ₂	CO ₂	N ₂	CO ₂
Devolatilization Region						
0.1	0.9881	0.9792	0.9869	0.9774	0.9880	0.9761
0.15	0.9926	0.9858	0.9917	0.9843	0.9944	0.9854
0.2	0.9966	0.9874	0.9962	0.9860	0.9982	0.9882
0.25	0.9969	0.9890	0.9965	0.9877	0.9983	0.9897
0.3	0.9984	0.9909	0.9981	0.9898	0.9989	0.9911
0.35	0.9983	0.9915	0.9981	0.9904	0.9984	0.9908
0.4	0.9985	0.9911	0.9983	0.9899	0.9980	0.9895
0.45	0.9983	0.9923	0.9981	0.9913	0.9973	0.9900
0.5	0.9986	0.9916	0.9984	0.9904	0.9972	0.9881
0.55	0.9981	0.9907	0.9978	0.9894	0.9958	0.9855
0.6	0.9972	0.9899	0.9967	0.9884	0.9930	0.9819
0.65	0.9959	0.9884	0.9951	0.9865	0.9876	0.9756
0.7	0.9942	0.9864	0.9931	0.9841	0.9786	0.9663
0.75	0.9923	0.9838	0.9907	0.9807	0.9654	0.9537
0.8	0.9884	0.9799	0.9859	0.9756	0.9450	0.9378
0.85	0.9830	0.9765	0.9788	0.9708	0.9218	0.9244
0.9	0.9759	0.9723	0.9690	0.9646	0.9019	0.9144
Char Formation Region						
0.1	0.9570	0.9864	0.9516	0.9852	0.9961	0.9849
0.15	0.9691	0.9898	0.9652	0.9887	0.9989	0.9904
0.2	0.9768	0.9903	0.9738	0.9891	0.9990	0.9880
0.25	0.9797	0.9912	0.9771	0.9900	0.9969	0.9823
0.3	0.9826	0.9899	0.9803	0.9884	0.9942	0.9735
0.35	0.9833	0.9884	0.9810	0.9867	0.9916	0.9700

0.4	0.9838	0.9892	0.9816	0.9874	0.9905	0.9782
0.45	0.9857	0.9900	0.9837	0.9883	0.9923	0.9884
0.5	0.9889	0.9910	0.9873	0.9894	0.9933	0.9954
0.55	0.9919	0.9916	0.9907	0.9901	0.9931	0.9973
0.6	0.9923	0.9919	0.9912	0.9904	0.9899	0.9956
0.65	0.9933	0.9933	0.9923	0.9921	0.9880	0.9917
0.7	0.9951	0.9937	0.9943	0.9926	0.9900	0.9859
0.75	0.9965	0.9945	0.9960	0.9935	0.9919	0.9813
0.8	0.9969	0.9951	0.9964	0.9942	0.9954	0.9799
0.85	0.9979	0.9944	0.9976	0.9934	0.9960	0.9850
0.9	0.9987	0.9938	0.9985	0.9927	0.9941	0.9845

Isoconversional plots of FWO, KAS and Friedman methods for Soma lignite in the first region (devolatilization region)

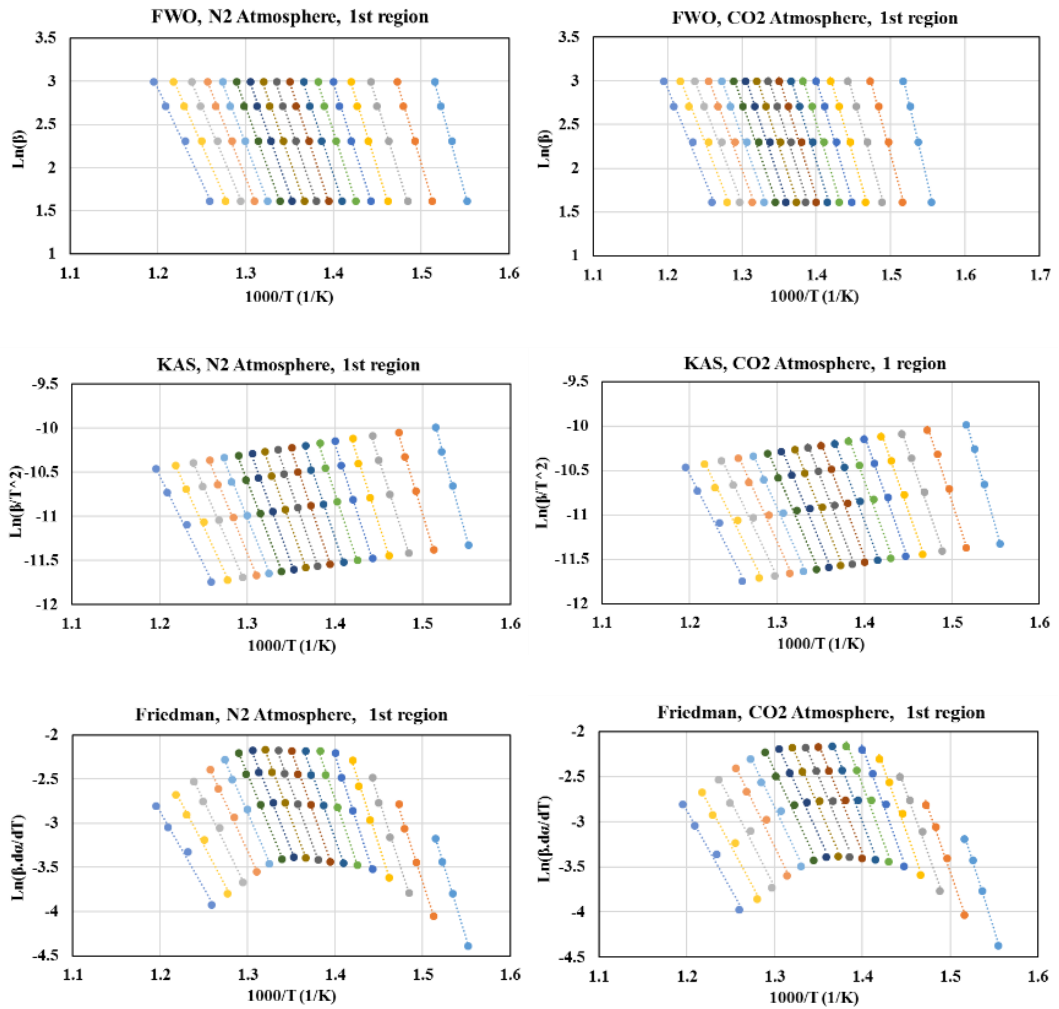


Figure A- 3 Isoconversional plots of FWO, KAS and Friedman methods for Soma lignite at different conversion values under N₂ and CO₂ atmospheres in the first region (devolatilization region)

Isoconversional Plots of FWO, KAS and Friedman methods for Soma lignite in the second region (char formation region)

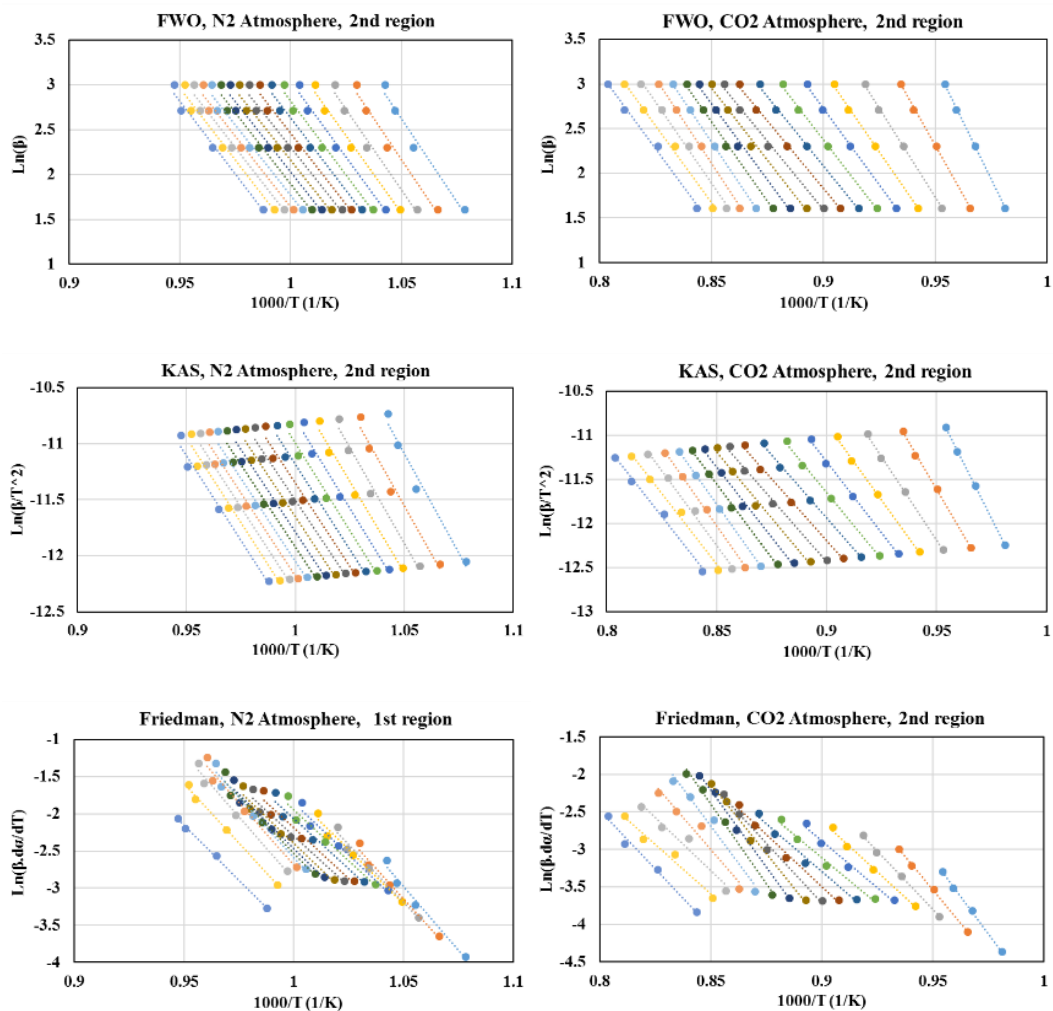


Figure A- 4 Isoconversional plots of FWO, KAS and Friedman methods for *Soma lignite* at different conversion values under N₂ and CO₂ atmospheres in the second region (char formation region)

Table A- 2 R^2 values for Soma lignite in N_2 and CO_2 atmospheres

Conversion values	FWO		KAS		Friedman	
	N_2	CO_2	N_2	CO_2	N_2	CO_2
Devolatilization Region						
0.1	0.9984	0.9981	0.9983	0.9979	0.9984	0.9984
0.15	0.9978	0.9941	0.9976	0.9936	0.9965	0.9965
0.2	0.9979	0.9947	0.9977	0.9942	0.9961	0.9961
0.25	0.9970	0.9942	0.9968	0.9936	0.9955	0.9955
0.3	0.9973	0.9925	0.9971	0.9917	0.9966	0.9966
0.35	0.9955	0.9900	0.9952	0.9888	0.9950	0.9950
0.4	0.9962	0.9890	0.9959	0.9877	0.9958	0.9958
0.45	0.9972	0.9861	0.9969	0.9845	0.9962	0.9962
0.5	0.9966	0.9849	0.9963	0.9831	0.9959	0.9959
0.55	0.9971	0.9891	0.9968	0.9877	0.9968	0.9968
0.6	0.9968	0.9885	0.9964	0.9870	0.9970	0.9970
0.65	0.9980	0.9881	0.9977	0.9864	0.9982	0.9982
0.7	0.9977	0.9879	0.9975	0.9861	0.9974	0.9974
0.75	0.9979	0.9878	0.9976	0.9859	0.9964	0.9964
0.8	0.9978	0.9812	0.9975	0.9783	0.9939	0.9939
0.85	0.9971	0.9855	0.9966	0.9830	0.9899	0.9899
0.9	0.9944	0.9879	0.9934	0.9856	0.9845	0.9845
Char Formation Region						
0.1	0.9763	0.9993	0.9738	0.9993	0.9984	0.9991
0.15	0.9798	0.9989	0.9776	0.9988	0.9965	0.9983
0.2	0.9833	0.9987	0.9815	0.9986	0.9961	0.9979
0.25	0.9869	0.9985	0.9854	0.9983	0.9955	0.9933
0.3	0.9846	0.9982	0.9827	0.9980	0.9966	0.9858

0.35	0.9857	0.9978	0.9840	0.9975	0.9950	0.9824
0.4	0.9836	0.9975	0.9815	0.9972	0.9958	0.9858
0.45	0.9810	0.9971	0.9784	0.9967	0.9962	0.9910
0.5	0.9798	0.9942	0.9770	0.9934	0.9959	0.9918
0.55	0.9786	0.9902	0.9757	0.9888	0.9968	0.9915
0.6	0.9776	0.9921	0.9745	0.9910	0.9970	0.9957
0.65	0.9774	0.9974	0.9744	0.9970	0.9982	0.9948
0.7	0.9770	1.0000	0.9738	1.0000	0.9974	0.9764
0.75	0.9778	0.9988	0.9747	0.9986	0.9964	0.9567
0.8	0.9786	0.9950	0.9757	0.9942	0.9939	0.9560
0.85	0.9799	0.9937	0.9772	0.9926	0.9899	0.9735
0.9	0.9824	0.9935	0.9801	0.9924	0.9845	0.9871